Single genes initiate novel epithelial structures in early fly development

presented by

M.Sc. Viola Noeske
born in: Villingen-Schwenningen

Dissertation
submitted to the
Combined Faculties for the Natural Sciences and for Mathematics of the
Ruperto-Carola University of Heidelberg, Germany for the degree of
Doctor of Natural Sciences

presented by

M.Sc. Viola Noeske
born in: Villingen-Schwenningen
Oral-examination: 24.09.2021

Single genes initiate novel epithelial structures in early fly development

Referees: Prof. Dr. Joachim Wittbrodt

Junior Prof. Dr. Steffen Lemke

Abstract

How does biology innovate? Ever since Darwin's famous visit of the Galapagos Islands and his studies beak shapes and food preferences of finches has this question been asked, addressed, and revisited. The study of biological innovation is at the core of all our attempts to explain morphological differences throughout different stages of animal development. Today, the availability of modern molecular techniques makes it possible to study biological innovations in great depth at the organismal, cellular, or genomic level. And still, it remains unclear how these different levels are linked to eventually produce something entirely new. In my thesis I identified two ways of how biology can create something new in the early stages of fly development, one at the cellular level and one at the tissue level. My discoveries are based on a comparison of the first hours of embryo development in the midge *Chironomus riparius* and the fruit fly *Drosophila melanogaster*. This comparison allowed me to identify and characterize cause and consequence of biological innovation, from new genes to new cell biology and putative adaptive benefits.

The first part of the results section comprises my comparative work on the formation of the first epithelium in insect embryos, the blastoderm. Here I identified tall blastoderm cells as a feature of presumably higher fly species and small blastoderm cells as a feature of more basal flies. To characterize the function of tall cells and how they emerged I used a comparative approach to distinguish tall from small blastoderm cells and their formation using the fruit fly *Drosophila melanogaster* as a representative of tall cells and the midge *Chironomus riparius* as a representative of small cells. By moving from tissue- to cell-level organization, I identified *slam*, as the first of a set of new genes, that act as headmaster of blastoderm columnarization in flies. By experimental engineering the blastoderm of *Chironomus* from a cuboidal to a columnar blastoderm I show that this novel Rho/F-actin regulator controls epithelial cell lengthening by an extension of E-cadherin based adhesion along the basolateral membrane. These experimentally columnized cells were less affected by desiccation suggesting an advantage by an increased barrier function of the epithelium.

The second part of my thesis focused on a previously identified diversity in extra-

embryonic tissue development within Diptera, where higher flies show a reduction in extraembryonic tissue development. More basal flies develop extraembryonic tissues that spreads over and covers the entire embryo. By studying interactions of yolk sac membrane with overlaying extraembryonic serosa cells in the scuttle fly *Megaselia abdita* I revealed decoupling of both tissues was necessary to ensure free spreading of the serosa to cover and protect the embryo. When interfering with the mechanism for decoupling, by interfering with yolk cortical actin or kock-down of *Megaselia-Matrix metalloprotease 1* (*Mab-Mmp1*), coupling of both tissues was prolonged and serosa stayed at a dorsal domain similar to a reduced extraembryonic tissue. The reduction of extraembryonic tissue here pretty much coincides with the transition from small to tall cells.

Zusammenfassung

Wie innoviert die Biologie? Seit Darwins berühmtem Besuch auf den Galapagos-Inseln und seinen Studien zu Schnabelformen und Nahrungsvorlieben von Finken wurde diese Frage gestellt, und immer wieder erneut aufgegriffen. Das Studium der biologischen Innovation steht im Mittelpunkt all unserer Versuche, morphologische Unterschiede in verschiedenen Stadien der Tierentwicklung zu erklären. Die Verfügbarkeit moderner molekularer Techniken ermöglicht es heute, biologische Innovationen auf organismischer, zellulärer oder genomischer Ebene eingehend zu untersuchen. Und dennoch bleibt unklar, wie diese verschiedenen Ebenen miteinander verbunden sind, um schließlich etwas völlig Neues hervorzubringen. In meiner Dissertation habe ich zwei Wege identifiziert, wie die Biologie in den frühen Stadien der Fliegenentwicklung etwas Neues schaffen kann, einen auf zellulärer Ebene und einen auf Gewebeebene. Meine Entdeckungen basieren auf einem Vergleich der ersten Stunden der Embryonalentwicklung bei der Mücke *Chironomus riparius* und der Fruchtfliege *Drosophila melanogaster*. Dieser Vergleich ermöglichte es mir, Ursachen und Folgen biologischer Innovation zu identifizieren und zu charakterisieren, von neuen Genen über neue Zellbiologie bis hin zu mutmaßlichen adaptiven Vorteilen.

Der erste Teil des Ergebnisteils umfasst meine vergleichenden Arbeiten zur Bildung des ersten Epithels in Insektenembryonen, dem Blastoderm. Hier identifizierte ich hohe Blastodermzellen als Merkmal vermutlich höherer Fliegenarten und kleine Blastodermzellen als Merkmal eher basaler Fliegen. Um die Funktion der langen Zellen und ihre Entstehung zu charakterisieren, habe ich einen vergleichenden Ansatz verwendet, um lange von kurzen Blastodermzellen und ihre Bildung zu unterscheiden, indem ich die Fruchtfliege *Drosophila melanogaster* als Vertreter der großen Zellen und die Mücke *Chironomus riparius* als Vertreter der kurzen Zellen verwendet habe. Durch Studieren der Gewebehin zur Zellebene identifizierte ich Slam, als das erste einer Reihe neuer Gene, das als Hauptorganisator der langen Blastodermzellen bei Fliegen fungiert. Durch experimentelles Einbringen von *slam* in das Blastoderm von *Chironomus* zeige ich, dass sich die Zellen von kurzen zu langen Blastodermzellen verändern. Dieser neuartige Rho/F-Aktin-Regulator verlängert die Epithelzellen durch eine Verlängerung der E-Cadherin-basierten

Adhäsion entlang der basolateralen Membran. Diese experimentell verlängerten Zellen wurden weniger durch Austrocknung beeinflusst, was auf einen Vorteil durch eine erhöhte Barrierefunktion des Epithels hindeutet.

Der zweite Teil meiner Dissertation konzentrierte sich auf eine zuvor identifizierte Diversität in der extraembryonalen Gewebeentwicklung innerhalb der Dipteren, bei der höhere Fliegen eine Reduktion der extraembryonalen Gewebeentwicklung zeigen. Mehr basale Fliegen entwickeln extraembryonales Gewebe, das sich über den gesamten Embryo ausbreitet und ihn bedeckt. Durch die Untersuchung der Wechselwirkungen der Dottersackmembran mit überlagernden extraembryonalen Serosazellen in der Buckelfliege *Megaselia abdita* zeigte ich, dass eine Entkopplung beider Gewebe notwendig war, um eine freie Ausbreitung der Serosa zu gewährleisten, um den Embryo zu bedecken und zu schützen. Bei einer Störung des Entkopplungsmechanismus durch Störung des kortikalen Aktins des Dotters oder durch einen knock-down der *Megaselia-Matrix metalloprotease 1* (*Mab-Mmp1*) wurde die Kopplung beider Gewebe verlängert und die Serosa blieb in einer dorsalen Domäne ähnlich einem reduzierten extraembryonalen Gewebe. Die Reduktion des extraembryonalen Gewebes fällt hier ziemlich genau mit dem Übergang von kleinen zu großen Zellen zusammen.

Contents

Abbreviations

A	Adenin
AJ	Adherens Junctions
AP	Anterior-Posterior
BMP	Bone morphogenetic protein
Bnk	Bottleneck
Bottleneck^{OE}	Bottleneck overexpression
C	Celcius
C. riparius	*Chironomus riparius*
cDNA	complementary DNA
cm	Centimetre
Cri	*Chironomus riparius*
D. melanogaster	*Drosophila melanogaster*
DAPI	4,6-diamidino-2-phenylindole
Ddc	Dopa decarboxylase
Dia	Diaphanous
DIC	Differential interference contrast
Dme	*Drosophila melanogaster*
DNA	Deoxyribonucleic Acid
dNTP	deoxynucleoside triphosphate
Dpp	Decapentalegic
dsRNA	double stranded RNA
Dunk^{OE}	Dunk overexpression
E-cad	E-cadherin
E. coli	Escherichia coli
EDTA	ethylendiamine tetraacetic acid
eGFP	enhanced green fluorescent protein
EtOH	Ethanol
F-actin	Filamentous actin
GBE	Germband extension
GEF	Guanine nucleotide exchange factor
GPCR	G-protein coupled receptor
GTP	guanosine triphosphate
H_20	Water
IAA	Isoamylalcohol
KD	kock-down
LB	Lysogeny Broth

M. abdita	*Megaselia abdita*
Mab	*Megaselia abdita*
MeOH	Methanol
min	Minutes
ml	Millilitre
Mmp1	Metalloprotease 1
mRNA	messenger RNA
mV	milliVolt
mya	million years ago
MyoII	Myosin II
myosin	Myosin II
NaOAC	Natriumacetat
ng	nano gram
nM	nano Molar
NTP	Nukleosidtriphosphate
PBS	Phosphate Buffered Saline
PBT	Phosphate Buffered Saline + Tween
PCR	polymerase chain reaction
PIV	Particle image velocimetry
Rho1/RhoA	Ras homolog family member A
RhoGEF2	Rho-guanine exchange factor 2
RNA	Ribonucleic Acid
Rok	RhoKinase
rpm	rounds per minute
SDS	Sodium Dodecyl Sulphate
sec	Seconds
Slam	Slow as molasses
Slam^{OE}	Slam overexpression in *Chironomus*
Sog	Short gastrulation
SPIM	Selective plane illumination microscopy
SURF	Synteny uncharacterized open reading frame
TAE	Tris-acetate-EDTA
Tris	Tris-(hydroxymethyl-) amino methane
UV	Ultraviolet
VE water	Deionized water
wt	wild type
Zen	Zerknüllt
µl	Microliter
µm	Micrometer

Contributions

In the following, people that contributed to the work presented in this thesis are listed. Their data has been used to create context and support observations. Contributions are listed below, and are also indicated on individual figures and in the main text.

Parts of this thesis are published or available as preprint:

Caroti, F., González Avalos, E., Noeske, V., González Avalos, P., Kromm, D., Wosch, M., Schütz, L., Hufnagel, L., & Lemke, S. (2018). Decoupling from yolk sac is required for extraembryonic tissue spreading in the scuttle fly Megaselia abdita. eLife, 7, e34616.

Noeske, V., Caglayan, E., Lemke, S. (2021). Single gene initiates evolution of epithelial architecture and function. Biorxiv https://doi.org/10.1101/2021.05.04.442636

Dr. Francesca Caroti: Performed and evaluated SPIM data in this Thesis. Cloning and synthesis of *zen* and *Mmp1* dsRNA and ddc probe.

Everado Gonzales: Performed quantitative evaluation of confocal microscopy recordings in Matlab for control embryos and *Mmp1* injected embryos. Wrote most of the Matlab skripts that are described in materials and methods and provided in the appendix.

Dr. Paula Gonzales: Performed volume rendering and assisted using Matlab.

Viola Kühnel and Yasmin Riesiger: performed injections of *cofilin* and subsequent DIC imaging and ddc in situ staining. Assisted PIV and flow analysis.

Clara Baader: performed injections of *bottleneck* and assisted characterize cell shape changes in these embryos.

Maike Fath: performed cloning: eGFP-slam, basigin-eGFP, Cofilin, SURF, Mab-slam, Lifeact-GFP, Lifeact-mCherry

Dr. Naima Ruhland: performed cloning: E-cadherin-GFP, Gap43-GFP (see PhD Thesis Naima Ruhland, 2020)

Emre Caglayan and Steffen Lemke: performed genomic survey for the cellularization genes s*erendipity alpha, nullo, bottleneck, dunk* and *slam*. Detailed description can be found in the Master Thesis of Emre Caglayan (2019) and preprint Noeske et al., 2021.

Dr. Atalay Tok: performed injectiond of Calyculin alpha (see PhD Thesis Atalay Tok, 2019).

1
Introduction

Biological innovations are a general feature of life and the evolution of new shapes and forms in animal development can often be associated with the origin of new phenotypes in the terminal development. The prime example and also one of the first studies on innovation in adult animals is the study of finches on the Galapagos islands, their different beak shapes and corresponding food preferences described by Darwin in 1839. Since then the development of new techniques, such as phylogenetic analysis and comparative developmental biology, provided a new level of studying biological innovations. This allowed to establish that morpohological innovations in evolution can be driven by a modification of molecular patterning, altered translation [Davies, 2013] or the gain or loss of gene activity. These innovations have particularly been described in related species and where phenotypic output can be associated with distinct patterns of gene expression like body pigmentation or the insect wing [Arnoult et al., 2013; Gompel et al., 2005; Wittkopp et al., 2002].

However, it remains unclear how genomic innovation can lead to an innovative output or adaptation via cell biological changes.

The complementary study of biological innovations on a genomic, cellular and molecular level thus requires the precise description of differences in cell shape and tissue behavior, the cellular components involved, the identification of phylogenetic novelties and a functional validation on the adaptive advantage.

In my thesis I focused on two innovations in early fly development where I observed a phenotypic difference in two distinct developmental tissues e.g., blastoderm tissue and extraembryonic tissue. I identified tall cells in the blastoderm stage and a reduced extraembryonic tissue spreading as a recent innovation in higher flies and aimed to characterize them using tools ranging from phylogenetic analysis via cell- to molecular- biology.

At blastoderm stage cell shape range from small and cuboidal [Bullock et al., 2004;

Benton et al., 2013; Urbansky et al., 2016] to tall and columnar [Lecuit and Wieschaus 2000; Acharya et al., 2014; Caroti et al., 2018], where the tall and columnar blastoderm is a rather recent innovation only found in higher fly species [Bullock, 2004]. To study the evolution of columnar blastoderm architecture typical for the fruit fly *Drosophila melanogaster* and other cyclorrhaphan flies, the nematoceran midge *Chironomus riparius* represents an excellent model system. *Chironomus* shared a last common ancestor with *Drosophila* 250 million years ago (MYA), and shows substantial differences in the cellular blastoderm stage. While cellularization in *Drosophila* results in cells that are about 30 µm tall, *Chironomus* cells only reach 13 µm [Urbansky et al., 2016; Wiegmann et al., 2011].

When cellularization is completed two adjacent structures form; the yolk sac surrounded by the blastoderm. Few cells from a dorsal domain decouple from the underlying yolk sac and spread over the embryo for protection and will not take part in embryonic development further on – the extraembryonic cells of serosa and amnion [Caroti et al., 2018; Schmidt-Ott and Kwan, 2016]. In *Drosophila* the cells of the extraembryonic anlage remain in a dorsal domain and do not spread over the embryo [Campos-Ortega and Hartenstein, 1997; Schmidt-Ott and Kwan, 2016] suggesting a difference in tissue to yolk sac coupling. To identify the unknown mechanism involved in extraembryonic tissue (de-)coupling *Megaselia abdita* represent an excellent model. *Megaselia* shared a last common ancestor with *Drosophila* 150 MYA [Wiegmann et al., 2011]. While overall embryonic development of both species is conserved and comparable [Wotton et al., 2014] *Megaselia*, in contrast to *Drosophila*, forms a closed serosa [Caroti et al., 2018; Rafiqi et al., 2012]. *Drosophila* as a well-studied model was my first entry into answering the questions on

1) how did tall cells emerge, and do they have an adaptive advantage? and
2) how gets coupling to the yolk sac resolved, to promote spreading of serosa cells over the embryo?

1.1 Early embryonic development in *Drosophila* forms a tall columnar blastoderm

1.1.1 Establishing a syncytial blastoderm in *Drosophila*

Like many other insects, early embryonic development in the fruit fly *Drosophila* is rapid and occurs in a syncytium, wherein a large mass of centrally located yolk confines cleavage to the cytoplasmic rim of the egg. One of the fascinating features of this cleavage type is that cells do not form until the nuclei have divided several times already [Leptin, 1999]. The first 13 nuclear divisions occur in absence of cytokinesis and consist of only S and M phases regulated by the cyclin dependent kinase (Cdk). After nuclei have been clustered together in the anterior part for the first three cycles, they become evenly distributed along the length of the embryo by a process called axial expansion. Astral microtubules play a key role during the first cycles and by their orientation prevent nuclear collision [Rothwell and Sullivan, 2000]. Starting from cycle 7 nuclei migrate to the cortex [Foe and Alberts, 1983]. During these cycles some nuclei fall back into the interior and become yolk nuclei. Starting from cycle 10 syncytial cleavages occur at the actin rich cortex just beneath the plasma membrane. Before the arrival of the nuclei and their associated centrosomes the F-actin is distributed evenly but becomes dramatically reorganized when nuclei reach the periphery. Plasma membrane and F-actin invaginate and form structures that are called metaphase or pseudocleavage furrows and then form around each nucleus and its associated centrosome [Riparelli et al., 2007]. These furrows have been described to be similar in structure and composition to cytokinesis furrows including actin, myosin, spectrins, anilin, septins and formins [Miller and Kiehart, 1995; Stevenson et al., 2002]. However, myosin is not required for metaphase furrow invagination. These metaphase furrows become essential to ensure separation of the individual nuclei when they divide in the tightly packed periphery [Sullivan et al., 1993]. During the last cycles' actin cap for-

mation above each nucleus can be observed. After 13 nuclear divisions nuclei are arranged in a closely packed monolayer, which is also characterized by an important transition in development the mid blastula transition, which in turn is characterized by a degradation of maternal RNAs and a dramatic activation of zygotic transcripts [Riparelli et al., 2007].

1.1.2 Cellularization dynamics in the *Drosophila* embryo

The blastoderm of insects is formed by a specialized form of coordinated cytokinesis – the so-called cellularization, where cells are formed by membranes invaginating between individual nuclei. The process occurs in animal but also in plant and unicellular eukaryote development [Hehenberger et al., 2012; Mazumdar and Mazumdar 2002]. Usually cellularization starts from a coenocyte (a multinucleated cell forming by sequential nuclear divisions without cytokinesis) and results in individual cell formation.

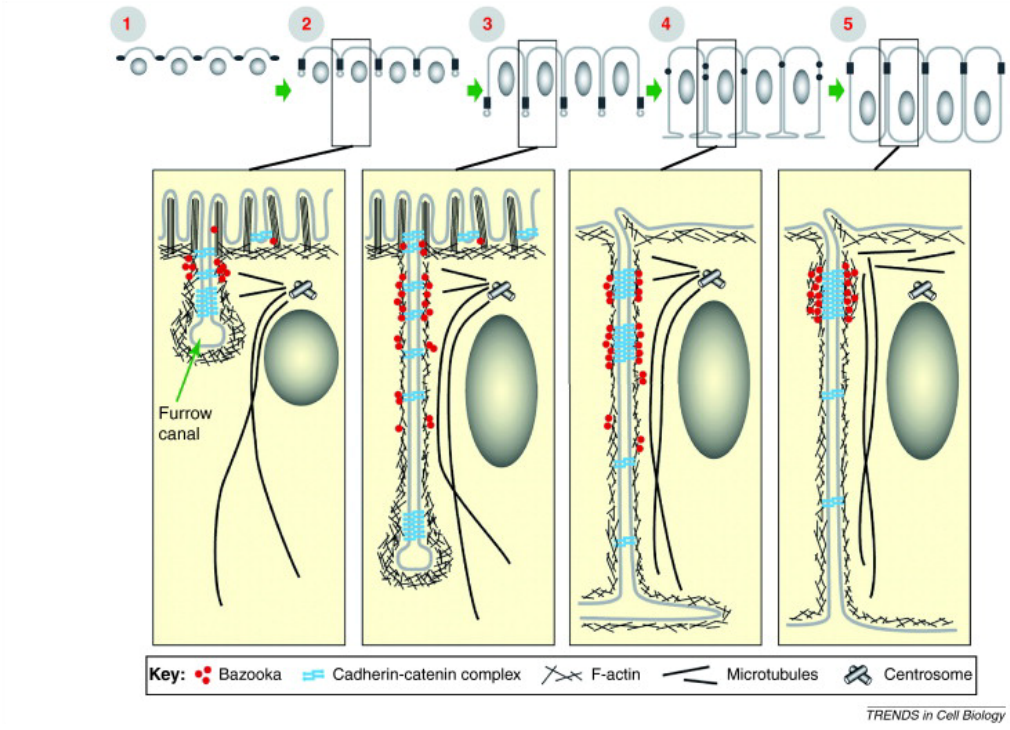

Figure 1.1: **Columnar blastoderm formation in the fruit fly *Drosophila melanogaster*.** Shown is a series of schemes representing the process of cellularization at the periphery of the developing egg. (1) before cellularization (2-4) during cellularization and (5) at blastoderm stage. The bottom series shows close-up views of the indicated stages. (Figure adapted from Laprise and Tepass, 2011)

During the process of cellularization, the plasma membrane invaginates between the cortical nuclei. As a result, the membrane surface in the embryo increases by a factor of about 30 and produces a polarized epithelium. Cellularization starts at the beginning of cycle 14, when the syncytial divisions stop and the membrane partition the cortical nuclei into individual cell units [Lecuit et al., 2002]. Above each nucleus the plasma membrane forms a somatic bud that is rich in villous projections. The somatic buds are separated by shallow invagination of the plasma membrane, which fold to form donut-shaped structures called furrow canals (FCs) (**Figure 1.1**) and are separated from the contiguous plasma membrane by basal adherens junctions (BAJs) [Lecuit, 2004]. The furrow canal constitutes the leading front of the ingrowing plasma membrane and contains specific sets of proteins where most of them are similar as in usual cytokinesis e.g., F-actin, myosin-II, anilin, septins and formins [Miller and Kiehart, 1995; Stevenson et al., 2002]. Here anilin and septins are important in contractile ring formation by crosslinking actin filaments and by order them in curved bundles [Piekny and Maddox 2010, Mavrakis et al. 2014]. It requires several F-actin nucleator such as Arp2/3 and Diaphanous [Afshar et al., 2000, Schmidt and Grosshans, 2018] and F-actin binding proteins including myosin II [Royou et al., 2002], septines [Adam et al., 2000], cofilin [Gunsalus et al., 1995] and profilin [Giansanti et al., 1998]. It also depends on junctional proteins supporting cell-cell adhesion including cadherin, alpha and beta catenin (**Figure 1.1**) [Hunter and Wieschaus, 2000]. Basal adheres junctions that contain the cadherin-catenin complex are assembled adjacent to the furrow canal. These are transient structures that are resolved at the end of cellularization. As the furrow canal is moving inward, the lateral membranes are forming. Membrane invagination requires trafficking of vesicles through subapical perinuclear recycling endosomes [Riggs et al., 2003, Lecuit and Wieschaus 2000].

Overall, the process of cellularization in *Drosophila* proceeds in two distinct phases. The first phase takes place in the first 35–40 minutes of cellularization, is slow (0.25 μm extension/minute), and membrane extension accounts for the first 10 μm of new membrane along the future basolateral cell surface. The second phase takes place from mitute 40-60 of cellularization, is fast (1.0 μm extension/minute), pushes the invagination rapidly towards the yolk, and stops when it is located about 30 μm inside the embryo [Lecuit and Wieschaus, 2000; Lecuit et al., 2002; Acharya et al., 2014].

1.1.3 The molecular initiation of cellularization

During initiation and much of the slow phase of cellularization, membrane growth is concentrated at the apical cell cortex, where actin forms caps apically to the nuclei. Within the next few minutes F-actin is reorganized and gradually accumulates at the tip of the forming furrow canal [Warn and Magrath, 1983, Schejter and Wieschaus, 1993]. This process of reorganizing the actin cytoskeleton dependents on the small GTPase Rho1, and inhibition of Rho1 leads to a disruption of the actin cytoskeleton and to severe defects in membrane invagination [Crawford et al., 1998]. Important for the cellular behavior and organization is the temporal and spatial control of Rho activation, which is achieved by a balance of GEF and GAP enzymes at selected membrane domains [Schmidt and Hall, 2002; Tcherkezian and Lamarche-Vane, 2007]. In the context of early embryonic development, Rho1 activity in *Drosophila* is regulated by RhoGEF2 [Barrett et al., 1997, Hacker and Perrimon, 1998; Kolsch et al., 2007]. In RhoGEF2 mutant *Drosophila* embryos, Rho1 fails to localize to the furrow canal; RhoGEF2 mutant embryos typically show incorrectly formed furrow canals [Grosshans et al., 2005]. During cellularization, Rho1 is specifically activated at the furrow canal by RhoGEF2, which is localized specifically at the furrow canal by interaction of its PDZ domain and Slow-as-molasses (Slam).

1.1.4 *Zygotic contribution in Drosophila* cellularization

Cellularization happens at an important transition, the so called mid blastula transition, where an extreme burst in zygotic transcription occurs. Five zygotic transcripts have been associated with the process of *Drosophila* cellularization: *nullo, serendipity-alpha, bottleneck, slam and dunk.*

1.1.4.1 *nullo* and *serendipity-alpha*

Nullo and Serendipity-alpha localize to the invagination front in the *Drosophila* embryo prior furrow canal formation, where they are required for proper infolding of the plasma membrane. There they colocalize with RhoGEF2 and Diaphanous [Grosshans et al., 2005]. *serendipity-alpha* acts in a genetic pathway in parallel to RhoGEF2 and Dia, controlling furrow canal formation [Mazumdar and Mazumdar, 2002]. During cellularization it is required for maintaining the integrity of microfilaments during cellularization. When *serendipity-alpha* is absent few multinucleated cells are forming [Mazumdar and Mazumdar, 2002]. The zygotic gene *nullo* has its peak expression at slow phase of cellularization and its level decreases during fast phase [Mazumdar and Mazumdar, 2002]. It is found at the cellularization front in the *Drosophila* embryo, where it is important for the organization of the furrow canal. It is required for the stabilization of a basal adhesive junction that isolates the furrow canal and allows the stable accumulation of myosin-II [Hunter and Wieschaus, 1994].

1.1.4.2 *bottleneck*

bottleneck reaches its peak expression when cellularization sets in and is required for proper organization of the actin filaments [Schejter and Wieschaus, 1993]. In absence of *bottleneck* hexagons change into rings much earlier and cells close too early, this sometimes resulting in nuclei being encompassed by the cellularization ring, which will give them a bottleneck-shape [Theurkauf, 1994]. *bottleneck* is specifically associated with actomyosin exclusively during the early phase of cellularization but gets lost from the invagination front when the hexagonal array breaks down into rings and the fast phase begins indicating a phase specific function [Schejter and Wieschaus, 1993; Theurkauf, 1994]. It is proposed that Bottleneck protein physically links actomyosin units within the hexagonal that facilitates tension at the invagination front [Schejter and Wieschaus, 1993; Theurkauf, 1994]. If this is balanced over the entire embryo, the network contracts as a whole resulting in an inward directed force. In this proposed model *bottleneck* acts to restrain

microfilament ring constriction by linking all the contractile units together.

1.1.4.3 *slam*

slam transcripts are provided maternally, and *slam* is also one of the first zygotically expressed genes. During the fast phase of cellularization, maternal *slam* transcript rapidly decreases and reaches low levels by the onset of gastrulation [Yan and Grosshans, 2018]. The expression of zygotic *slam* is rapidly induced during the slow phase at beginning of cycle 14 and is required for timely invagination of the membrane furrows [Lecuit et al., 2002; Stein et al., 2002; Yan and Grosshans, 2018]. Maternal as well as zygotic *slam* expression is required for complete furrow canal extension during the fast phase of cellularization. If either contribution is missing, the furrow canal forms slower and remains much shorter [Acharya et al., 2014].Such defects have been associated with several critical roles that *slam* plays during cellularization: it is required for localization of RhoGEF2 to the furrow canal, it is required for accumulation of junctional components at the ingrowing lateral cell membrane, it is involved in membrane trafficking, and, together with *dunk*, *slam* is required for the recruitment of non-muscle myosin-II to the furrow canal [Wenzl et al., 2010; Acharya et al., 2014; Lecuit et al., 2002; Mazumdar and Mazumdar, 2002].

1.1.4.4 *dunk*

dunk transcripts are provided only zygotically and transcription starts immediately before the onset of cellularization [He et al., 2016]. Dunk protein is specifically required to maintain myosin at the cortex. During cellularization myosin acts in consecutive phases: in the first 12 minutes of the flow phase, myosin is recruited to the apical cortex and rapidly flows towards the base of the newly formed furrows. In the second phase of the slow phase (12-30 min), myosin is directly recruited to the leading edge without cortical flow [Mazumdar and Mazumdar, 2002]. Dunk seems to play a crucial role in this process: in *dunk* mutant embryos, myosin rapidly dissociates from the cortex after the onset of the flow phase. The recruitment phase however takes place in a *slam* dependent but *dunk* in-

dependent direct myosin recruitment pathway [He et al., 2016]. These *dunk* dependent stabilization of myosin recruitment sites enable the establishment of an interconnected actomyosin network that maintains tension and provides a mechanical mechanism to guide the anisotropic myosin flow [He et al., 2016].

1.1.5 The first embryonic epithelium in insects: innovation of tissue architecture

The blastoderm formation driven by cellularization is a common feature found in most insect species. However tall cells in the blastoderm stage are suggested to rather be a recent innovation mostly found in higher flies [Bullock et al., 2004]. *Tribolium castaneum* is one representative species consisting of small cuboidal cells in its blastoderm stage [van der Zee et al., 2015]. A striking difference from *Tribolium* to *Drosophila* cellularization is the formation of junctions between the forming basal membrane and the yolk plasmalemma by innexin 7 [van der Zee et al., 2015]. Additionally, the rapid phase of invagination is missing in *Tribolium* and cells closing directly underneath the spherical nuclei leading to a much thinner blastoderm cell with cuboidal cells [van der Zee et al., 2015].

The observed differences in blastoderm stage found in Tribolium and described by Bullock et al., 2004 suggest that the blastoderm architecture has changed over the past millions of years however when and how remains unclear. This suggest that the blastoderm presents a perfect model to study the biological innovation of tall blastoderms including studies on cellular and molecular changes as well as a phylogenetic analysis.

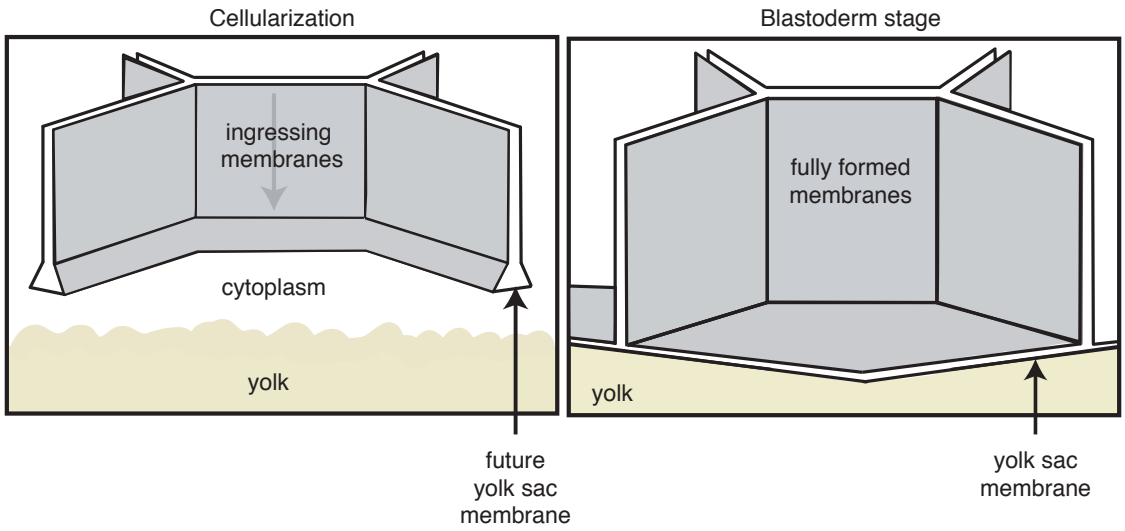

Figure 1.2: **The yolk sac forms as a consequence of cellularization.**
Yolk sac formation by the process of cellularization shown in a scheme. Shown is the process of cellularization that is forming blastoderm cells (grey) around the yolk (yellow) and the yolk sac membrane formation. Apical up basal down.

1.2 Early embryonic development of the two overlaying structures – yolk sac and serosa

1.2.1 The process of cellularization forms two distinct structures - blastoderm cells and yolk sac membrane

The next part focuses on a biological innovation on the tissue level, where I used a previously described observation on differences in extraembryonic tissue spreading [Kwan et al., 2016; Schmidt-Ott and Kwan, 2016; Caroti et al., 2018; Rafiqi et al., 2008]. I aimed to study how and whether tissue-tissue interaction can alter the spreading behavior of the extraembryonic tissue. In detail, serosa cells that sit at a dorsal domain in the fly embryo has to separate from the underlaying yolk sac to spread free and cover the embryo for protection. In higher fly species, such as *Drosophila* the extraembryonic tissue does not spread over the entire embryo and thus show a reduced extraembryonic tissue the so called am-

nioserosa [Rafiqi et al., 2008]. The yolk sac membrane and extraembryonic tissue anlage form by the process of cellularization when membranes fuse basal to the nuclei.

Blastula formation is completed when membranes fuse basal to the blastoderm nuclei. At this time two distinct structures arise (I) the blastoderm epithelium and (II) a single continuous plasma membrane around the yolk – the yolk sac membrane (**Figure 1.2**) [Schmidt-Ott and Kwan, 2016; Lemke et al., 2020]. These structures are fundamentally different in structure but also in their contribution to development. However, the contribution of the yolk sac to gastrulation and extraembryonic tissue development remains poorly understood.

1.2.2 Extraembryonic epithelia in the context of fly development

The blastula is the source to form a three-layered embryo and additionally for the formation of the extraembryonic epithelia serosa and amnion (or amnioserosa in case of *Drosophila*) that cover and protect the embryo [Schmidt-Ott and Kwan, 2016].

The serosa is derived from a spheroidal extraembryonic anlage in the anterior/dorsal portion of the blastoderm, it spreads over the entire embryo and completely engulfs it at the end of gastrulation [Kwan et al., 2016; Schmidt-Ott and Kwan, 2016; Caroti et al., 2018; Lemke et al., 2020]. The amnion is specified in a circumferential ring next to the serosa and connects to the embryo; as the serosa spreads over the embryo, the amnion folds underneath and in most insects' spreads between serosa and embryo to eventually cover the posterior/ventral side of the embryo [Schmidt-Ott and Kwan, 2016; Caroti et al., 2018; Lemke et al., 2020]. Cells of the serosa and amnion do not divide or intercalate, indicating that extraembryonic tissue spreading is achieved by changes in cell shape and dependent on the initial size of the extraembryonic anlage. In a subset of flies, including the fruit fly *Drosophila*, only a single tissue is formed, the amnioserosa; it stays on the dorsal side of the embryo and does not spread [Rafiqi et al., 2008; Schmidt-Ott and Kwan, 2016; Lemke et al., 2020]. The dynamics of extraembryonic tissue and cell behavior have been studied extensively in the fruit fly *Drosophila* [Rafiqi et al., 2008; Pope and Harris, 2008; Lacy and Hutson, 2016].

1.2.3 Gastrulation and extraembryonic tissue development in *Drosophila*

After blastula formation cells start to invaginate at the ventral side of the embryo in a coordinated manner forming the tube-like ventral furrow [Leptin and Grunewald, 1990]. This tube collapses, when invaginated and cells migrate along the lateral epithelium establishing the mesoderm. To separate head from trunk the transient cephalic furrow forms. In the next step cells germband starts to elongate by elongation of the ventral side and the pole cells are pushed to the dorsal side of the embryo [Turner and Mahowald, 1977]. The germband extension starts with a first fast phase and slows down in the second phase when pole cells are internalized and the posterior midgut starts to invaginate. The germband elongates until it almost reaches the germband [Anderson 1966, Campos-Ortega and Hartenstein 1997]. As germband gets elongated cells at the dorsal side spread transforming from a columnar to a squamous epithelium – the extraembryonic amnioserosa [Turner and Mahowald, 1977]. When germband elongation is completed the germband start retracting and amnioserosa spreads out. After complete retraction of the germband the amnioserosa, that sits on top of the yolk, contracts and reduces its area and starts dorsal closure [Turner and Mahowald, 1979]. At complete dorsal closure amnioserosa is degraded and the dorsal hole is completely healed.

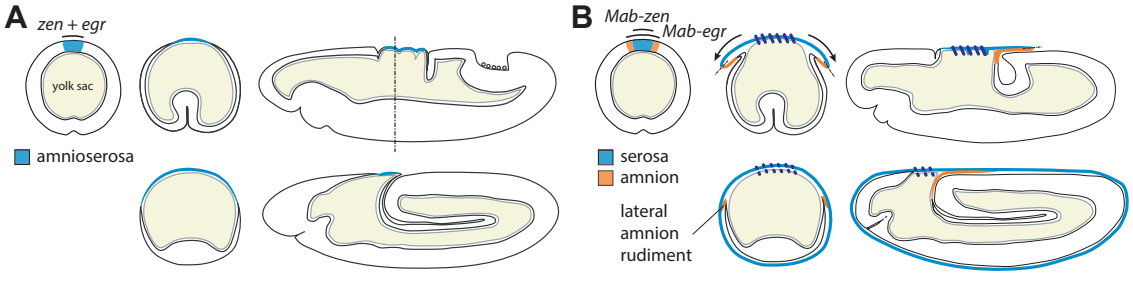

Figure 1.3: **Extraembryonic tissue anlage is defined by *zen* and *eiger* (*egr*).**
A-B, Schematic illustration of extraembryonic tissue development at two stages of gastrulation in *Drosophila* and *Megaselia*. (A) Coinciding expression of *zen* and *egr* define the anlage of amnioserosa at blastoderm stage (blue). (B) *Mab-zen* defines serosa anlage (blue) and *Mab-zen* amnion anlage at blastoderm stage in *Megaselia*. (Figure adapted from Lemke et al., 2020)

1.2.4 Extraembryonic tissue development in other insects

The extraembryonic amnioserosa is an evolutionary novelty found only in a subset of flies [Rafiqi et al., 2008]. Most other insects develop two extraembryonic tissues – the serosa and the bordering amnion. The extraembryonic membranes show different morphologies between insect species. The serosa is set up from blastoderm cells along the dorsal midline, similar to the amnioserosa. The topology of the amnion is different between species; in *Tribolium*, *Chironomus*, *Anopheles* and other basal branching flies the amnion is in close contact to the serosa and follows around the poles and closes ventral as does the serosa resulting in a covered embryo with an additionally thin amnion at its ventral site [Goltsev et al 2009; Lemke et al., 2020]. In *Megaselia* and *Episyrphus*, examples from the basal cyclorrhaphan flies, serosa, as it expands, separates from the amnion [Lemke et al., 2020]. The amnion in *Megaselia* remains at the dorsal side with a thin line of cells at the lateral sites of the embryo and stays in contact with the embryo proper [Caroti et al., 2018].

1.2.5 Genetics of extraembryonic tissue development

The dorsal domain from which extraembryonic cells form are defined by a peak of BMP signaling in *Drosophila* and also other flies [Kwan et al., 2016, Rafiqi et al., 2012]. The width of the domain is defined by the BMP ligand Decapentaplegic (Dpp) and its positive feedback. The long range Dpp transport depends on two other secreted proteins; Short gastrulation (Sog) and Tolloid, a metalloprotease. Sog and Dpp form a diffusible complex that hinders its receptor interaction. This is released in presence of Tolloid, which releases the ligand again [Shimmi 2005; Umulis 2010; Wang and Ferguson 2005]. The local activity of Dpp is promoted by *eiger* (tumor necrosis factor alpha) which is activated by *zerknüllt* (*zen*) (**Figure 1.3 A**). The highest concentration of Dpp is in the dorsal midline of the embryo and decreases towards the lateral sites which defines the amnioserosa

anlage. In *Drosophila, eiger* has been reported to remodel extracellular matrix (ECM) by promoting *Mmp1* (*Matrix metalloprotease 1*) activity in later stages (larvae stage) and therefore not reported to be involve in amnioserosa development.

In *Megaselia* this pathway is in parts conserved and long-range transport of Dpp functions as in *Drosophila* by the expression of essential BMP signaling factors [Kwan et al., 2016, Rafiqi et al., 2012]. However, the domain of *zen* appears overlapping with *eiger* only in a dorsal domain which is explained by *Mab-eiger*'s expression under control of dorsocross, a zen independent Dpp target. This leads to a domain where *zen* and *eiger* expression overlap giving rise to serosa cells and a domain with only *eiger* defining the bordering amnion (**Figure 1.3 B**) [Caroti et al., 2018; Lemke et al., 2020].

1.2.6 Yolk sac in the context of early embryonic development

The yolk sac is defined as a membranous sac filled with yolk attached to the embryo proper during early embryonic development [Schmidt-Ott and Kwan, 2016]. The yolk sac is common to all insect species which develop from a centrolecithal yolk rich egg, but the developing embryos differ substantially among insect species. Beside its function providing nutrition for the embryo studies indicate that the huge multinucleated yolk cell actively contributes to early embryonic development [Reed et al., 2004, Goodwin et al., 2016]. Very early in development observations made in the beetle *Callosobruchus maculatus* showed rhythmic movements of the yolk that can be associated with the nuclear divisions. These movements are suggested to be important for nuclei movements during syncytial cleavages [Miyamoto et al., 1982]. The yolk sac membrane is formed at the end of cellularization underneath the blastoderm where cells close up at the basal site forming one continuous membrane around the yolk. This membrane is covered by cortical actin and recent studies showed integrins to be actively involved in early embryo development at distinct places and phases in development [Reed et al., 2004, Benton et al., 2013].

In *Drosophila* the huge polynucleated cell is attached to the amnioserosa via a laminin containing extracellular matrix and integrins which is essential for the amnioserosa

contraction contributing to the closing force [Narasimha and Brown, 2004]. When integrin function is inhibited a premature death of the overlaying amnioserosa cell layer is observed. It is suggested that the contractile yolk sac in interaction with overlaying amnioserosa cells use an apicobasal pulling force [Reed et al., 2004]. The expression of integrins is also involved other developmental processes i.e., midgut formation [Narasimha and Brown, 2004] or germband retraction [Schöck and Perrimon, 2003]. In the flour beetle *Tribolium castaneum* the yolk sac as well as the amnion fold over the extending germband [Handel et al., 2000; Schmidt-Ott and Kwan 2016] and a physical connection has been suggested [Benton et al., 2013]. When the involution of the amnion ends this fold retracts allowing serosa and amnion to close. These investigations suggest an essential role of the yolk cell and its nuclei however the molecular basis for the involvement on gastrulation remains poorly understood.

Aim

The aim of this thesis was to characterize and identify the genetic basis of early embryonic innovations during fly development for two distinct embryonic structures: (1) cell height differences in the blastoderm and (2) the connection of the two extraembryonic structures yolk sac and serosa.

(1) Despite epithelia diversity in form and function, it is still fundamentally unclear how major differences in tissue architecture evolved. Here I aimed to take advantage of a recent innovation in fly cell anatomy to address the molecular mechanism that once transformed a cuboidal epithelium of small and short cells into a columnar epithelium of long and tall cells. First, I aimed to use a comparative approach to distinguish tall from small blastoderm cells and their formation using the fruit fly *Drosophila melanogaster* as a representative of tall cells and the midge *Chironomus riparius* as a representative of small cells. By combining this comparative approach with a deliberate addition and removal of selected molecular components into the *Chironomus* embryo I aimed to identify differences in early embryonic tissue diversity on a molecular, cellular, genetic and evolutionary level.

(2) At blastoderm formation two adjecent structures form – the blastoderm epithelium and the yolk sac. The blastoderm cells are the source for gastrulation and have been studied intensively, however little is known about the involvement of the yolk sac to gastrulation and early fly development. I aimed to study the involvement of the yolk cell membrane to allow free serosa spreading. The serosa is an extraembryonic tissue that develops from cells that are set aside from the embryo, cover the embryo and are described to protect the embryo. However not all flies develop a serosa that spreads over the whole embryo and cells from extraembryonic- anlage remain at a dorsal position in connection with the underlaying yolk sac i.e., the amnioserosa in *Drosophila*. I aimed to investigate the coupled and decoupled state of the two extraembryonic structures yolk sac and overlaying serosa cells in the scuttle fly *Megaselia abdita* using live imaging of both structures and aimed to identify whether a prolonged coupling would result in a *Drosophila*-like phenotype.

2
Results

2.1 The fly blastoderm – a model to study tissue architecture divergence

2.1.1 A tall columnar blastoderm is a recent innovation of higher flies

The architecture of tissues differs within organisms and between species and cell architecture can range from flat and wide to tall and narrow. These differences are often associated with a difference in function, though it remains elusive whether differences in cell height and function are linked. To address putative mechanisms underlying tissue architecture divergence, it would be ideal to investigate an epithelium that appeared once with small and once with tall cells to compare their function.

One promising framework that fulfills these criteria is the first embryonic epithelium of flies, the so-called blastoderm. At this stage the blastoderm cells of different fly species show differences in their cell architecture. More basal flies consist of small and cuboidal cell where the more derived flies are made of tall columnar cells (**Figure 2.1**) [Schwalm et al., 1988; Bullock et al., 2004; Wiegmann et al., 2011].

To address the questions of how blastoderm architecture relates to blastoderm function, I compared two fly species that each represent a distinct type of blastoderm architecture; *Drosophila melanogaster* features a columnar blastoderm, the midge *Chironomus riparius* represents the ancestral cuboidal architecture [Urbansky et al., 2016; Klomp et al., 2015 Ritter, 1890] (**Figure 2.2**).

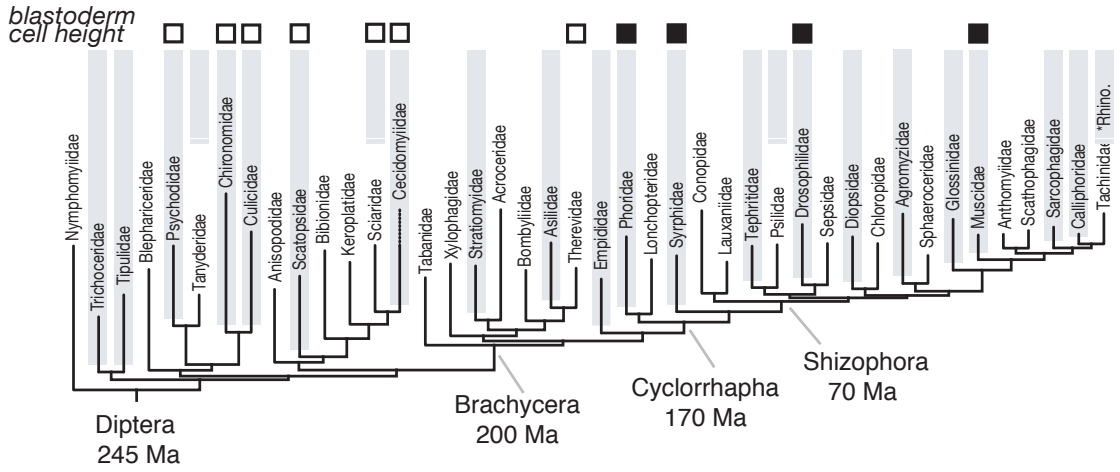

Figure 2.1: **Tall cells are a feature found in higher fly species (black box).**
Phylogeny of major fly families, with selected minor families added (asterisk; Chaoboridae, Bolitophilidae, Rhinophoridae) [Wiegmann et al., 2011]. Blastoderm cell height indicated; empty box: small cuboidal cells, filled box: tall columnar cells.
Species from left to right: Psychoidae - *Clogmia albipunctata*; Chironomidae – *Chironomus riparius*; Culicidae – *Anopheles gambiae*; Scatopsidae – *Coboldia fucipes*; Sciaridae – *Bradysia hygida*; Cecidomyiidae – *Aphidoletes aphidimyza*; Therevidae – *Bactrocera dorsalis*; Phoridae – *Megaselia abdita*; Syrphidae – *Episyrphus balteatus*; Drosophilidae – *Drosophila melanogaster*; Muscaidae – *Musca domestica*
[Bullock et al., 2004; Havelka et al., 2007; Jiménez-Guri et al., 2014; Urbansky et al., 2016; Suksuwan et al., 2017; Uliana et al., 2018; Caroti et al., 2018]

2.1.2 Cuboidal versus columnar blastoderm: a quantitative characterization

To characterize general differences between embryos of the two species, I first compared the egg shape and quantified the *Chironomus* embryo to be 2 times smaller (average of 240 µm in length, 110 µm in width) compared to *Drosophila* (average of 485 µm in length, 180 µm in width) (**Figure 2.2 A-B'**). Despite the differences in surface area (*Chironomus*: 2.12 cm^2; *Drosophila*: 5.884 cm^2), nuclear density appeared to be similar (*Cri*: 4.9 +/- 0.7 versus *Dme*: 5.1 +/- 0.7), suggesting some differences in the developmental processes leading up to blastoderm formation (see below). To address differences in cell architecture, I conducted a quantitative comparison of cell shape in the short and tall blastoderms of the two species. This included quantification of height and width of cells, but also how closely cells mirrored the shape of true columns or whether they tapered at their apical and basal sides (**Figure 2.3**). To reveal cell outlines, I used cortical F-actin and found that blastoderm cells in *Chironomus* were about half as tall compared to *Drosophila*

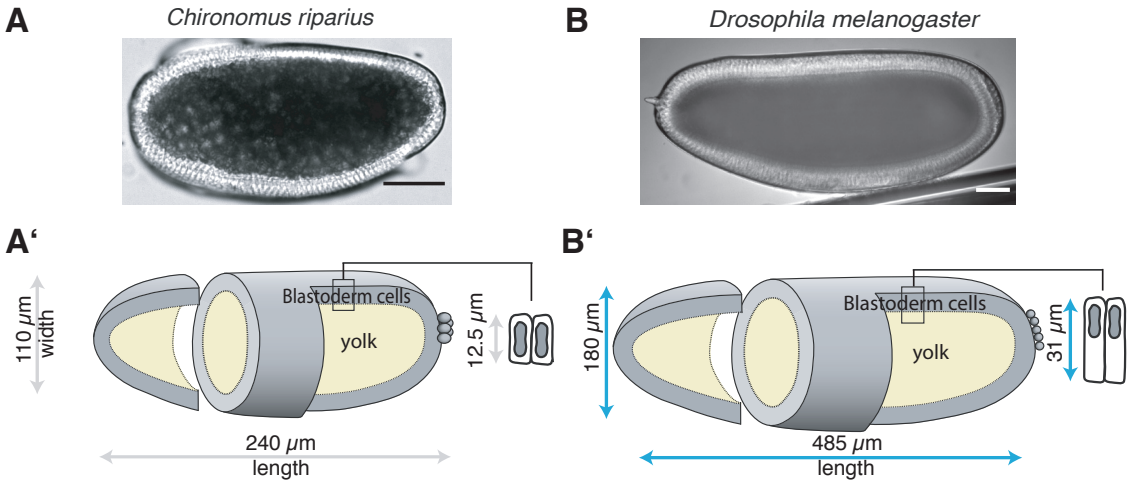

Figure 2.2: **Representative fly species display either a short or a tall blastoderm cell architecture.** **A,A'**, The *Chironomus riparius* embryo is a representative species consisting of small cells in the blastoderm stage; **B,B'**, *Drosophila melanogaster* a representative of tall cells in the blastoderm stage. DIC image and sketch of a *Chironomus riparius* embryo (A-A') and of a *Drosophila melanogaster* embryo (B-B') (anterior left, dorsal up, dimensions indicated in the sketch). Scale bar 50 µm.

(12.8 +/- 1.0 µm (*Cri*) versus 32.3 +/- 0.9 µm (*Dme*)) (**Figure 2.3 A,B,D**). At the apical side, neither species showed apical cell tapering (**Figure 2.3 F**); at the basal side, cells in *Chironomus* tapered, while cells in *Drosophila* remained connected and appeared as columns (**Figure 2.3 G**).

With cell density similar between cuboidal *Chironomus* and columnar *Drosophila* blastoderm, my results establish cell height and the degree of basal cell-cell contacts as primary differences between the two blastoderm epithelia.

2.2 Setting the stage: establishing *Chironomus* as comparative pair for studying differences in blastoderm formation

To compare *Chironomus* to the well-studied *Drosophila* model, I began by investigating the early development from egg lay to blastoderm establishment in *Chironomus*. Specifically, I first explored the nuclear divisions in the syncytium necessary to build up

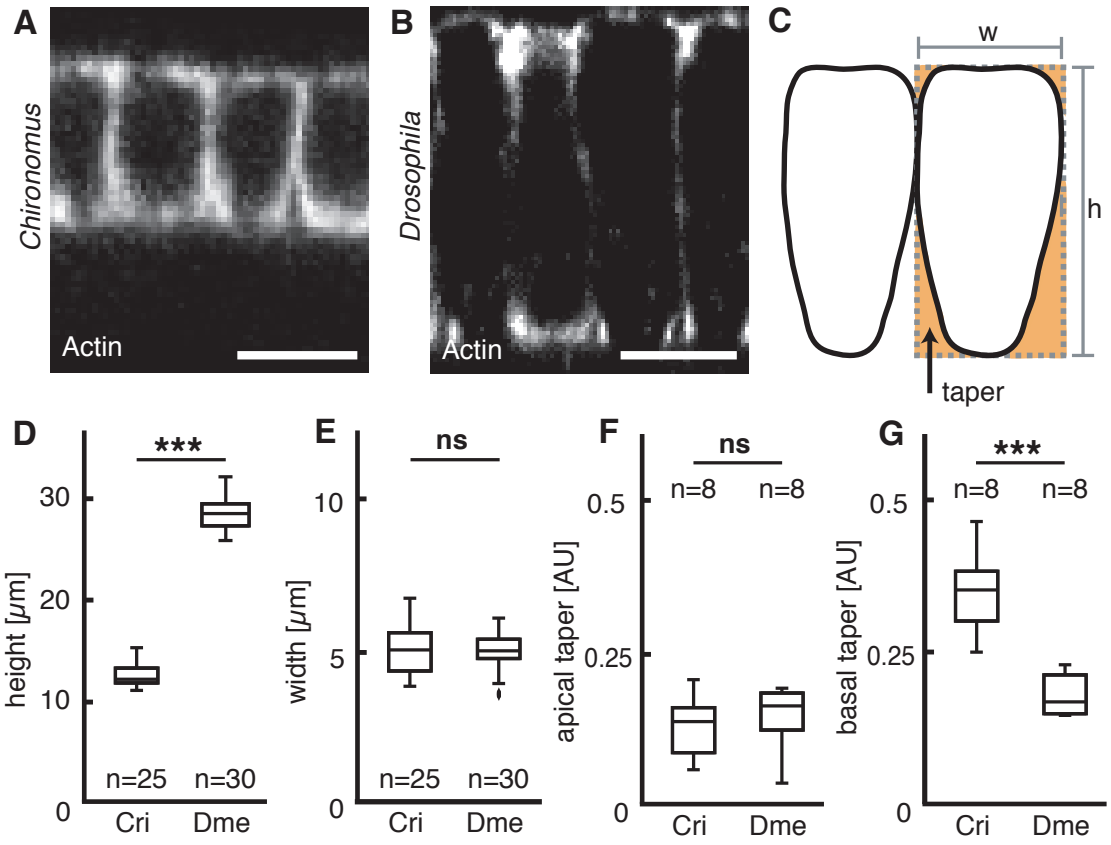

Figure 2.3: **Blastoderm cell architecture differs between *Chironomus* and *Drosophila*.**
A-B, Blastoderm cells in *Chironomus* (A) and *Drosophila* (B). **C**, Sketch indicating cell width (w), height (h), and taper as measures of blastoderm cell architecture. **D-G**, Comparisons of height (D; *** P<0.0001), width (E; ns. P=0.76), apical (F; ns. P=0.73) and basal taper (G; *** P<0.0001) indicate differences in *Chironomus* cuboidal (Cri) and *Drosophila* columnar (Dme) cell architecture. P-values calculated with t-test, scale bars 10 µm.

the material for blastoderm formation. I then investigated the process of *Chironomus* cellularization and ended with a side-by-side comparison of the two species.

2.3 From a fertilized egg to a syncytial blastoderm in *Chironomus*

2.3.1 The syncytial blastoderm in *Chironomus* is based on 12 nuclear divisions

To characterize the syncytial cleavages (from egg lay to start of blastoderm forma-

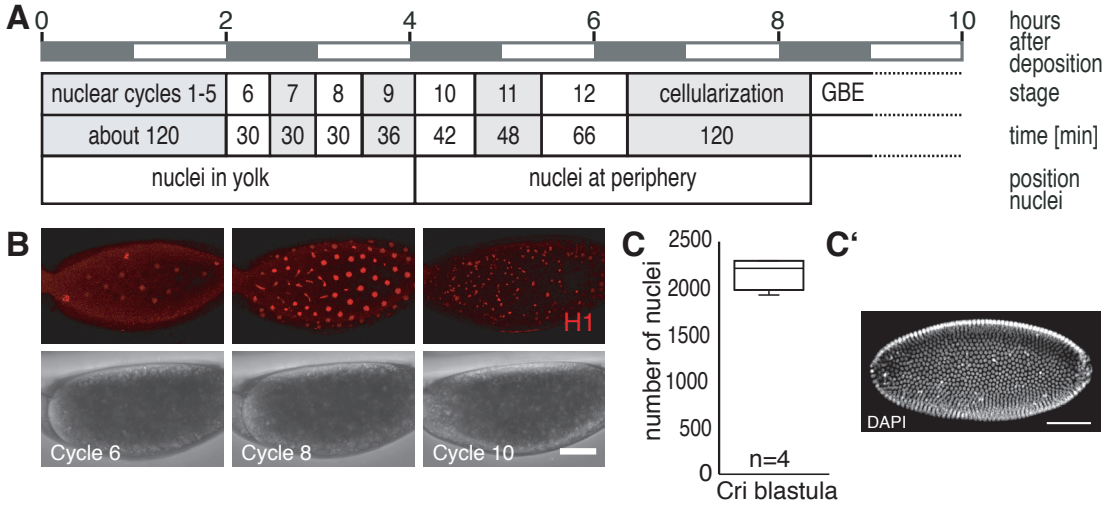

Figure 2.4: **Early embryonic development in *Chironomus riparius* takes about 8 hours and 12 nuclear cycles until the end of cellularization.**
A-B, Timing and duration of nuclear cleavage cycles (A), observed by brightfield and confocal time lapse recordings in embryos injected with fluorescently labeled Histone-H1-texasRed (B). **C**, Number of nuclei in *Chironomus* blastoderm stage (at periphery).

tion) in *Chironomus* I used two ways to determine timing of the divisions 1) DIC movies and 2) *Chironomus* transiently labeled with HistoneH1-texas red (injected embryos at pole cell stage) to follow nuclei cleavages. I found the *Chironomus* embryo underwent one nuclear cycle less (12 cycles, **Figure 2.4 A,B**) with about 2300-2500 nuclei at the periphery before cellularization set in (**Figure 2.4 C**). This diverged from the expected number of 4096 nuclei in the egg after 12 divisions. In the literature of *Drosophila* a similar phenomenon is described, where [Reed et al., 2004; Caroti et al., 2018] nuclei were not dividing anymore or nuclei remained in the yolk not moving to the periphery resulting in a smaller number of nuclei at the periphery as expected.

In summary I found syncytial blastoderm formation took about 2 times longer in *Chironomus* to complete 12 nuclear divisions (about 6 hours) compared to *Drosophila*, which took only 2.5 hours [Mazumdar and Mazumdar, 2002] to complete 13 nuclear divisions, while cell density appeared similar in both species. This suggest that *Chironomus*' smaller egg size results in a reduced number of cycles (12) necessary to reach the same cell density as *Drosophila*.

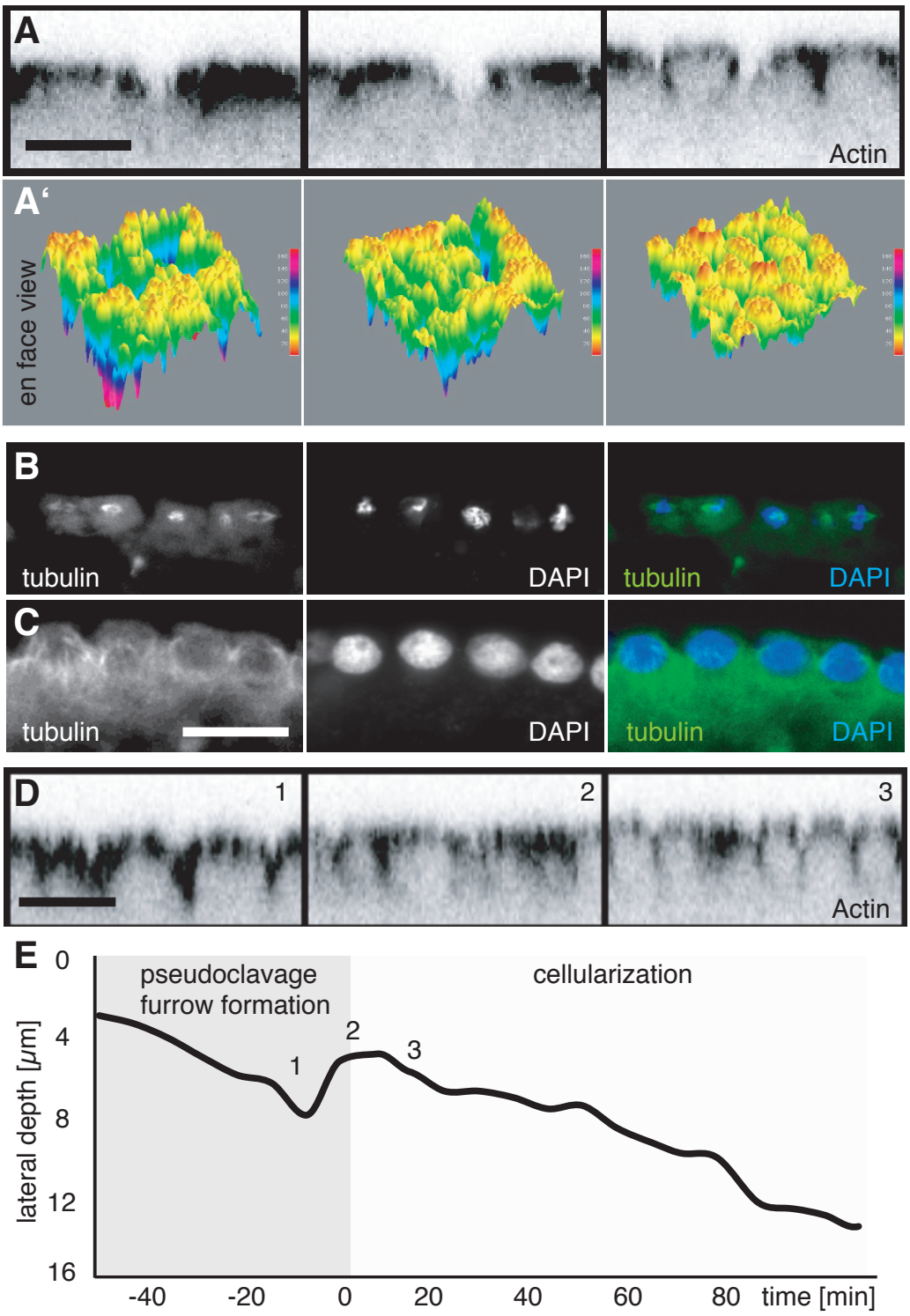

Figure 2.5: **The establishment of the syncytial blastoderm in *Chironomus* coincides with the formation of actin rich villi above individual nuclei and microtubules.**
A-A', Actin cap establishment above individual nuclei and membranes starting invaginating to separate individual spaces around individual nuclei. Shown are Lifeact-mCherry stainings in a cross-section and an en face view indicating thickness of the actin caps (thickness indicated in px [16 px = 6.7 µm], **B**, Microtubules organization during M-Phase and **C**, Microtubules organization during S-Phase. **D-E**, Metaphase furrow formation before cellularization starts shown by a Lifeact-mCherry staining (D) and its progression over time (E).

2.3.2 Cytoskeletal dynamics during *Chironomus* syncytial nuclear divisions

During syncytial cleavages in *Drosophila* a dramatic reorganization of the cortical cytoskeleton takes place that results in the formation of discrete cytoskeletal domains around each nucleus [Schejter and Wieschaus, 1993]. This becomes especially important when nuclei reach the periphery, where they must establish enough membrane material for subsequent cellularization. In *Drosophila* this membrane reservoir is stored in actin rich villi above each individual nucleus [Stevenson et al., 2002; Figard et al., 2013; Figard and Sokac, 2014; Figard et al., 2016]. To follow the F-actin dynamics in *Chironomus* I injected Lifeact-mCherry when nuclei were at the periphery and found F-actin organized in caps above individual nuclei. These caps became disassembled in the mitotic phase when nuclei divided and reorganized again (**Figure 2.5 A, A'**). In later cycles (starting from cycle 10) while caps were re-established, I observed membranes starting to invaginate (similar to the later process of cellularization). The invagination of this intermediate membrane elongation protruded up to 8 µm deep into the egg which represented more than half the lateral cell height of *Chironomus* blastoderm cells (**Figure 2.5 E**). When actin caps disassembled microtubules started to re-organize as well. As they were organized as inverted baskets during S-phase, they reorganized in a 90° angle in M-Phase and re-established as inverted baskets afterwards (**Figure 2.5 B,C**). These observations were similar to previous findings in *Drosophila* [Riparelli et al., 2007].

2.3.3 Syncytial nuclear divisions in *Chironomus* require the cytoskeletal elements F-actin, myosin-II and microtubules

To address how F-actin, myosin-II and microtubules function in *Chironomus* cuboidal syncytial blastoderm formation, I took advantage of small compound inhibitors that rapidly interfere with the cytoskeleton upon injection and can thus decribe their function

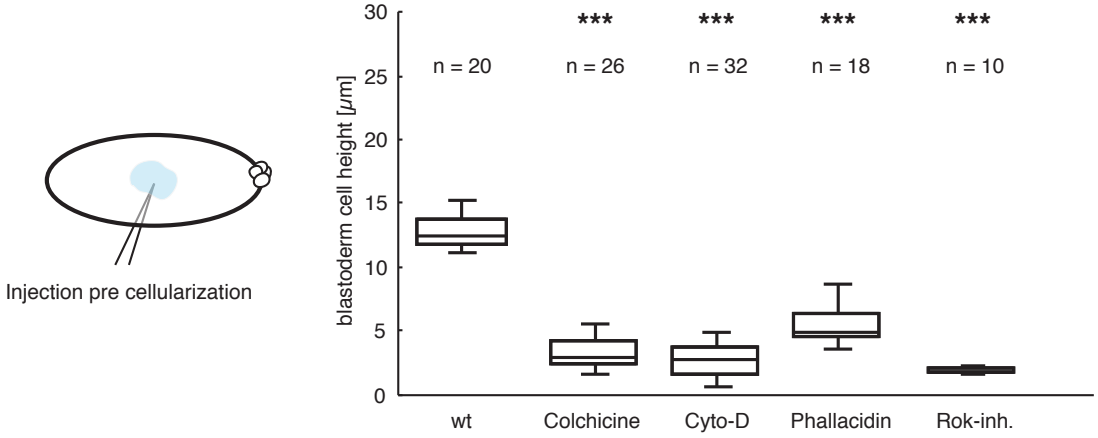

Figure 2.6: **Syncytial blastoderm formation in *Chironomus* depends on F-actin, microtubules and myosin.**
Blocking microtubules (Colchicine), actin (Cytochalsin D, Phallacidin) or myosin (Rok-inhibitor) before onset of cellularization impairs blastoderm formation in the *Chironomus* embryo. P-values calculated with t-test (*** <0.0001).

before cellularization. In addition to drugs targeting microtubules (Colchicine) and F-actin (Cytochalasin D, Phallacidin) directly [Harris and Peifer, 2005; Planques et al., 1991], I used H1152 as inhibitor of the Rho-associated protein kinase ROK, which activates non-muscle myosin-II and modulates F-actin binding of various proteins [Munjal et al., 2015]. Before the onset of cellularization, any interference with microtubules assembly, F-actin stability, and ROK activity prevented blastoderm formation (**Figure 2.6**). These results correspond to previous findings in *Drosophila* and likely reflect critical functionality of the cytoskeleton in the embryonic syncytium [Crawford et al., 1998; Planques et al., 1991; Xue and Sokac, 2016].

Taken together these results indicate early development of meroblastic cleavages to be similar in their cytoskeletal organization in flies forming small cuboidal or tall columnar cells.

2.4 Transforming a syncytial into a cellular blastoderm in *Chironomus*

2.4.1 Cellularization in *Chironomus* is a single-phase process that takes 120 minutes

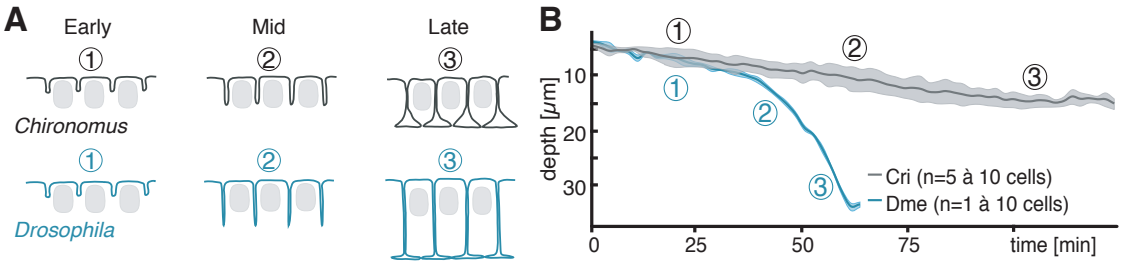

Figure 2.7: Cellularization of the *Chironomus* blastoderm follows a linear time course
A, Sketches and **B**, measured progression of blastoderm formation in *Chironomus*; the dynamics from a *Drosophila* embryo illustrate previously described dynamics [Xue et al., 2016].

At onset of cycle 13 when nuclei sit at the periphery, blastoderm formed by the process of cellularization, which I characterized as a linear invagination of plasma membrane lasting for 120 minutes with a speed of 0.1 +/- 0.02 µm/min in between nuclei that resided underneath a cortical actin pool. This process appeared to be very different from that in *Drosophila* where blastoderm cells form by a multi-phased membrane ingression lasting for 60 minutes with an average speed of 0.5 +/- 0.02 µm/min (**Figure 2.7 B**).

These results suggest fundamental differences in the molecular processes underlying short and tall blastoderm formation, as opposed to being simply a matter of time, where an abbreviated cellularization process would result in short cells, while an extended process would result in tall cells.

2.4.2 Cytoskeletal dynamics during *Chironomus* cellularization

To address which molecules could contribute to cytoskeletal scaffolding in the *Chironomus* blastoderm cell formation, I compared F-actin, myosin-II and microtubules between the two blastoderms types. Cytoplasmic intermediate filaments are considered absent from most insects and were thus not considered [Mencarelli et al., 2011]. In the cuboidal blastoderm, microtubules were organized in an inverted basket, and F-actin was enriched in a cortical domain (**Figure 2.8 A-E"**), similar to previous findings for the columnar blastoderm in *Drosophila* [Lecuit and Wieschaus 2000; Figard et al., 2013]. Myosin appeared to not be localized to the membrane, but remained in the cytoplasm over the whole course of cellularization (**Figure 2.8 F-F"**).

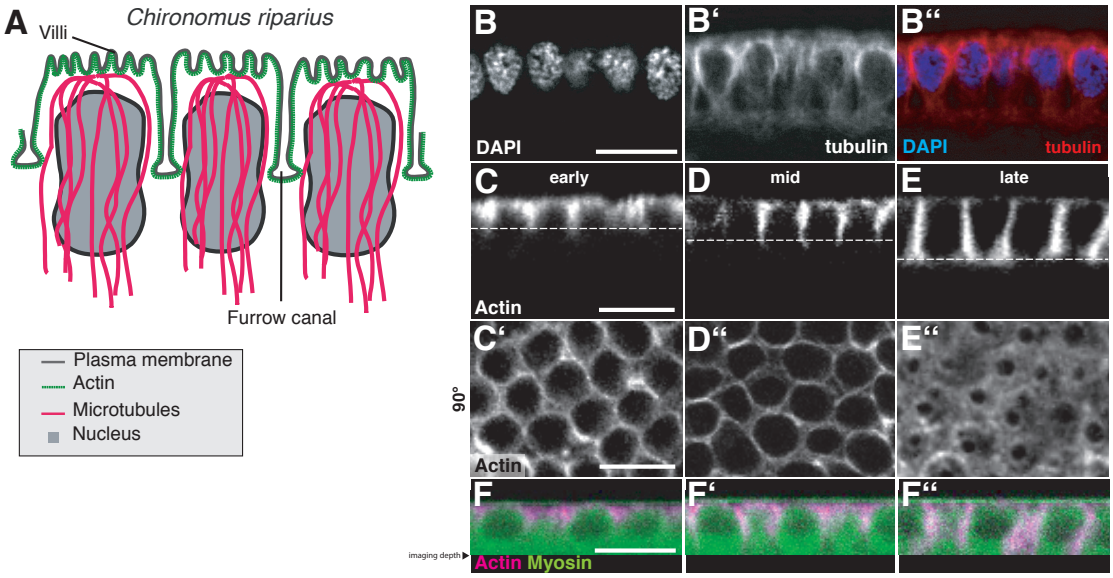

Figure 2.8: Cellularization in *Chironomus* is characterized by an inverted basked of microtubules and a basally extending front of F-actin.
A, Sketch illustrating cytoskeletal organization in the process of cellularization in *Chironomus*. **B-B“** Doble stainings of DAPI (nuclei) (B and B”) and anti-tubulin staining (microtubules) (B and B”) showing microtubules organized as inverted baskets and elongated inside the embryo. **C-E”** Shown is the F-actin organization over the course of cellularization where early corresponds to 0-5 µm membrane depth, mid 5-10 µm and late 10-13 µm in fixed samples. Corresponding stages are shown in a cross-section (C-D) and respectively in an en face view from the basal actin organization (shown plane is indicated by a dotted line) (C’-E’). **F-F”**, Myosin staining over the course of cellularization visualized by injection of myosin-GFP and followed live over time together with an F-actin staining visualized by an injection of Lifeact-mCherry. Scale bars 10 µm.

2.4.3 Actin is the key structural element in *Chironomus* cellularization

To address how F- actin myosin-II and microtubules function during the process of cellualrization I took advantage of the same small compound inhibitors as used before (**Figure 2.6**) i.e., microtubules (Colchicine) and F-actin (Cytochalasin D and Phallacidin) and myosin-II (H1152 as inhibitor of the Rho- associated protein kinase ROK [Crawford et al., 1998]).

When drugs were applied after the onset of cellularization, I found only injection of Cytochalasin D, an F-actin depolymerization drug could prevent cellularization itself (**Figure 2.9**). To confirm actin as an essential molecule I used Phallacidin, an F-actin stabilizing drug as another method to interference and found cellularization impaired

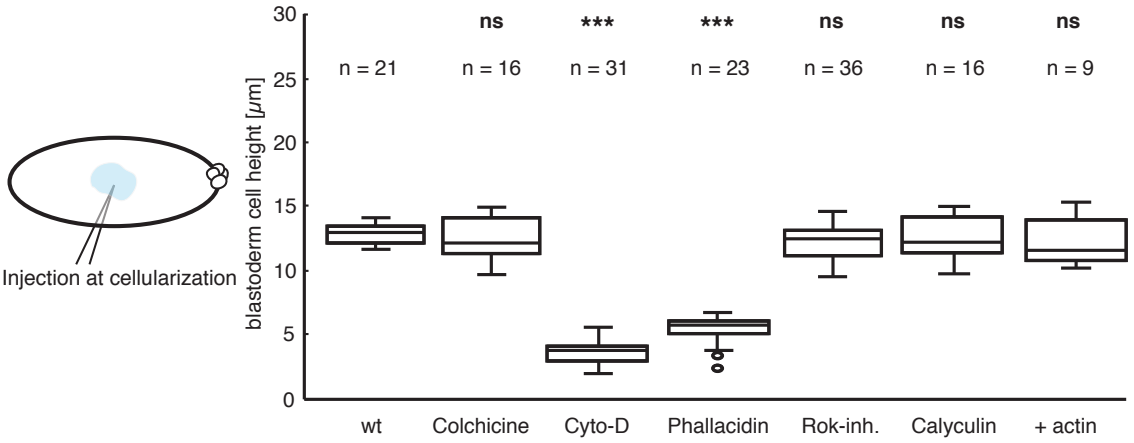

Figure 2.9: **Cellularization in *Chironomus* depends on F-actin but is independent of microtubules and myosin.**
Blocking actin (Cytochalsin D, Phallacidin) after onset of cellularization impairs blastoderm formation in the *Chironomus* embryo. Blocking microtubules (Colchicine), myosin (Rok-inhibitor) or over activate myosin (Calyculin alpha) has no effect on blastoderm formation. P-values calculated with t-test (*** <0.0001; ns >0.05).

(**Figure 2.9**).

Notably, and in contrast to columnar blastoderm formation in *Drosophila* [Crawford et al., 1998; Xue and Sokac, 2016], I found cuboidal blastoderm formation unaffected by inhibiting Rho kinase activity. To test whether simple over-activation of myosin-II would be sufficient for cell elongation Calyculin was injected into the developing embryo (performed by Atalay Tok), which is a serine/threonine phosphatase inhibitor that acts on myosin phosphatase and leads to increased myosin at the cortex [Fernandez-Gonzales et al., 2009; Ishihara et al., 1989]. The increased myosin-II activity did not affect cell height (12.48 µm +/- 1.69 µm) suggesting ROK-regulated processes provide a limited, if any, contribution to cuboidal blastoderm formation. To sum up, cellularization in *Chironomus* appeared to rely predominantly on F-actin as the key structural element; the observed differences in the sensitivity to ROK inhibition furthermore suggest that the capacity for F-actin modulation differs between cuboidal and columnar blastoderm formation.

To test whether simple enrichment of basal F-actin levels could be sufficient for blastoderm cell elongation, I artificially increased basal F-actin through injection of actin monomers. This increased overall actin levels but did not affect cell height (12.78 +/- 1.84 µm) (**Figure 2.9**), suggesting a difference on the molecular regulation.

2.4.4 F-actin dynamics at *Chironomus* cellularization

To understand how modulations of F-actin could contribute to the final shape of the epithelium, I asked where F-actin was present during the process of cellularization. I used Lifeact-mCherry as a reporter and monitored the dynamic distribution of F-actin during cuboidal blastoderm formation. I could observe cortical F-actin continuously expanded along the apical-to-basal cell membrane. The double staining of membrane and F-actin revealed that the membrane was ingressing in front, followed by F-actin (**Figure 2.10 A-B**). Only when cells started closing up at their basal site actin cought up and po-

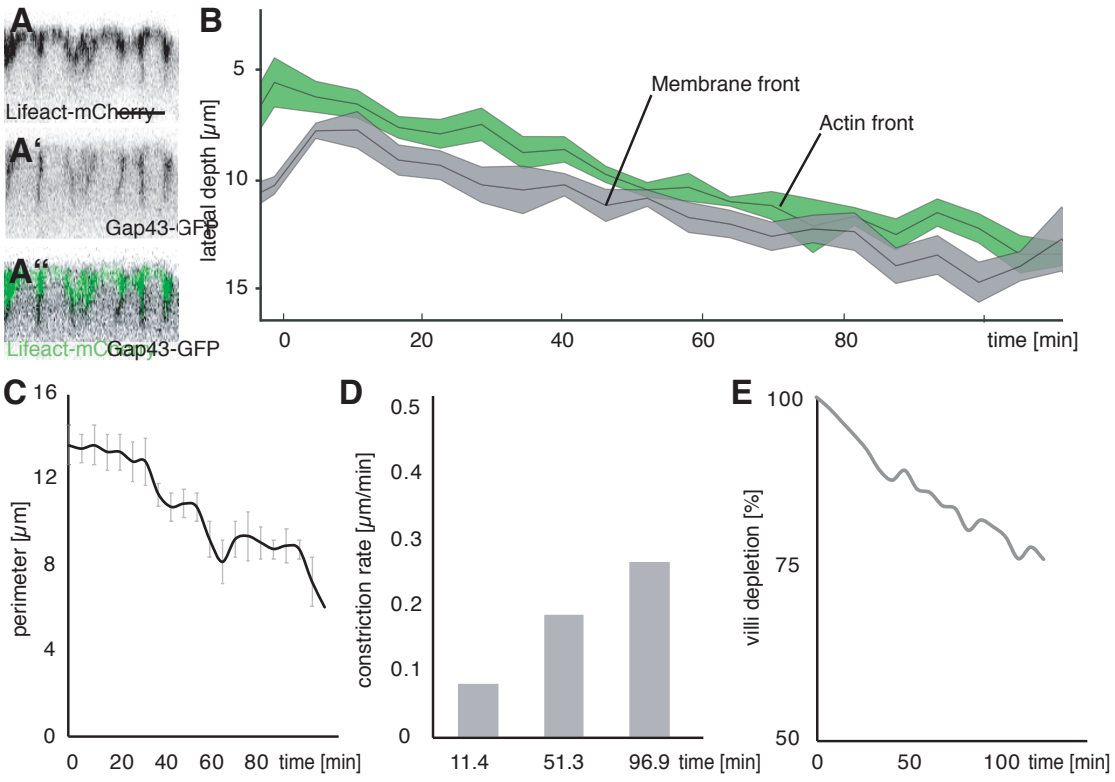

Figure 2.10: **Cellularization in *Chironomus* coincides with active F-actin remodeling at the cell cortex.**
A-B, Membrane invaginates in front of actin revealed by a live double staining of F-actin (Lifeact-mCherry) and membrane (Gap43-mCherry) shown is one representative timepoint (A-A"). Cellularization progression is shown in a plot following the basal tip of either actin or membrane. **C**, Graph shows the average perimeter of 5 cells over time. **D**, Reduction in perimeter measured as constriction rate within the last 5 minutes of cellularization (timepoints of measurement indicated on x-axis). **E**, Indicates the average depletion of villi (n=5) showing a leftover of apical villi when cellularization is completed. Scale bar is 10 µm.

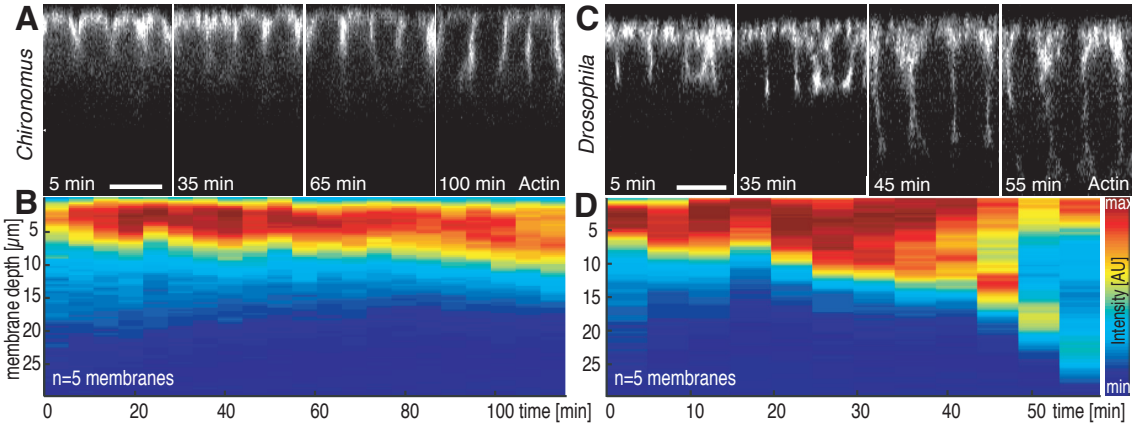

Figure 2.11: **During blastoderm formation F-actin dynamics in *Chironomus* differ from actin dynamics in *Drosophila*.**
A-D, Actin dynamics during blastoderm formation in *Chironomus* (A,B) and *Drosophila* (C,D) visualized by the F-actin reporter Lifeact-mCherry. Heatmap kymographs illustrate basolateral distribution of F-actin during blastoderm formation in *Chironomus* (B) and *Drosophila* (D).

tentially helped closing cells by actively decreasing the perimeter of the "cellularization ring". To follow the ring establishment in the beginning (0-3 µm) and its closure (at about 12 µm) over time I analysed ring perimeter and closure rate using Lifeact-mCherry as a proxy. I found the ring perimeter to be constant between 12 and 14 µm for approximately the first 40 minutes and then decreasing for 70 minutes showing ring closure with a closing rate up to about 0.3 µm/min (**Figure 2.10 C-D**). Over time the apical surface area (0-3 µm) (actin rich villi) decreased by about 1/3 while the lateral membrane surface area increased, suggesting a remaining membrane reservoir at the apical side (**Figure 2.10 E**).

2.4.5 Cellularization and F-actin dynamics differ between *Chironomus* and *Drosophila*

When comparing *Chironomus* cellularization dynamics to literature on *Drosophila*, *Chironomus* temporal and F-actin dynamics appeared to diverge during the process of cellularization. In order to confirm previous findings from *Drosophila*, I investigated the process of cellularization in *Drosophila* and briefly reviewed temporal and F-actin dynamics. The cellularization dynamics appeared as a bi-faced process with a first slow phase (about 0.1 µm/min) followed by a second fast phase (about 1 µm/min). Following cortical F-actin dynamics using Lifeact-mCherry. I found a non-continuous expansion

of F-actin, which gave rise to two domains of F-actin i.e., apical and basal (**Figure 2.11**). These results were consistent with data from the literature [Acharya et al., 2014; Wenzl et al., 2010; Lecuit and Wieschaus, 2002].

In conclusion, the most likely demonstrated difference between columnar and cuboidal blastoderm formation was the tight spatial and temporal F-actin regulation in *Drosophila*, which diverged from the dynamics in *Chironomus*.

2.5 The fly blastoderm as model to distinguish tissue architecture divergence

I found that *Drosophila* and *Chironomus* share a similar early development with similar molecules involved but the divergence in cell height in blastoderm stage as major difference. This gave me experimental access to use *Chironomus* as a test-tube-like system to address the mechanism of blastoderm columnarization.

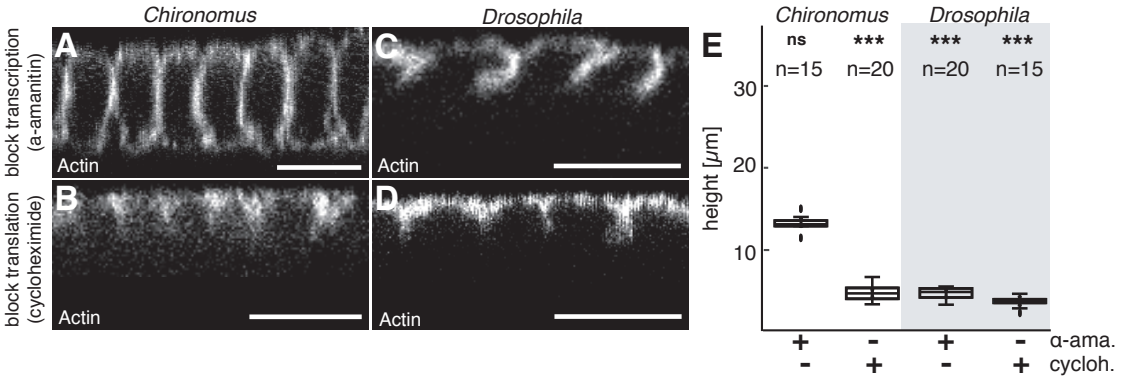

Figure 2.12: **Cellularization in *Chironomus* requires maternal transcripts.**
A-D, Blastoderm formation in *Chironomus* and *Drosophila* following inhibition of transcription with α-amanitin (α-ama., A,C) and translation with cycloheximide (cycloh. B,D). Blocking transcription (α-ama.) impairs blastoderm formation in *Drosophila* (***P<0.0001), not *Chironomus* (n.s. P=0.945); blocking translation (cycloh.) impairs both (Cri.cycl ***P<0.0001, Dme.cycl.***P<0.0001). P-values calculated with t-test, scale bars 10 µm.

2.5.1 *Chironomus* cellularization is driven maternally and lacks zygotic genes known for *Drosophila* cellularization

Because the F-actin dynamics in *Chironomus* and *Drosophila* blastoderm formation appeared to be different, I hypothesized that cell height differences were driven by timing and efficiency of their assembly. In *Drosophila*, cellularization has been associated with the activity of a small set of dedicated zygotically genes expressed throughout the embryo [Mazumdar and Mazumdar, 2002; Merrill et al., 1988; Schejter and Wieschaus, 1993; Zheng et al., 2013; Lecuit et al., 2002; He et al., 2016]. To narrow down the pool of potential candidates, I used drugs to specifically block transcription (alpha amanitin) and translation (Cycloheximide) after the last syncytial nuclear cycle.

I found that without translation, neither *Chironomus* nor *Drosophila* developed a blastoderm (**Figure 2.12 A,C,E**). Without transcription, *Drosophila* blastoderm formation failed, but the *Chironomus* blastoderm still formed (**Figure 2.12 B,D,E**). These results suggest that cuboidal and columnar blastoderm formation differ through the activity of at least one zygotic transcript or that the cellularization genes were provided maternally.

To test whether the transcripts were provided maternally, I aimed to identify their orthologues in *Chironomus* and determine their expression (in collaboration with Emre Caglayan and Steffen Lemke). Surprisingly, for most of the known *Drosophila* cellularization genes no orthologues could be indentified in *Chironomus*. To test whether these genes could have been lost specifically in *Chironomus* or were overlooked due to imperfect genome assembly, a systematical screen for the presence of known *Drosophila* cellularization genes in available dipteran genomes and selected additional insects was done. Mapping all identified orthologues onto a phylogenetic tree revealed a striking presence of cellularization genes throughout cyclorrhaphan flies, which have been previously described with stereotypical columnar blastoderm [Bullock et al., 2004]. By contrast, non-cyclorrhaphan insects consistently lacked clear orthologues (in collaboration with Emre Caglayan and Steffen Lemke) (**Figure 2.13**).

These results suggest that a previously mainly maternal driven process, found in non-Cyclorrhaphan flies, was shifted to a zygotic supported process.

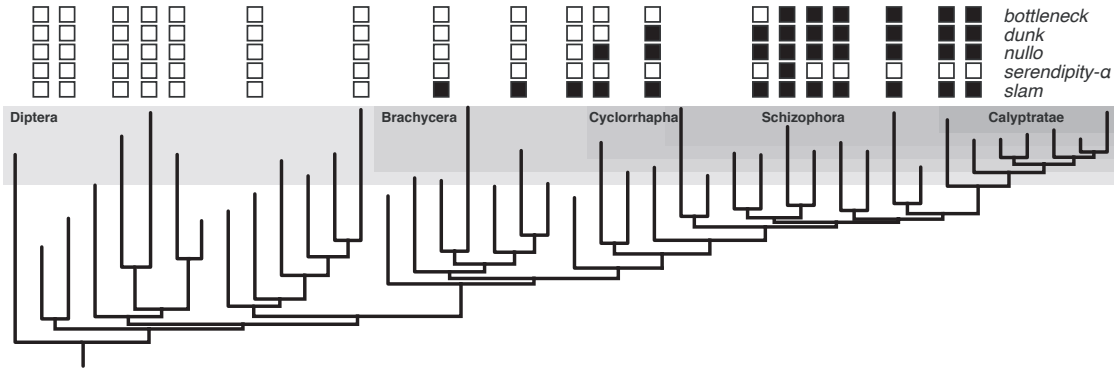

Figure 2.13: ***slam* is the first of several newly emerged cellularization genes.**
Initial genomic survey suggests *slam* to be the oldest known zygotic cellularization gene.
Shown are phylogeny of major fly families, with selected minor families added (asterisk; Chaoboridae, Bolitophilidae, Rhinophoridae) [Wiegmann et al., 2011]. Emergence of individual novel cellularization genes are indicated with filled boxes. Genomic analysis for 131 fly species was done in collaboration with Steffen Lemke and Emre Caglayan [Caglayan Master Thesis, 2018].

2.6 The origin of a novel developmental program

From the screen I selected three candidates to test them functionally. The most prominent gene was a gene called *slam*. *slam* in *Drosophila* is described to be the main organizator of cellularization and its KO results in a lethal phenotype with no blastoderm forming. It also appeared to be the first novel cellularization gene. This suggested *slam* to be most prominent conditate gene for cell coumnarization. To verify that it is the oldest of all cygotic genes a survey of all available fly genomes was conducted and mapped on the phylogenetic tree (in collaboration with Emre Caglayan and Steffen Lemke) showing *slam* emerged about 190 MYA (**Figure 2.14**). *dunk* as second candidate is described to act together with *slam* to recruit myosin to the invagination front. The third candidate was *bottleneck*, which is a scaffolding protein needed to physically link the actomyosin contractile unit in *Drosophila* [Schejter and Wieschaus, 1993; Theurkauf, 1994]. I hypothesize that the process of cellularization was shifted to a zygotic supported process by a stepwise addition of these and maybe other (novel) factors in Cyclorrhaphan flies.

To test for this stepwise addition of genes, I aimed to introduce them into the developing context of *Chironomus* to test for differences during the process of cellulariza-

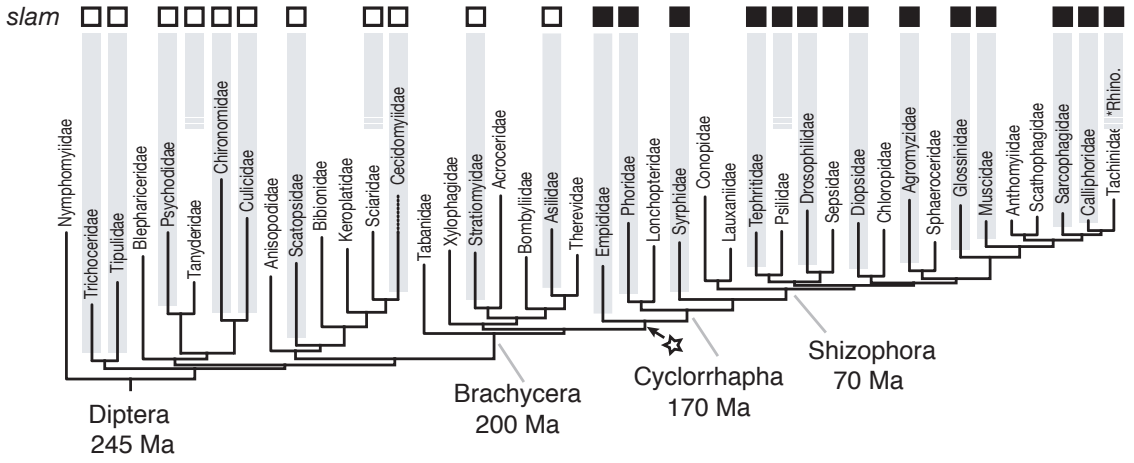

Figure 2.14: **Exhaustive comparative genomics in 172 fly species points to the emergence of *slam* about 190 MYA.**
Genomic survey suggests *slam* emerged about 190 MYA and can be found in Empididae and Cyclorrhaphan flies. Shown is the phylogeny of major fly families, with selected minor families added (asterisk; Chaoboridae, Bolitophilidae, Rhinophoridae) [Wiegmann et al., 2011]. Families with sequenced genomes in individual species indicated (grey bar). Indicated counts of high-quality genomes (light), genomes with identified *slam* ortholog (bold), character state of *slam* in individual families (open if absent, filled if present), and *slam* emergence (star). Genomic analysis was done in collaboration with Steffen Lemke and Emre Caglayan [Caglayan Master Thesis, 2018].

tion. I started with *slam*, which appeared to be the oldest of the zygotic expressed genes. It also appeared to be the only one found in all fly species once it emerged. To test for the subsequent emerged genes, I aimed to introduce *dunk* and *bottleneck* alone and in a combination with *slam* into the developing context of *Chironomus*.

2.7 A novel developmental program I: the contribution of *slam*

2.7.1 *Slam* induces a *Drosophila*-like phenotype in *Chironomus* blastoderm formation

Based on the finding that *Chironomus* lacks *slam* raised the question of how cuboidal blastoderm formation in *Chironomus* would be affected by the presence of *slam* activity.

To address this question, I injected mRNA of *slam* into early *Chironomus* embryos

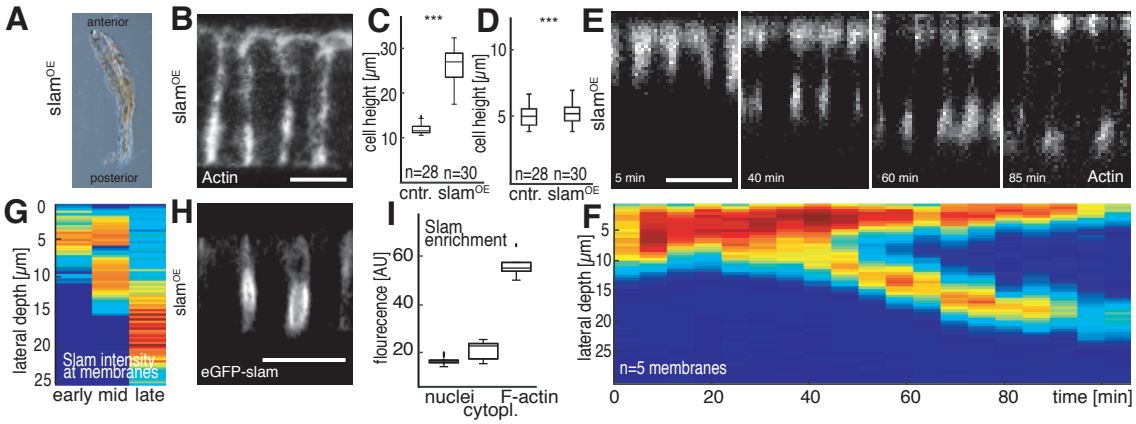

Figure 2.15: **Overexpressing *slam* in *Chironomus* transforms short-cell into tall-cell blastoderm.** **A-D**, Expression of *slam* in *Chironomus* embryos (slam^{OE}) results in viable embryos (A) and tall cells at blastoderm stage (B) with increased height (C; *** P<0.0001) and unchanged width (D; *** P<0.0001). **E-F,** F-actin in slam^{OE} embryos with linear cell extension (E) and basal F-actin (F). **G-I**, Slam-eGFP (G) colocalizes with F-actin (I) and is enriched at basolateral cell faces (H). P-values calculated with t-test, scale bars 10 µm.

(slam^{OE}embryos). I first asked whether embryos injected with *slam* have a similar survival rate as water injected embryos. I found slam^{OE}embryos developed with a similar survival rate as control injected embryos (88% control, 64% slam^{OE}embryos into larvae stage); the larvae appeared motile and showed a normal feeding behavior.

To test whether blastoderm cell architecture was affected, I over expressed *slam* and fixed the embryos at blastoderm stage to identify cell shape changes by staining for F-actin (Phallacidin). Strikingly, the blastoderm in slam^{OE}embryos had a total cell height of 28.15 +/- 4.7 µm (**Figure 2.15 B,C**), which was more than double the height of wildtype and close to the columnar blastoderm of *Drosophila* (**Figure 2.3 D**). Cells were not larger overall, but specifically increased in cell height; the width of cells remained unchanged at 5.1 +/- 0.8 µm (**Figure 2.15 D**). Together, these results indicate that the expression of *slam* was sufficient to initiate a *Drosophila*-like, columnar blastoderm architecture in *Chironomus*.

2.7.2 *Slam* reorganizes F-actin during the process of cellularization

To address whether F-actin reorganization during blastoderm formation in *Chironomus* slam^{OE}embryos was altered and comparable to *Drosophila*, I analyzed the F-actin dynamics of slam^{OE}embryos. Remarkably, columnarization of the *Chironomus* blastoderm coincided with a *Drosophila*-like appearance of a basal F-actin pool. I observed the establishment of two, non-continuous apical and basal domains of F-actin (**Figure 2.15 F**). To establish whether these F-actin dynamics in *Chironomus* were similar to a basolateral enrichment of Slam protein, I injected mRNA encoding an eGFP-fusion as a reporter and asked where Slam protein was localized within the cell. I found eGFP-Slam at lateral and basal positions at the cell outline (revealed by F-actin) (**Figure 2.15 G-I**). The localization of Slam was very similar to the protein localization observed in in *Drosophila* (Lecuit et al., 2002) This suggest that injected *slam* in *Chironomus* embryos functions as in *Drosophila*.

2.7.3 Redistribution of actin polymerization sites in the presence of *slam*

In *Drosophila*, basolateral F-actin enrichment requires local enrichment of the widely conserved F-actin polymerizing formin Diaphanous (Dia) [Afshar et al., 2000; Grosshans et al., 2005]. Here, Rho1 activity is required, which in *Drosophila* is recruited to the basolateral membranes by a direct interaction of RhoGEF2 with Slam [Wenzl et al., 2010]. I used the previously described GFP-Dia-N reporter [Rousso et al., 2013] to indicate sites of F-actin polymerization in *Chironomus* control and slam^{OE}embryos. In control embryos, I observed fluorescence in a single domain at and just below the apex of the cuboidal blastoderm (**Figure 2.16 A-C**). The localization of GFP-Dia-N in slam^{OE}embryos could be observed in two pools, i.e., at the apex and, separately, at lateral and basal membranes (**Figure 2.16 D-F**) similar to the localization of Slam (**Figure 2.15 G-H**). To test whether Dia activity was required for cellularization and columnar cell

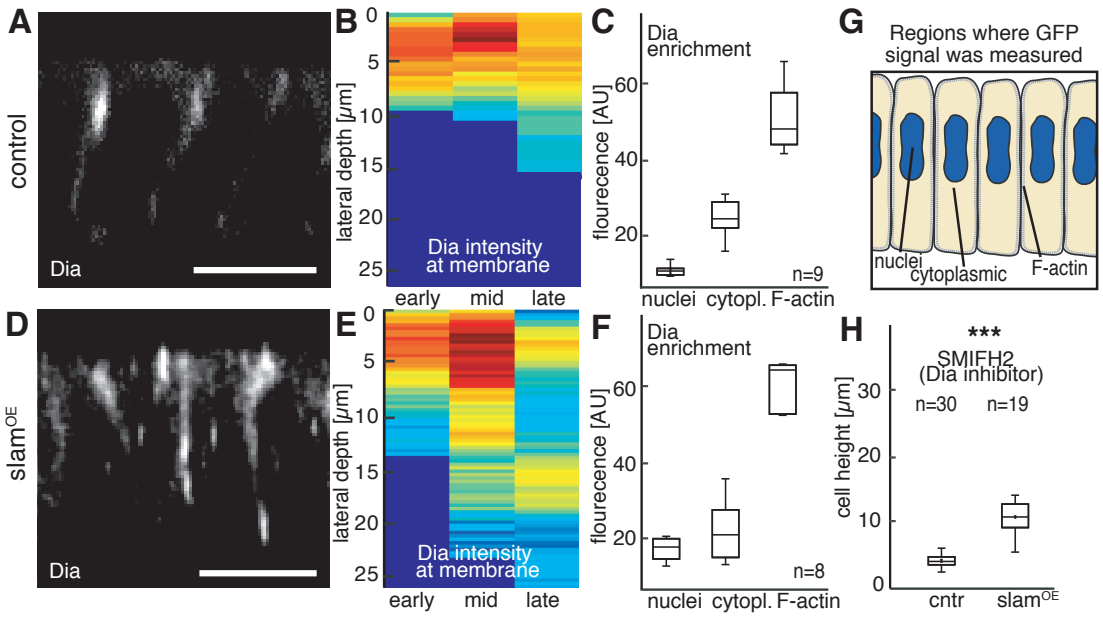

Figure 2.16: ***slam* expression results in basolateral enrichment of Diaphanous.**
A-C, Dia-eGFP (A) enriched in a narrow subapical band (B) in colocalization with F-actin (C,G). **D-G**, In slam^{OE} embryos, Dia localizes to subapical and basolateral domains (D) and two separate pools over time (E) in colocalization with F-actin (F,G). **H**, Inhibition of Dia activity by injection of SMIFH2 attenuates cell height, which is partially rescued in slam^{OE} embryos (***P<0.0001). P-values calculated with t-test, scale bars 10 µm.

formation, I used a small compound inhibitor of formin activity (SMIFH2) [Rizvi et al., 2009], which allowed me to inhibit Dia activity at or briefly after the onset of blastoderm formation. Consistent with a role in basolateral F-actin polymerization, cell height was reduced to about wild type in SMIFH2-treated slam^{OE}embryos (**Figure 2.16 H**). Taken together, these results suggest that expression of *slam* enables a locally restricted F-actin polymerization at a basolateral site promoted by Diaphanous.

2.7.4 *Slam* does not induce a globally contracting basal F-actin web in *Chironomus*

To address how the formation of a distinct pool of F-actin polymerization could contribute to tissue columnarization, I considered the possibility that the basal F-actin pool generated a supracellular and globally contractile actin web. In such a web, the sum of basal blastoderm cell constriction amounts to global cortical constriction of the yolk cell, with a resulting force that not only condenses yolk content but also collectively

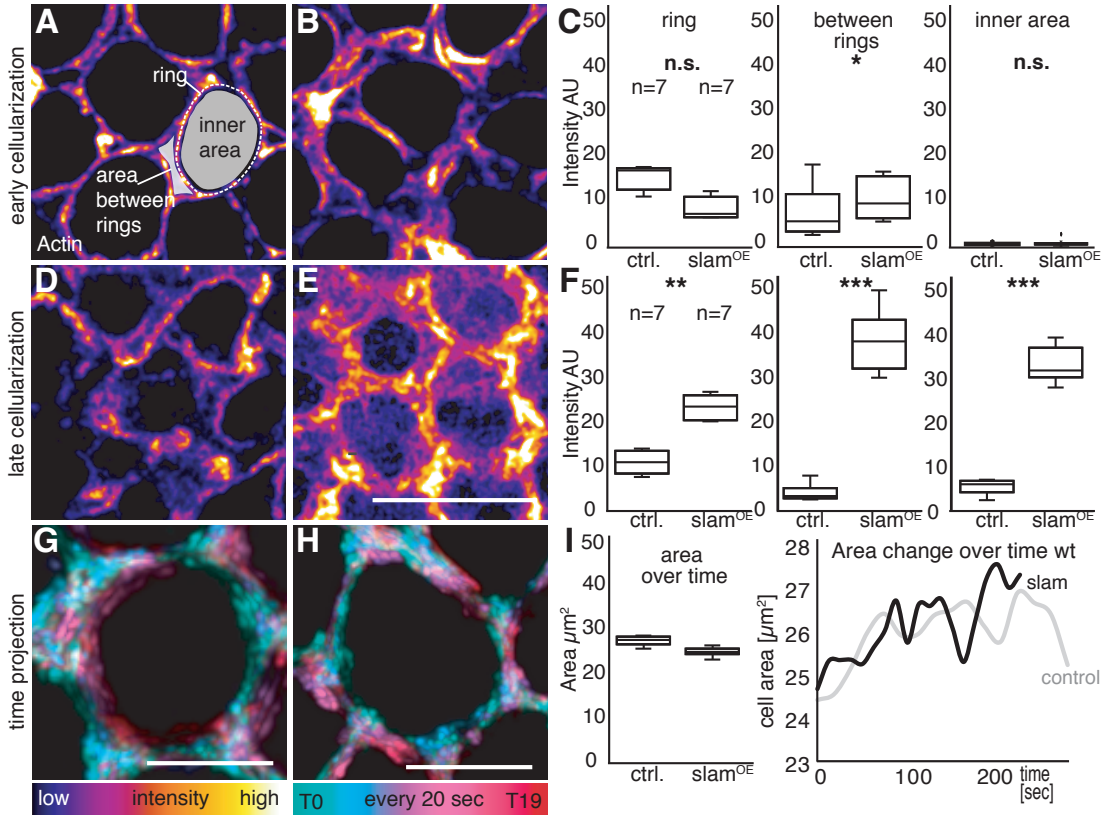

Figure 2.17: ***slam* expression does not effect contractility in basal actin web.**
A-B,D-E, Average projections of basal F-actin (Lifeact-mCherry) in high resolution for control (A,D) and slam^{OE}embryo (B,E). **C,F**, F-ctin intensity measurements for three regions at the basal site: I) ring, II) between rings and III) inner area for control and slam^{OE}embryo. (G,H) Cell area change over time in the basal area and area change over time plotted (I). Scale bar 10 µm (A-E) and 5 µm (G,H). P-values calculated with t-test.

pulls the attached bases of each blastoderm cell further towards the centre of the embryo [Schejter and Wieschaus, 1993]. To address whether *slam* could promote the generation of a supracellular actin web, I distinguished between a shape-scaffolding F-actin pool and a putatively web-supporting pool between and beneath cells (**Figure 2.17 A-C**). I asked how relative F-actin levels in each pool were increased in *slam* expressing cells and found a significant increase in web-supporting F-actin levels, supporting the idea of a *slam*-induced supracellular F-actin web (**Figure 2.17 D-F**). To address whether this basal actin web was contractile, I monitored changes in basal area of individual cells and supracellular clusters (**Figure 2.17 G-I**). I found cells to be similarly contractile in wt and slam^{OE}embryos with the difference that slam^{OE}embryos showed a reduction in perimeter only at the ring closure suggesting that basal cell tapering was reduced in these cells which coincides with an overall tighter basal coupling (**Figure 2.3 G**).

2.7.5 Ecad organizes a zipper at lateral membranes

The overexpression of *slam* in *Chironomus* resulted in the establishment of a second actin pool promoted by Dia accumulation, indicating a comparable function of *slam* in *Chironomus.* However the basal mesh contractility remained unchanged between control and slam^{OE}embryos. It remained unclear by which mechanism an overexpression of *slam* is linked to global cell elongation.

One possible scenario for cell elongation comes from planar cell-cell dynamics, where Dia (via cortical F-actin) was described to actively reshape epithelia through establishing patches of E-cadherin [Levayer et al., 2011; Cavey et al., 2008].

In cellularization, apical-to-basal extending F-actin/E-cadherin patches along adjacent lateral cell membranes could possibly "zip" cells together which might be similar to planar adhesion zippers in cell culture [Vasiouhin et al., 2012]. The expansion of lateral cell-cell contacts, could then result in taller cells during cellualrization.

Furthermore, tighter cell-cell coupling at the inside of a forming epithelium has been previously associated with the increase of cell adhesion, which is typically based on spot-like adherens junctions made from cytoskeletal F-actin support and homophilic adhesion molecules such as E-cadherin [Cavey et al., 2008].

To test the prediction of a lateral zipper, I first asked whether cell-cell contacts were increased by Slam activity by comparing cell tapering in wildtype and slam^{OE}embryos. (**Figure 2.18 A-B**) I found an increase of basolateral cell-cell adhesion and cell tapering at the basal site significantly reduced in slam^{OE}embryos compared to the control (**Figure 2.18 B**). To test whether the columnar shape of the cells in slam^{OE}embryos coincided with an increased lateral cell-cell adhesion in slam^{OE}embryos, I used a *Drosophila* E-cadherin-GFP reporter to visualize and quantify adherens junctions (AJs). In control embryos injected only with E-cadherin-GFP reporter, AJs were found mostly just below the apex in a subapical domain (0-5 µm below the apex displays 88.7 +/- 3.5% of all GFP signal, **Figure 2.18 C,D**). In slam^{OE}embryos, I found AJs still enriched subapically (49.6% +/- 3.7%), but also distributed along the the lateral cell membrane from apical to basal(50.4% +/- 3.6%, **Figure 2.18 G,H**). These results suggest the existence of a zippping mechanism

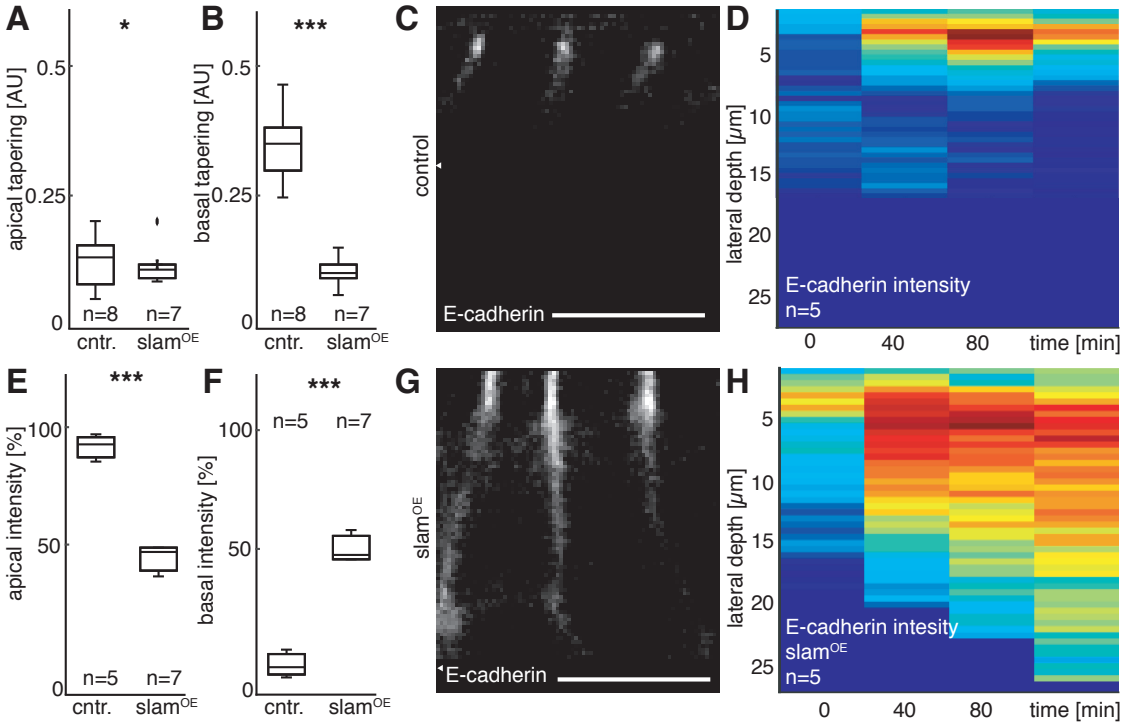

Figure 2.18: **E-cadherin based adhesion progresses along the basolaterl membrane in slam^{OE} embryos.**
A-B, Lateral cell-cell contact increased in slam^{OE} embryos; apical (A; * P=0.0401) and basal taper (B; *** P<0.0001) is reduced. **C-D**, E-cad-eGFP (C) enriched in narrow subapical domain throughout blastoderm formation (D). **E-H**, Relative E-cad in slam^{OE} embryos reduced apical (E) and increase basolateral (F) as reporter (G) distributes over the full basolateral range (H). P-values calculated with t-test, scale bars 10 µm.

at the lateral membranes. It is possible that the continuous generation of lateral F-actin/E-cadherin patches drives cell elongation to a columnar shape.

To understand whether lateral cell adhesion is driving cell elongation, I tested the function of E-cadherin during cellularization in slam^{OE}embryos. I found E-cad was needed before onset of cellularization and a knockdown during syncytial cleavages had a lethal phenotype (**Figure 2.19 A**). To overcome the requirement during early stages of development I locally knocked down *Chironomus* E-cadherin (Cri-E-cad RNAilocal) by timing injection shortly before onset of cellularization, which established a central domain of an incomplete cellularization and a flanking domain with complete cellularization and the formation of complete cells. When I performed the local KD in slam^{OE}-embryos, I observed a blastoderm of 12.64 +/- 3.59 µm in the central domain, compared to 19.34 +/- 3.37 µm in the flanking domain (**Figure 2.19 C,E**). The inverse experiment in which E-cadherin was knocked down completely (early injection) in slam^{OE}embryos,

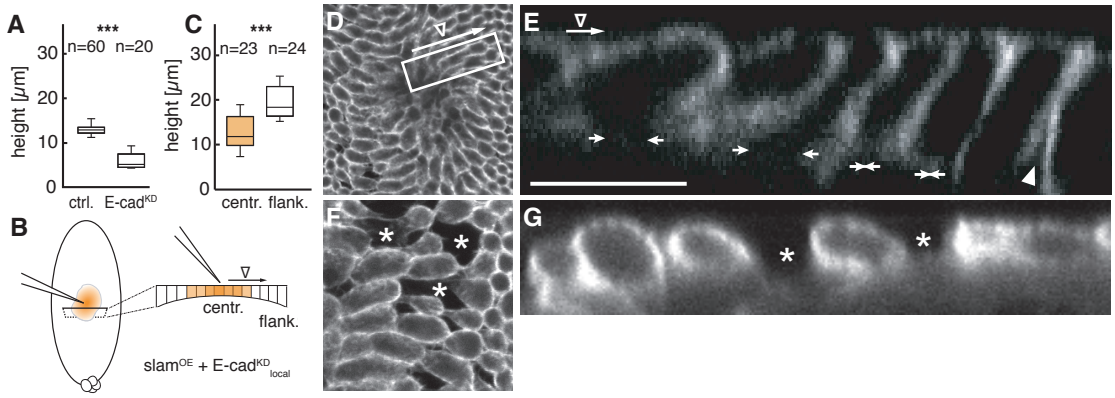

Figure 2.19: **E-cadherin is necessary for *slam* promoted cell elongation and blastoderm integrity.** Effect of E-cad knockdown on *Chironomus* blastoderm formation. **A**, In embryos injected with dsRNA against Cri-E-cad during nuclear migration stage, blastoderm formation stalls (*** P<0.0001). **B**, Sketch outlining the experimental approach to study the effect of local Cri-E-cad knockdown in slam^{OE} embryos. **C-D**, Blastoderm in a representative Cri-E-cadKDlocal slam^{OE} embryo at site of maximal E-cadKD effect, with typical signs of cell individualization (asterisks) within the blastoderm in areas of poor adhesion, shown as a maximum intensity projection en face (C) and in a xz-reslice (D). **E-G**, Graded response to local Cri-E-cad knockdown in slam^{OE} embryo shown en face (E) and in a xz-reslice of a selected window (F). The inferred activity gradient of Cri-E-cad knockdown is indicated with long arrow, short arrows indicate completion of blastoderm formation as cell base is open or closed. P-values calculated with t-test, scale bars 10 µm.

I introduced a local rescue through the injection of mRNA encoding *Drosophila* E-cadherin-GFP. The local rescue through *Drosophila* E-cadherin in Cri-E-cad RNAiglobal embryos resulted in a central domain where columnar cells formed, which could be identified by junctional GFP signal (**Figure 2.20 A-D**). Cells in the flanking region, however formed wt-like cuboidal cells (**Figure 2.20 D,F**), suggesting cellularization of individual cells is a cell autonomous process. In summary, these results suggest that columnar cell elongation is promoted by basolateral extension of F-actin/E-cadherin patches likely driven by *slam* localization. This suggests that *slam* could integrate seamlessly into an exciting developmental program by reorganizing pre-exciting proteins to change cell architecture dramatically.

2.7.6 *Slam* was integrated into blastoderm formation and became essential quickly

Experiments from *Drosophila* show that *slam* is essential for columnar cell formation and leads to a lethal phenotype when knocked down [Acharya et al., 2014; Wenzl

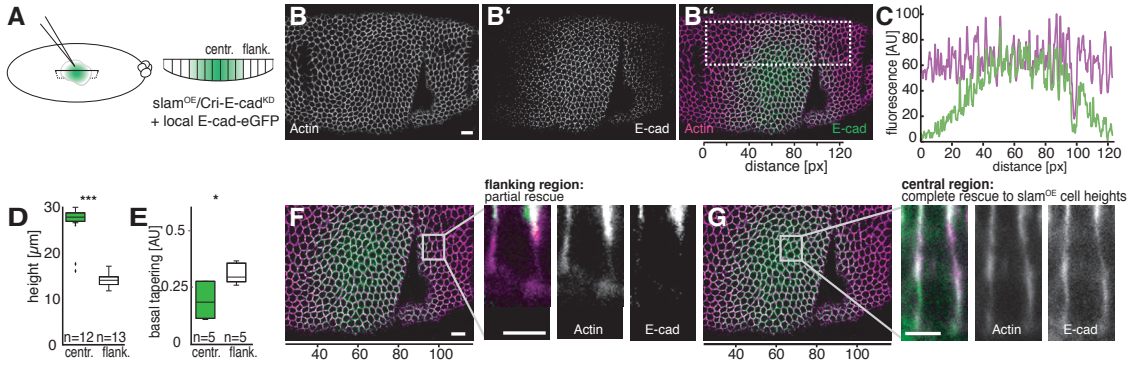

Figure 2.20: **A local source of E-cadherin is sufficient for the autonomous formation of columnar cells in slam^{OE} embryos.**
Local E-cad rescue of blastoderm formation in slam^{OE}/Cri-E-cad RNAi embryos. **A**, Sketch outlining the experimental approach to study the effect of local E-cad availability in slam^{OE}/Cri-E-cad RNAi embryos. **B-B"**, F-actin and E-cad levels visualized by fluorescent reporters (Lifeactin-mCherry and E-cad-eGFP). **C**, Quantification of fluorescent signal in subapical plane (3-5 µm) over the area shown in B". **D**, Distribution of F-actin and E-cad in a cell (shown in a xz-reslice) representative of the blastoderm flanking maximal E-cad levels seen in (C). **E**, Distribution of F-actin and E-cad in a cell representative of the blastoderm with maximal E-cad levels. P-values calculated with t-test, scale bars 10 µm.

et al., 2010; Lecuit et al., 2002]. It is be possible that in a more basal cyclorrhaphan fly, which is not yet as derived as *Drosophila*, a knock down would result in a cuboidal blastoderm. To understand when *slam* became essential to the process and whether I could induce a cuboidal blastoderm in a fly which usually forms a columnar one, I conducted a knock down experiment in a basal cyclorrhaphan fly i.e., the Phoridea fly *Megaselia abdita*, which appeared to be one of the first species to express *slam*. *Megaselia* shared a last common ancestor with *Drosophila* about 150 MYA. I found after cellularization was initiated, at about 10 µm membrane invagination, the process stalled and led to a lethal phenotype with no completion of cell formation. These results suggest that *slam* became essential to the cellularization process quickly after it emerged and likely replaced the more ancestral mechanism.

2.7.7 *Slam*-induced tall blastoderm cells slow down gastrulation

The putative benefits of a columnar tissue architecture still remained less clear. It could be speculated, that increased cell height and cell volume increased dramatically after overexpressing *slam*, this could be beneficial for subsequent gastrulation. During

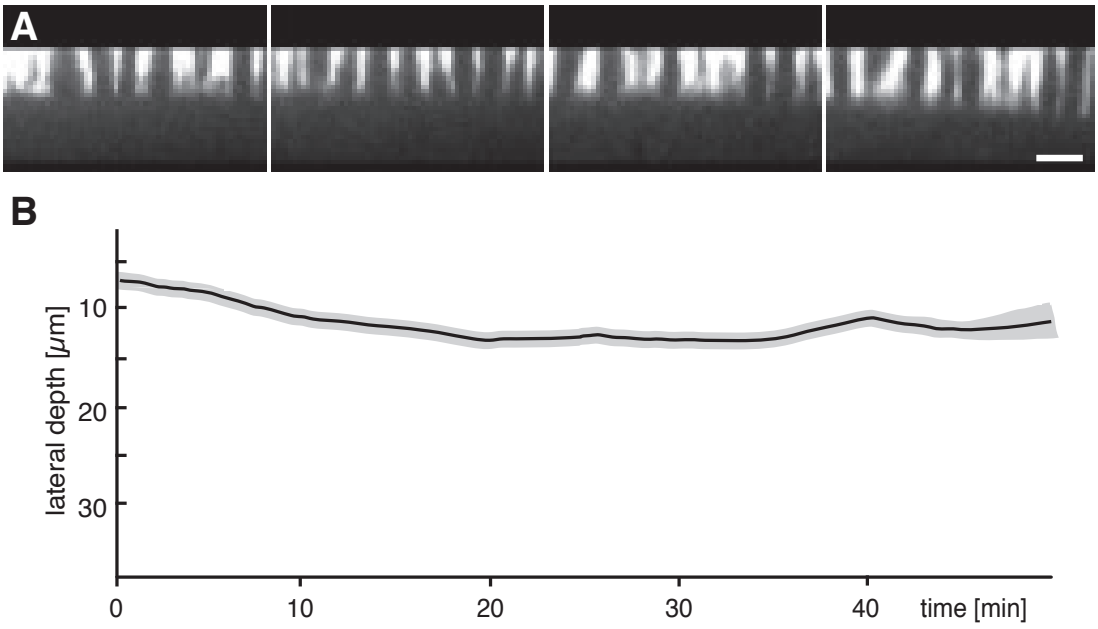

Figure 2.21: ***Mab-slam* is required for cellularization in *Megaselia*.**
A-B, Knock down of *Mab-slam* in *Megaselia abdita*, as representative of one of the earliest species expressing *slam*, showing no progression of lateral cell lengthening (A-B). (B) Plot shows basal tip of the actin front revealed by Lifeact-mCherry staining. Scale bar 5µm.

gastrulation cells change their shape dramatically and rearrange, which depends on a sufficient supply of membrane material. In *Chironomus* wt, remaining membrane is stored in apical villi in contrast to slam^{OE}embryos where membrane is found along lateral membranes. Potentially affecting cell rearrangements during gastrulation. To test whether columnar cells result in a faster germband elongation I compared germband elongation in wt to slam^{OE}embryos and found gastrulation movements to be significantly slower in slam^{OE}embryos. In addition, the germband extended to only 60% of egg length compared to 75% in wt (**Figure 2.22**). These results suggest that tall cells alone where not sufficient to speed up the process of germband elongation.

The organized rearrangement of cells depends on molecular regulation and subsequent reorganization of cytoskeletal elements and junctions. Important here is RhoGEF2, which is a protein involved in actin organization and contractility. RhoGEF2 acts in the GPCR signaling cascade and the GPCR secreted ligand Fog is involved in accumulation of RhoGEF2 to the apical cell membrane and thus promotes actomyosin constriction and T1 transitions important for germband elongation [Kolsch et al., 2007; Sawyer et al., 2010]. If RhoGEF2 was a limiting factor for cell rearrangements (T1 transitions) during

gastrulation in slam^{OE}embryos the slow-down in speed could be explained. To increase RhoGEF2 activation during gastrulation I took advantage of Fog to coordinate cell shape changes during gastrulation as previously shown by Urbansky et al., 2016 to be affective after overexpression in *Chironomus*. To test whether gastrulation in embryos with tall cells following overactivation of RhoGEF2 would increase speed I injected *slam* together with fog (slam^{OE}fog^{OE}embryos) and found speed again comparable to *Chironomus* wt and elongation to a similar length (72% egg length). Not only did the speed change but also the dynamics during the elongation; while in wt germband elongation was paused from 55 – 75 min after onset of GBE in slam^{OE}fog^{OE}embryos this plateau was not found suggesting a continuous elongation of the germband in presence of *fog* (**Figure 2.20**). The observed dynamics in these embryos mirrored the dynamics in *Drosophila*, where the elongation is also a continuous process. However, germband elongation in *Drosophila* proceeds twice as fast, indicating that gastrulation is a very orchestrated process in *Drosophila* and changing cell height in *Chironomus* alone is not sufficient to increase speed to a *Drosophila*-like phenotype.

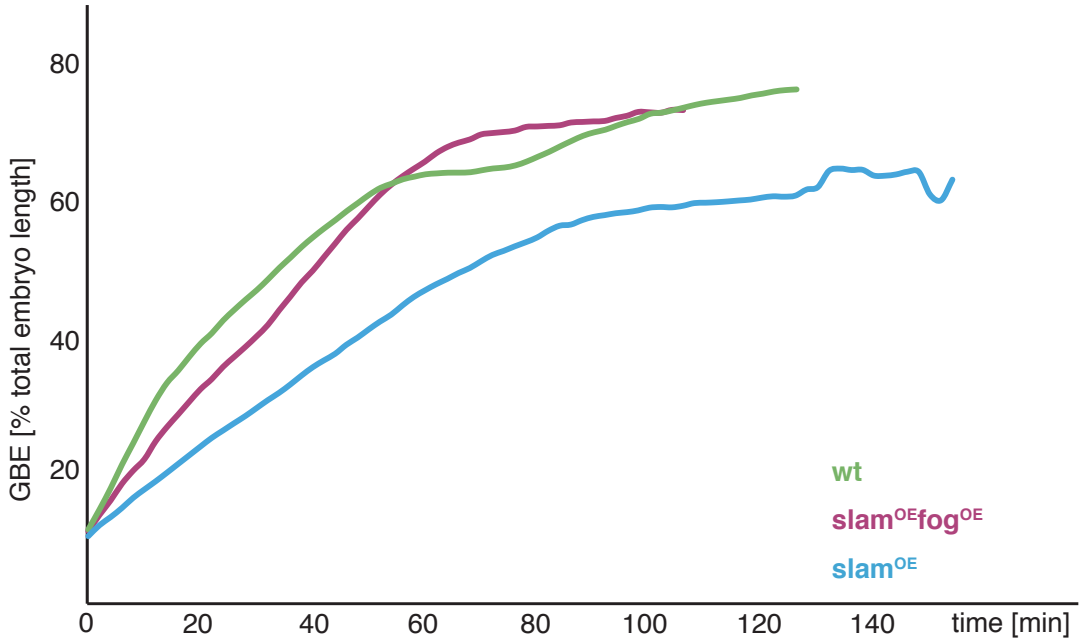

Figure 2.22: **Overexpression of *slam* slows down *Chironomus* gastrulation.**
Progression of gastrulation followed by germband elongation tracking in relation to total embryo length (100%). Graph shows the average position of the germband tip over time for wt (n=3), slam^{OE} (n= 10) or slam^{OE}fog^{OE} (n=12) embryos.

Taken together tall cells in *Chironomus* came at a price and were not immediately beneficial for the process of germband elongation. This raised the question whether tall cells were advantageous at blastoderm stage.

2.7.8 *Slam*-induced tall cells improve epithelial barrier function

To test whether tall cells were advantageous I hypothesized that tall cells could provide a protective environment to the outside by acting as a selective barrier. I tested the effectiveness of this barrier in *Chironomus*, by placing the embryos in a high salt solution and tested for shrinkage of the embryo, due to water efflux (**Figure 2.23**). When I placed unfertilized eggs that do not form a blastoderm and embryos with a blastoderm into the salt solution, then unfertilized eggs shrank substantially faster than embryos with a blastoderm (**Figure 2.23 A,D**), demonstrating how an epithelium reduces water exchange between yolk and outside. To address whether a columnar blastoderm in *Chironomus* embryos improved its function as an epithelial barrier, I compared rates of embryo shrinking in control and slam^{OE}embryos. Strikingly, I found a substantially reduced embryos shrinkage in slam^{OE}embryos. The rates of shrinkage were depending on salt concentration (**Figure 2.23 B-D**). These results suggest that water loss in the yolk was reduced in embryos with a columnar blastoderm and indicating that a columnar cytoarchitecture provides an increase in epithelial barrier function.

Taken together, the presented data identified a particularly simple and novel mechanism for the making of a tall epithelium: the accumulation of basal F-actin via a novel membrane anchor that re-localizes the F-actin assembly machinery, in addition to a lateral zipper promoted by E-cadherin, provided long term stability for an apical-to-basal progression of lateral cell-cell adhesion. The data provide evidence that the columnar epithelium functions as a protective barrier to reduce water permeability.

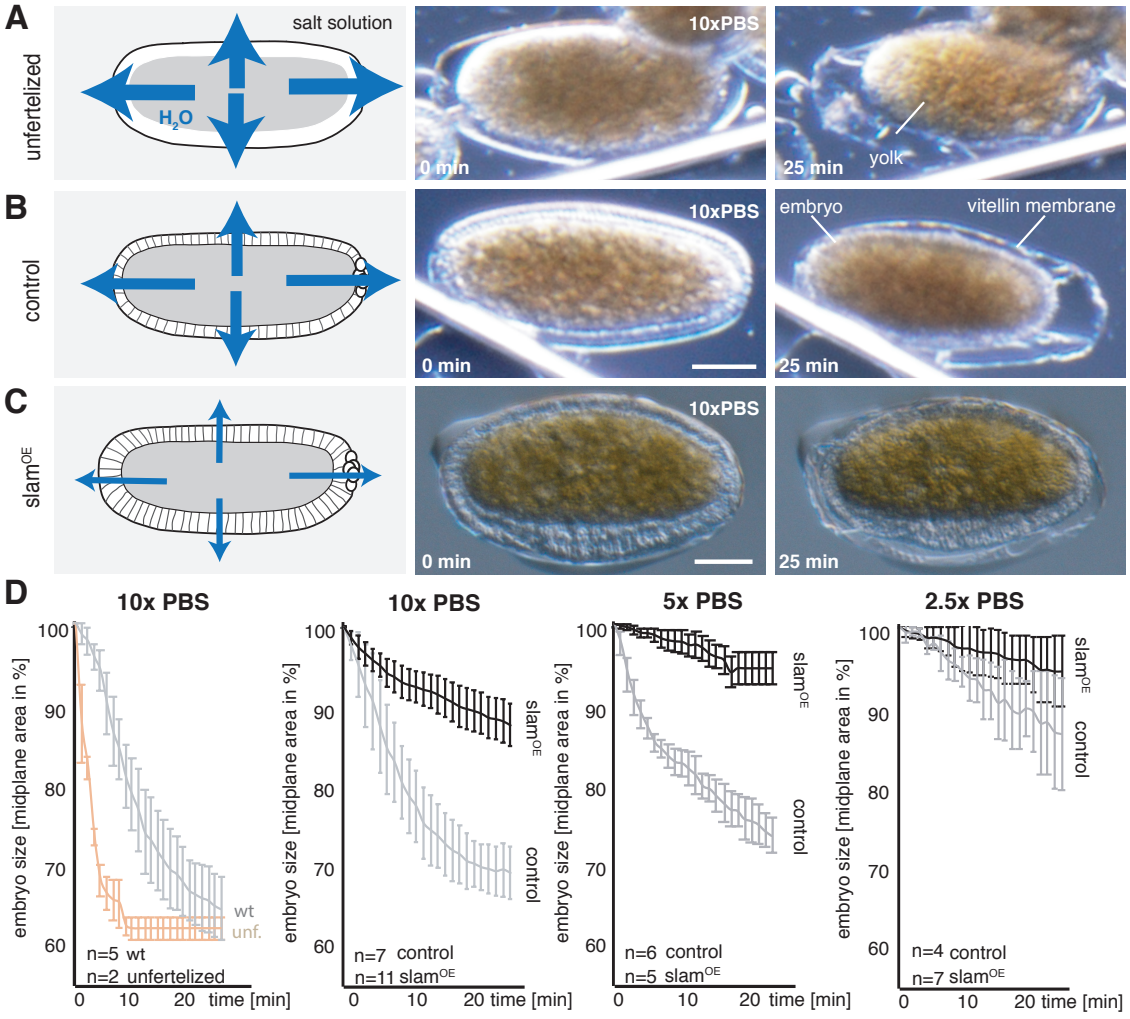

Figure 2.23: **Overexpression of *slam* provides blastoderm with protection against water loss.** **A-C**, *Chironomus* embryo deformation as response to inferred water loss in unfertilized egg cell without blastoderm (A), with a cuboidal (B) and a *slam*-induced columnar blastoderm (C). **D**, Embryo shrinkage is a function of salt concentration and cell height. Scale bars 50 µm.

2.7.9 *Slam* is the likely evolutionary founder and driver of columnar blastoderm formation

The findings that *slam* had the ability to jump on an existing mechanism and reshuffle the existing elements in a way to alter cell architecture completely made me wonder whether I find any evidence of how it evolved and whether there was any sequence similarity to another gene. From earlier studies in *Drosophila*, it is known that the structure of *slam* is intrinsically disordered and misses well-defined structural motifs [Wenzl et al. 2010; Acharya et al., 2014]. Therefore, I first aimed to find evidence of its emergence

by synteny analysis (This analysis was done in collaboration with Emre Caglayan and Steffen Lemke and the work can be found in E. Caglayan Master Thesis 2019 and biorxiv Noeske et al. 2021).

The search for sequence similarity to another gene showed no similarity could be found suggesting *slam* did not emerge by duplication. The synteny analysis showed that *slam* was localized within intron 4 of a conserved but uncharacterized gene CG42748, and *slam* appeared very close to the 3' end of the intron, except in the Drosophilidae. The same intron exon structure was also identified over the whole dipteran lineage and suggest that CG42748 was conserved. This enabled a direct comparison to identify any sequence similarity to *slam* in non-cyclorrhaphan flies. No putative conserved gene was found in that region, but an open reading frame (ORF) very similar to the conserved region of *slam* was discovered. Since the ORF was identified by synteny conservation it was named 'Synteny Uncharacterized ORF' (SURF).

To test whether SURF was involved in *Chironomus* cellularization and possibly was the ancestor of *slam* I performed a knock down by injecting SURF dsRNA in the developing *Chironomus* embryo and found cellularization not affected and cells at a similar height and cellularization speed as observed for *Chironomus* control embryos (**Figure 2.24 A-B**).

This suggest that SURF was not involved in cell formation in *Chironomus* and provided evidence that *slam* was a novel gene found in synteny with the ORF SURF.

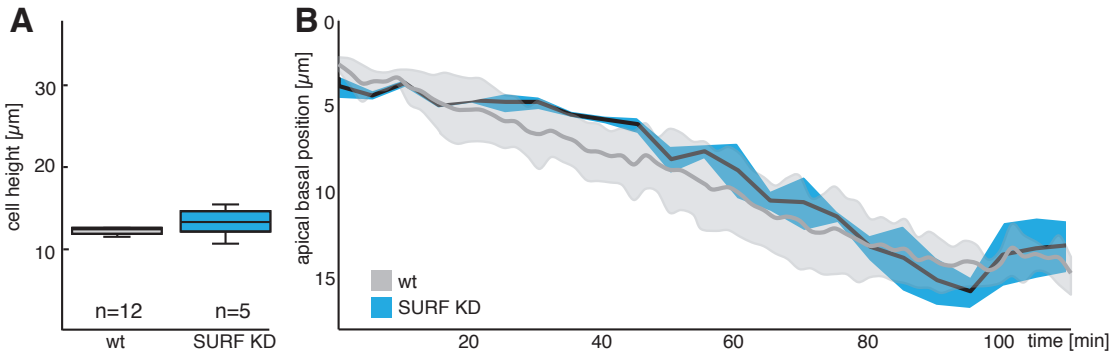

Figure 2.24: **Candidate for gene with *slam* like genomic localization in *Chironomus* is not required for cellularization**
A-B, Knock down of synteny uncharacterized ORF (SURF) has no effect on *Chironomus* cellularization; neither on cell height (A) nor cellularization progression (B).

2.8 A novel developmental program II: the contributions of *dunk* and *bottle-neck*

In the following two sections I aimed to get a lead for the stepwise addition of genes to the process of cellularization. Results from **Figure 2.13** indicated that new zygotic genes appeared after *slam* e.g., *dunk* and *bottleneck*. To test for their function in *Chironomus* I introduced them either alone or in combination with *slam* into the developing embryo and asked for a change in tissue architecture and the process of cellularization. The presented data are yet less complete as for *slam* and partly preliminary.

2.8.1 *Dunk* is supporting innovation towards robust columnar blastoderm formation

dunk in the context of *Drosophila* cellularization is described to be specifically required to maintain and stabilize myosin II at the cortex [He et al., 2016]. The *dunk* dependent stabilization of myosin recruitment sites enables the establishment of an interconnected actomyosin network at the invagination front that maintains tension and provides a mechanical mechanism important for cell elongation to form a complete blastoderm [He et al., 2016].

As indicated in **Figure 2.13** no clear orthologue of *dunk* in more basal fly groups (lower Diptera and basal Brachycera) could be identified suggesting *dunk* to be a novel gene evolved about 150 MYA (**Figure 2.13**). Synteny analysis of the *dunk* locus indicate it to be conserved throughout Cyclorrhapha and located upstream of *slam*. Since the search of ORFs in synteny with *dunk* could not resemble any protein in *Drosophila* or any ORF with the size larger than 100aa it is possible that *dunk* arose de novo (E. Caglayan Master Thesis, 2019).

I could show that the development in a lower Dipteran species i.e., *Chironomus* is characterized by a slow development and short cuboidal blastoderm cells as opposed to

fast development and tall columnar blastoderm cells of Cyclorrhapha i.e., *Drosophila*. This argues that *dunk* could also have played a role in the phenotypic differences.

To test whether the placing of *dunk* in the developing context of *Chironomus* also has an effect on cellularization in *Chironomus*, *Drosophila-dunk* mRNA was injected at pole cell stage.

Following the injection of *dunk* into *Chironomus* embryos, an increase in cell height was clearly visible in the raw images and changed the cell architecture significantly. While in mock injected *Chironomus* cells had a cell height of about 12 µm in average, this range of cell height shifted to 18-22 µm in average following the injection of *dunk* mRNA (**Figure 2.25**).

To test whether the combined ectopic expression of *slam* and *dunk* together had a stronger effect on cell height increase than either of the genes alone, mRNA of both genes were co-injected and cell height was analyzed (**Figure 2.25**). In two different embryos the median cell height had an average height of about 18 µm in average (sample size 2 embryos) (**Figure 2.25**). The analysis suggests that there is not a significant difference on cell height change when *slam* and *dunk* act together compared to a configuration where the genes act individually.

In summary, *Chironomus* dunk^{OE}embryos and dunk^{OE}slam^{OE}embryos showed a changed cell architecture where cell height increased significantly by the factor of 1.5.

2.8.2 *Bottleneck* is supporting innovation towards robust columnar blastoderm formation

Another zygotic expressed gene involved in *Drosophila* cellularization is *bottleneck* (bnk). The search for orthologues outside of *Drosophila* failed to identify any orthologue outside Shizophora. In the Shizophoran families were bnk orthologues could be identified it is found to be located in the first intron of a gene called mesh.

Bnk in *Drosophila* is described to be involved in slow phase of cellularization where it is important organizing actin filaments [Mazumdar and Mazumdar, 2002] and is proposed to physically link actomyosin units within the hexagonal array by providing a con-

nection of the contractile unit [Schejter and Wieschaus, 1993]. This generates an inward directed force that invaginates membranes [Xue and Sokac, 2016]. This phase, rich in tension, can be followed by shape changes at the invagination front (basal site) where high tension can be seen by cell boundaries that appear more straight round compared to less tensile phases in cellularization [Xue and Sokac, 2016] (**Figure 2.26**).

To follow these differences over the process of cellularization I analyzed actin-stained cells at different stages of cellularization. I measured the shape differences as circularity (C), where C = 1 for a circle and C < 1 for angular shapes (e.g., C = 0.6 for a triangle) [Xue and Sokac, 2016]. Circularity got lost in the transition from slow to fast phase in *Drosophila* which can be seen by a dramatic drop in circularity at a furrow depth of 6-8 µm (**Figure 2.26 A**) as previously described by Xue and Sokac, 2016, suggesting Bnk activity results in a tension rich phase and in a loss of circularity. Accordingly, I was conducting the same analysis for *Chironomus* mock injected embryos and no transition in phases could be observed suggesting membranes do not straighten as observed in *Drosophila* and remain circular over the whole course of cellularization.

Drosophila bottleneck (Dme-bnk) mRNA was injected in pole cell stage *Chironomus* embryos (in collaboration with Clara Baader (Lab-report Clara Baader)) in order to test whether the placement of *bnk* in *Chironomus* influenced forming more straight cell borders resulting in clear hexagons in cellularization. After ectopic expression of Dme-bnk prliminary data suggest cell borders to be straighter which can be seen a dropped of circularity at about 6-8 µm membrane invagination.

In addition to the straighter cell borders I observed cells to be taller in blastoderm stage after overexpressing *bnk* in *Chironomus* and cells appeared to be about 18-20 µm in height and equates 1.6-fold increase.

Taken together these results showed that *bnk* may arose *de novo* and altered the developmental program of *Chironomus* after its over expression and cell borders appeared straighter in the first phase of cellularization and cells elongate taller.

The preliminary data of *dunk* and *bottleneck* and the extensive study of *slam* give evidence that the previously maternal driven process got stepwise revised by the addition of zygotic genes. These results support the hypothesis that the addition of new genes rearranged the elements of the ancestral process to a more efficient process of cellularization.

2.9 The fly yolk sac – A model to study tissue-tissue interaction

2.9.1 The yolk sac is in direct contact with the extraembryonic tissue anlage

After cellularization is completed two adjacent structures form: 1) the one layered blastoderm epithelium which forms around the yolk and 2) the underlaying yolk sac enclosed by a single continues membrane (**Figure 2.27**). In consequence the blastoderm cells sit on top of the yolk sac membrane however it remains unclear whether this contact has any consequence in early development.

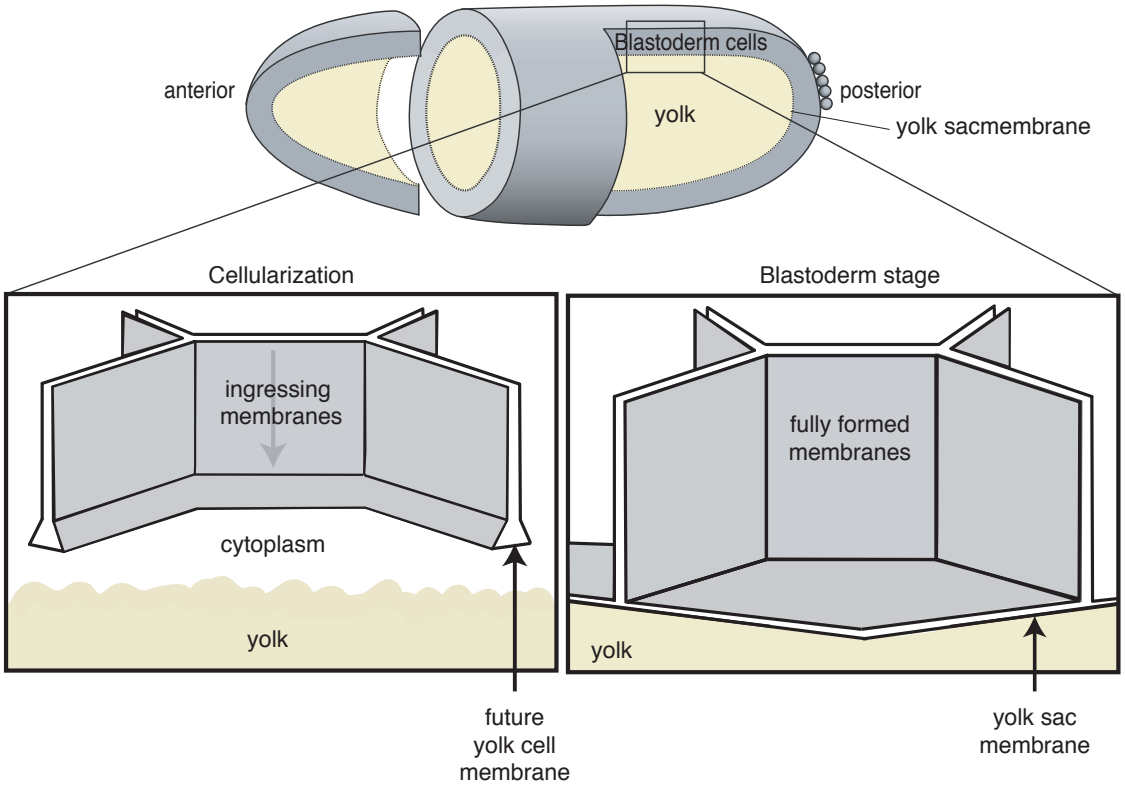

Figure 2.27: **The yolk sac forms as a consequence of cellularization.**
Yolk sac formation by the process of cellularization shown in a scheme. Close up is showing the process of cellularization that is forming blastoderm cells around the yolk (grey) and the yolk sac membrane formation.

One possibility to reveal effects of blastoderm/yolk sac connections on early development is to follow a developmental process in which the state of connection changes. Such a developmental process takes place after blastoderm and yolk sac formation are completed. A promising developmental process that could be used to illuminate this question is the formation of the extraembryonic tissues. This tissue starts forming the extraembryonic tissue from blastoderm cells at a dorsal domain and the individual cells begin to increase their area to spread over the entire embryo proper.

To study the interaction of yolk sac and serosa cells I investigated and characterized both structures in early and late stages of the scuttle fly *Megaselia abdita*.

2.9.2 Extraembryonic cells form from a dorsal domain and increase dramatically in apical area

To investigate whether the interaction of yolk cell and serosa affected extraembryonic development I first aimed to describe cell shape changes of serosa cells before and towards the state of free tissue spreading. I quantified their cell properties and compared them to embryonic cells in comparison in fixed samples. Therefore, I fixed *Megaselia* embryos at three subsequent stages of development, and the cell outline was revealed by staining filamentous actin (F-actin). Cell height and area, were measured at various positions along the anterior-posterior axis and the embryonic circumference (i) in the blastoderm before the onset of gastrulation, (ii) after germband extension and the initial formation of a dorsal extraembryonic tissue, (iii) during or briefly after detachment of the serosa (**Figure 2.28 A-D**) [Caroti et al., 2018]. During blastoderm stage, all cells appeared to be tall and equal in size, shape, and volume (**Figure 2.28 B-B"**). After the onset of germband extension but prior to detachment of the serosa, two classes of cells appeared to be qualitatively distinguishable based on differences in cell shape: cells of the lateral region of the embryo were characterized by a slight decrease in cell height but maintained apical area and circularity, while cells along the dorsal midline appeared flattened and stretched and deviated from the ideal circular apex (**Figure 2.28 C-C"**). Similarly, during or briefly after detachment of the serosa, cells shapes were observed to fall into two qualitatively distinct

classes, i.e., tall cells with a round apex and a small apical cell area (embryonic cells) (**Figure 2.28 C',D'**), and thin cells with a stretched and flat cell area (extraembryonic cells) (**Figure 2.28 C",D"**).

These dramatic changes in cell shape coincides with a spreading of cells over the embryo proper. This was possible when cells could detach from the underlaying yolk sac. It remained unclear whether shape changes were sufficient for decoupling from underlaying yolk sac or whether further regulations would be necessary. To understand how cell shape changes might be involved time lapse recordings were taken and analyzed, i.e., whole embryo (SPIM (SPIM-imaging and evaluation in collaboration with Francesca Caroti [Caroti et al., 2018]) or heigh (temporal) resolution of the dorsal serosa anlage and underlaying yolk sac.

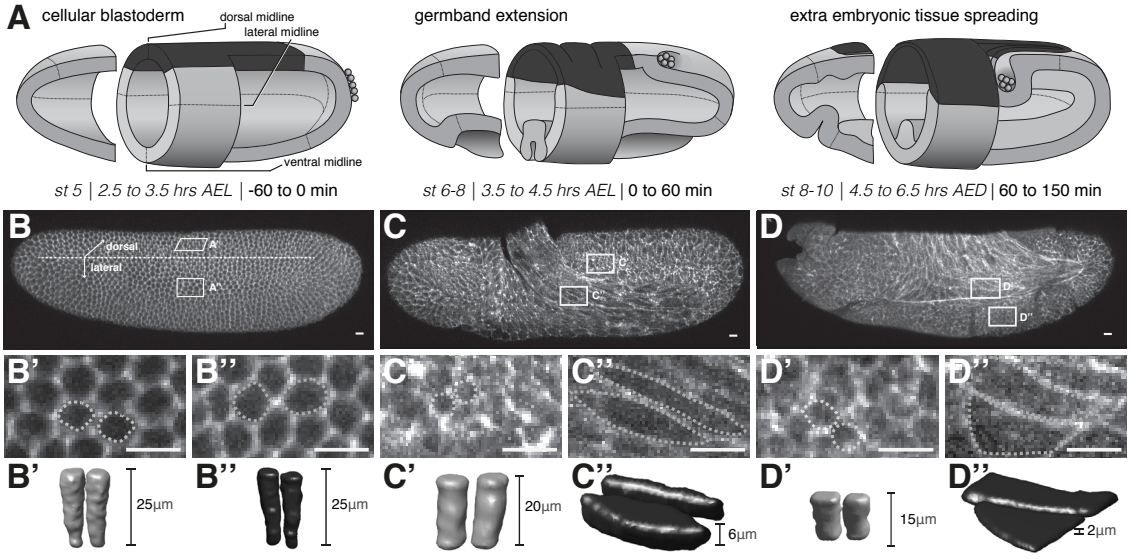

Figure 2.28: *Megaselia* serosa cells develop dorsal over the yolk sac and change their shape during gastrulation.
A, Model of early extraembryonic development in *Megaselia* without distinction of amnion and serosa (extraembryonic tissue labeled in black). **B–D"**, Global embryonic view of fixed embryos stained for Phallacidin to outline actin cytoskeleton (B–D), with close-up views (B'-D") and three dimensional volume renderings (B'-D") of embryonic (B', C', D') and extraembryonic cells (B", C", D"). (Volume rendering was conducted in collaboration with Paula Gonzalez) (Figure adapted from Caroti et al., 2018).

2.9.3 Serosa spreading is a non-continuous process interrupted by a pause of spreading just before disjunction to spread free

The observed cell shape changes as measures of extraembryonic tissue were further confirmed in whole embryo time lapse recordings (SPIM) [Caroti et al., 2018]. The analysis of these time lapse recordings suggest that the movements are non-continuous in the case of serosa area increase (**Figure 2.29 A-D**) [Caroti et al., 2018]. In the first phase of serosa spreading serosa area increased at a constant rate, which was followed by a break in tissue expansion, during which the serosa area did not increase substantially. In this time period, serosa cells displayed increased pulsations. After the pause of about 30 minutes, it continued to expand over the embryo proper (**Figure 2.29 D**) [Caroti et al., 2018]. These findings suggested that extraembryonic tissue and yolk sac were initially connected and were then required to break apart from each other in order for the serosa to spread freely over the embryo.

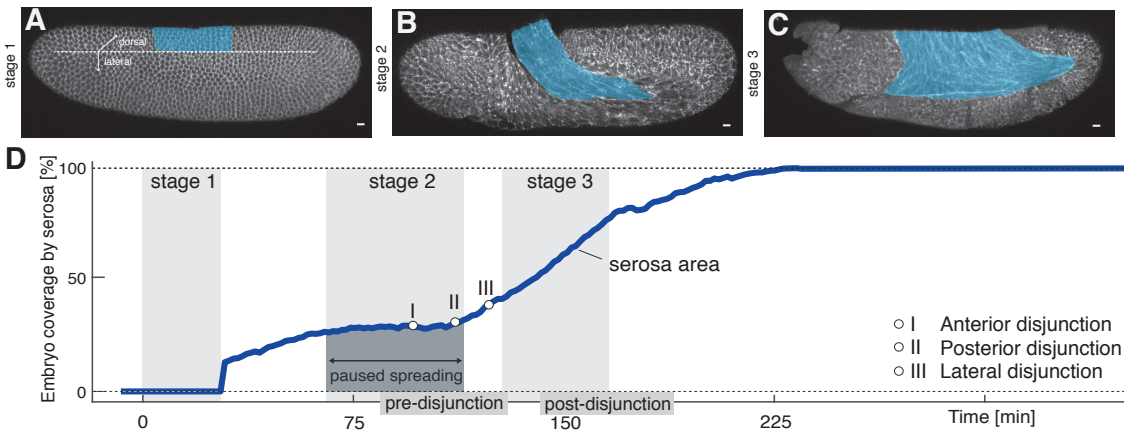

Figure 2.29: **Serosa spreading is a dynamic process that is interrupted by a pause before cells start to spread free.**
A-C, Global embryonic view of fixed *Megaselia* embryos stained for Phallacidin to outline actin cytoskeleton indicating the serosa anlage (blue) in (A) blastoderm in blastoderm stage, (B) during paused spreading and (C) after serosa disjunction. **D**, Serosa spreading plotted over time with indicated timepoints of paused serosa spreading, anterior, posterior and lateral disjunction (based on SPIM data, experiment performed and evaluated by Francesca Caroti). (Figure adapted from Caroti et al., 2018).

2.9.4 Decoupling of serosa cells and yolk cell is important for subsequent free serosa spreading

To investigate this postulated connection of serosa and yolk sac I aimed to monitor extraembryonic cells together with the yolk sac membrane and investigate whether they move together.

For this analysis a marker that could visualize the yolk sac membrane had to be established first. The *Megaselia* orthologue of *basigin* (Mab-bsg) appeared to be possible candidate, which encodes a trans-membrane protein that in *Drosophila* is enriched in the yolk sac membrane [Reed et al., 2004; Goodwin et al., 2016].

To establish Mab-bsg as a faithful reporter of the yolk sac membrane, I first asked whether the gene was expressed at the yolk sac membrane. I performed in situ hybridizations and found specific staining at the yolk sac membrane of different staged *Megaselia* embryos (**Figure 2.30 A,B**). I then asked whether a fusion of Basigin and eGFP (Basigin-eGFP) could be used to visualize the yolk sac membrane like in *Drosophila* [Goodwin et al., 2016]. To express the basigin-reporter specifically in the yolk sac I injected the capped mRNA of Mab-bsg-eGFP after cellularization was completed and germband extension had started [Rafiqi et al., 2010]. I could observe a specific stable staining of the

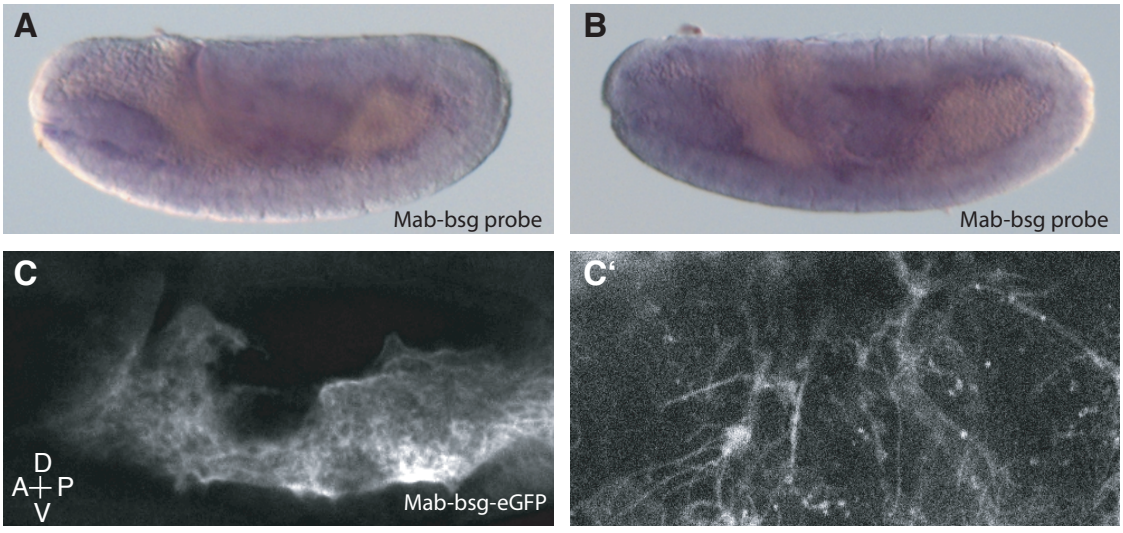

Figure 2.30: **Mab-basigin is expressed at the yolk cell membrane.**
A-C', *Megaselia* embryo at germband extension stage; staining for Mab-bsg probe detected at yolk cell membrane (n=40) (A-B) and Mab-bsg-eGFP expression visualized by confocal imaging (C-C').

yolk sac membrane enabling a live observation of specific movements of the yolk.

To quantify the movements of yolk sac membrane and serosa cells together, their respectively movements had to be imaged individually and analyzed together subsequently. Therefore, the Basigin reporter was specifically expressed in the yolk sac and combined with a Lifeact-mCherry staining of serosa cells. Visual inspection of time-lapse recordings along the dorsal midline indicated that fluorescent signals in serosa and yolk sac could be separated, allowing me to distinguish between movements in either tissue (**Figure 2.31 A-C**).

With Basigin-eGFP established as reporter for the yolk sac membrane in *Megaselia*, I used its fluorescent signal to track movements at the yolk sac surface by optical flow (in collaboration with Everdo Gonzales) (see Materials and Methods) [Caroti et al., 2018]. These analyses detected oscillations in serosa cells before free spreading, which seemed to coincide with oscillations at the yolk cell membrane (**Figure 2.31 D**). The direct comparison by cross-correlation analysis of movements in yolk cell and serosa cells revealed a strong positive correlation, which was very specific to individual serosa cells and the yolk sac membrane directly underneath (**Figure 2.31 F,G**). Such positive correlation of movements is indicative of strong mechanical coupling between yolk cell membrane and extraembryonic tissue [Goodwin et al., 2018]. I found coupling to be significantly reduced after serosa had started to spread freely over the embryo proper (**Figure 2.31 E,G**). Notably, coupling was not completely lost, suggesting that yolk sac and serosa remained physically associated, but loosely enough to slide past each other. Possibly further tissue spreading was hindered by an adhesion to an underlaying substrate first i.e., the yolk sac before a free spreading was possible

In summary together, I showed that serosa cells were in tight contact with the underlaying yolk sac before they decouple, and serosa can spread freely over the *Megaselia* embryo.

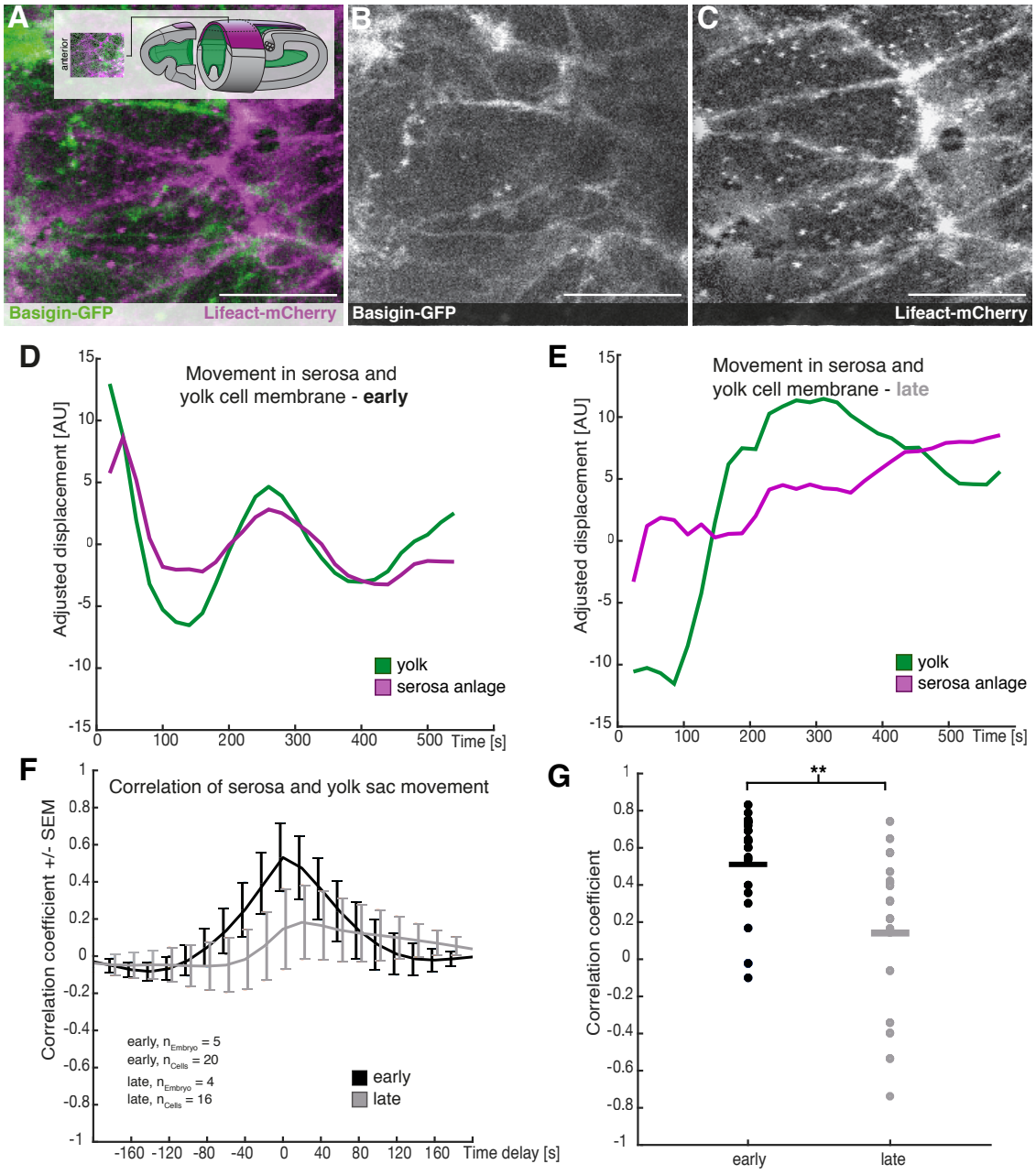

Figure 2.31: **Yolk cell membrane and serosa cells are coupled pre-disjunction and decoupled after-disjunction of serosa.**
A-C, Average intensity projections of serosa (visualized with Lifeact-mCherry) and underlaying yolk cell membrane (expressing Basigin-eGFP). Shown are stills from time lapse recordings taken along the dorsal midline and anterior of the germband (indicated in the scheme in A). **D-E**, Serosa (magenta) and yolk cell membrane (green) displacement measured by optical flow analysis and plotted over time before serosa disjunction (early) (D) and after disjunction (late) (E). **F**, Average cross-correlation function of serosa cells and yolk cell indicate coupling early (black) and de-coupling (late) of serosa cells. Standard deviation of mean indicated as bars. **G**, Collective comparison of correlation coefficients for individual cells early and late; bar indicates the mean (quantitative evaluation of confocal microscopy recordings in collaboration with Everado Gonzales) (Figure adapted from Caroti et al., 2018, Scale bars 20 µm).

2.9.5 Free serosa spreading is interrupted by a phase where active pulsations can be observed

Serosa cells and yolk sac membrane not only appeared to be in tight contact in early stages of development but also showed a distinctive oscillating behavior seen in rhythmic pulsations in both structures especially strong during paused serosa spreading.

Tissue contractions are often correlated to contractions in the actin cytoskeleton [Martin et al., 2009]. To verify that the yolk sac had a separate actin pool, I firstly injected Lifeact-mCherry before cellularization was completed. Secondly, I injected Lifeact-GFP after cellularization was completed around 4.5 h after egg lay, to ensure fully closed membranes and both pools of actin to be stained autonomously (**Figure 2.32 A-C**). The results verified that the basal blastoderm actin cytoskeleton is independent from yolk sac actin cytoskeleton suggesting yolk sac actin could have an active role in building a mechanic force (pulsations).

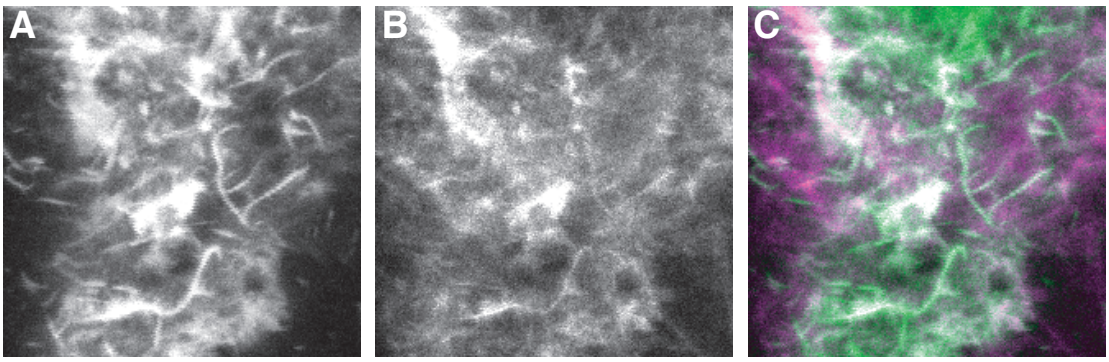

Figure 2.32: **The yolk sac membrane is a separate tissue with an independent actin pool.**
A, Basal serosa F-actin stained with Lifeact-mCherry. **B**, Yolk cell actin stained with Lifeact-GFP. **C**, Merge of serosa cells and yolk cell F-actin staining.

To understand whether these pulsations were important drivers for serosa decoupling from the yolk sac I first aimed to characterize them before and after disjunction. Therefore, I took confocal movies of *Megaselia* injected with Mab-bsg-eGFP in high temporal resolution and analyzed the direction of movements by using the Matlab toolbox PIV-Lab, where velocity of individual particles in the movie are followed, direction of the movement extracted and exported as directional vectors (**Figure 2.33 A-A"**) and

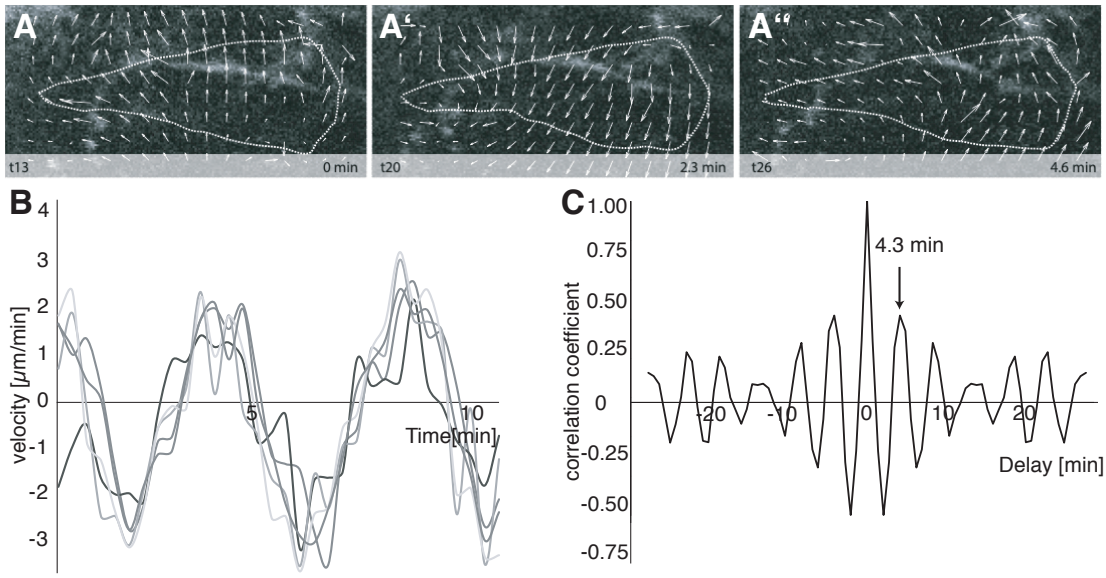

Figure 2.33: **Yolk sac membrane oscillates between 90 – 120 min after onset of germband extension.** **A-A'',** Yolk flow analyzed on Mab-bsg-eGFP stained embryos, movements visualized by particle velocity toolkit (PIVLab-Matlab) and directionality of movements indicated by arrows (vector velocities). **B**, Yolk flow directionality analyzed at different regions in one embryo and plotted over time indicating a uniform movement within the yolk tissue. **C**, Autocorrelation analysis of movements from PIV velocities showing a frequency of 260 sec (4.3 min). Dotted line outlines one serosa cell.

velocity plotted over time. The analysis of different regions within one embryo suggested that in pulsatile phase the yolk sac membrane is highly contractile and seems to pulsate in a rhythmic matter.

To verify that those movements were rhythmic and pulsatile I performed autocorrelation analysis of these oscillating movements suggesting a contraction rate of 260s/pulse (4.33 min/oscillation cycle) (**Figure 2.33 B,C**) (in collaboration with Viola Kühnel).

PIV analysis and respectively autocorrelation analysis at later stages confirmed that the oscillating behavior observed in earlier stages was not found anymore. The PIV analysis clearly showed that different regions within one embryo were moving independent of each other as was also seen in the respectively autocorrelation analysis (**Figure 2.34 B,C**).

In summary these results showed that the pulsations were observed during early phases in serosa spreading coincidentally with the pause in serosa spreading (90-120 min) and frequent oscillation behavior was not found in later stages anymore. This suggests that pulsations in that time window might be important for subsequent free serosa spreading. However, it was not yet clear what is driving these pulsations and whether they are the drivers for the decoupling.

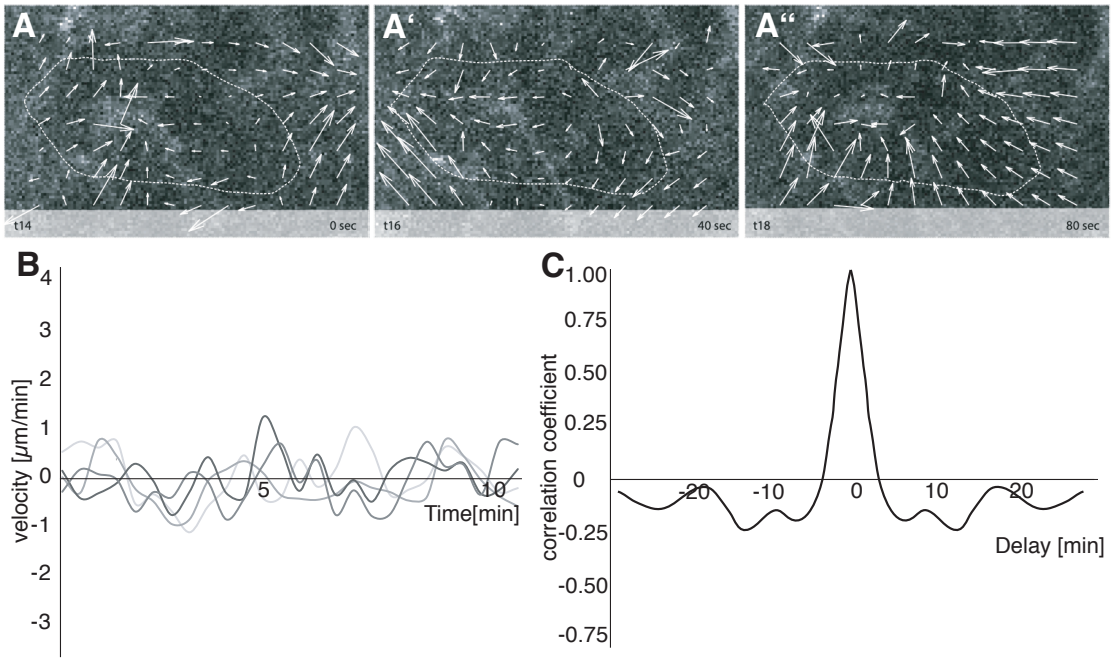

Figure 2.34: **Yolk cell membrane shows no frequent oscillations 140-200 min after onset of germband extension.**
A-A”, Yolk flow analyzed on Mab-bsg-GFP stained embryos, movements visualized by particle velocity toolkit (PIVLab-Matlab) and directionality of movements indicated by arrows (vector velocities). **B**, Yolk flow directionality analyzed at different regions in one embryo and plotted over time indicating disordered movements. **C**, Autocorrelation analysis of movements from PIV velocities indicating no frequent oscillation. Dotted line outlines one serosa cell.

2.9.6 Pulsations in paused spreading can be altered by the interference with yolk sac F-actin

To test whether contractions were caused by the yolk sac I aimed to interfere with the actin cytoskeleton specifically by using *cofilin* mRNA which is described to disassemble actin specifically (in collaboration with Viola Kühnel). To test whether Cofilin was effective, injections before cellularization was completed where conducted and showed a lethal phenotype (16/17 lethality) suggesting Cofilin to be interfering with F-actin, which is essential for cellularization to complete. To ensure Cofilin affects yolk sac F-actin only injections were conducted just after cellularization was completed (about 4.5 h after egg lay).

Pulsations could still be observed in treated *Megaselia* embryos but appeared to

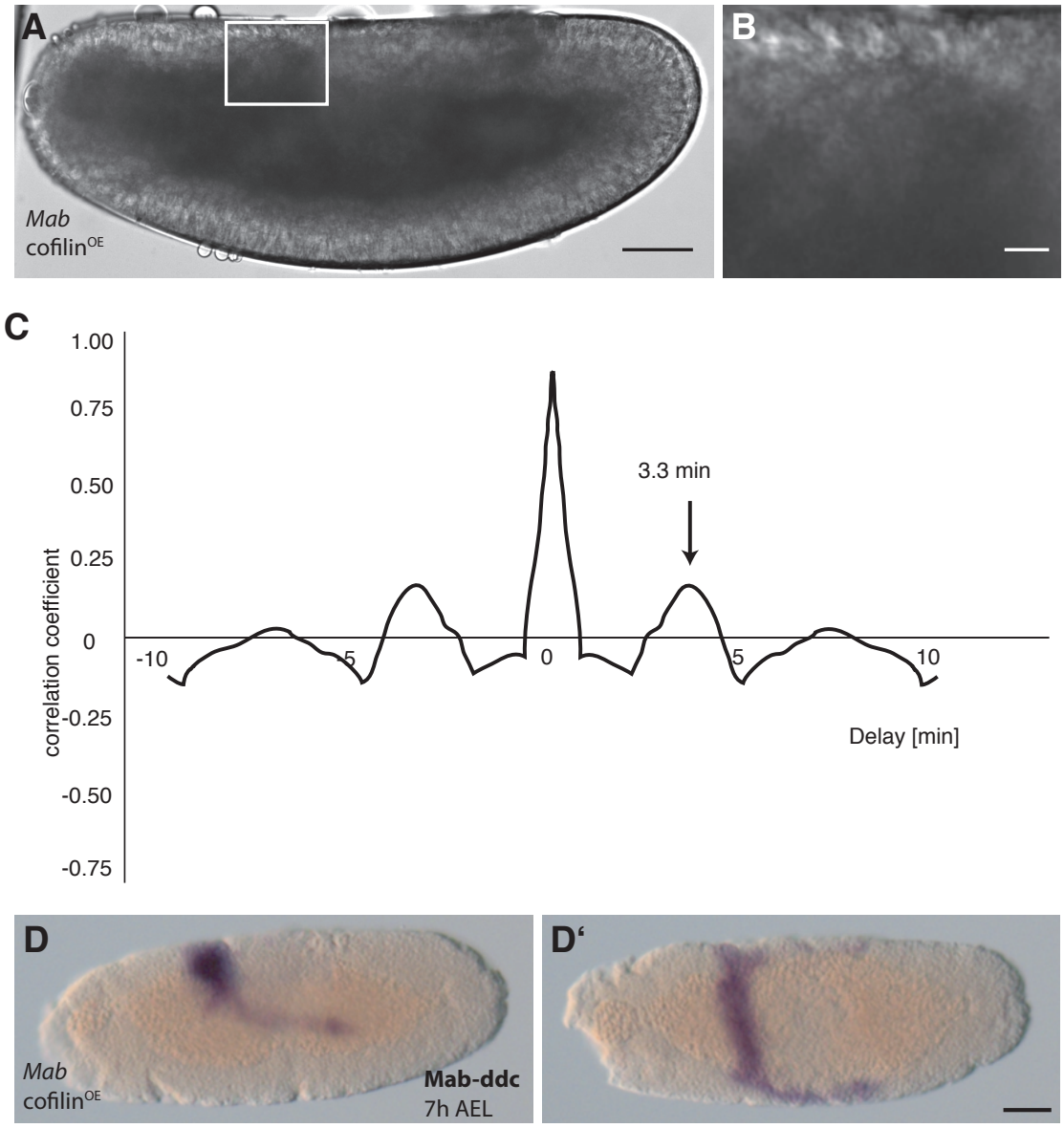

Figure 2.35: **Injection of *cofilin* mRNA alters yolk sac oscillation, presumably by changing actin dynamics.**
A-C, *Megaselia* embryo at GBE-stage (A) indicating the region of pulsations, (B, scale bar 10 µm) shown in a close up, which was analyzed by autocorrelation in (C). **C**, Pulsations analyzed by optical flow analysis and plotted in an autocorrelation graph indicating a frequency of 3.3 min. **D-D'**, Expression of *Mab-ddc* as serosa marker during GBE-stage (7 h AEL) in cofilin^{OE} embryos. Scale bar 50 µm. (in collaboration with Viola Kühnel).

be in a different frequency, which could be verified by the respectively autocorrelation analysis, which was adapted for DIC movies (**Figure 2.35 A,B**). The oscillating behaviour was analysed in direction A-P (X) and D-V (Y) showing the strongest pulsations in D-V direction with a frequency of 190-200 seconds (**Figure 2.35 C**). This is in contrast to the 260 seconds that were observed in the wildtype condition suggesting the interreference

with yolk sac F-actin did have an effect on the oscillations. Consequently, active pulsations possibly have an effect on serosa spreading.

To test whether yolk sac actin (part-)disruption had an effect on development and especially serosa spreading putative effects on serosa development was tested by staining embryos for the serosa specific marker gene dopa decarboxylase (Mab-ddc) [Rafiqi et al 2010]. In wildtype embryos the serosa closes about 7 – 7.5 h after egg lay, which in corresponding fixed stages is reflected by uniform staining of Mab-ddc [Caroti et al., 2018]. Following F-actin disruption by Cofilin, *Mab-ddc* expression most embryos (8/10) showed a wildtype like expression where serosa was closed over the whole embryo. However, two embryos showed a staining reduced to a dorsal domain at corresponding stages suggesting serosa spreading was impaired in these embryos (**Figure 2.35 D D'**).

The finding that the frequency of the pulsations was altered when interfering with cortical yolk actin suggest that pulsations might not only come from the yolk but depend on the overlaying serosa cells.

2.9.7 Pulsations are abolished after fate change of serosa cells

To investigate whether tissue interaction and /or pulsations were altered after changing fate of serosa cells I analyzed Mab-zen RNAi embryos in which the serosa and was replaced by amnion. Previous work has shown that knockdown of *zen* activity transformes serosa into amnion cells [Rafiqi et al., 2008], thus allowing me to analyze tissue and cell behavior in an enlarged amnion.

Similar as for wildtype I used, similar as for wildtype, the *basigin* reporter to investigate movements specific for the yolk cell and combined it with Lifeact-mCherry-staining of the overlaying serosa cells. The subsequent autocorrelation analysis showed that the fate change led to abolish pulsations in stages where they were observed in a wildtype situation (90-120 min) and were not detectable in later stages (**Figure 2.36 A-B**). These results suggested that serosa cells were actively involved in inducing the oscillatory behaviour and may implicate that serosa cells were the source of such movements.

Earlier I could show that the oscillatory behaviour was seen in both serosa cells and yolk sac membrane and that they would pulsate together in early stages suggesting they were tightly coupled (**Figure 2.31**) and a non-simultaneous movement in later stages when serosa spreads free (**Figure 2.31**). Even though no oscillations were observed after *zen* knock down cross-correlation analysis was performed to test whether both (amnion cells and yolk sac membrane) would move together suggesting a tight coupling of both. I found they move together in early and in late stages suggesting amnion cells and yolk sac membrane were tightly connected over the whole course of germband elongation and cells would not loosen up as described for wildtype (**Figure 2.36 C-E**).

In summary I could show that pulsations depend on tissue fate and differentiation than yolk sac actin alone. This shows that mechanical forces were part of the decoupling but suggest another mechanism to be involved dissolving the tight coupling.

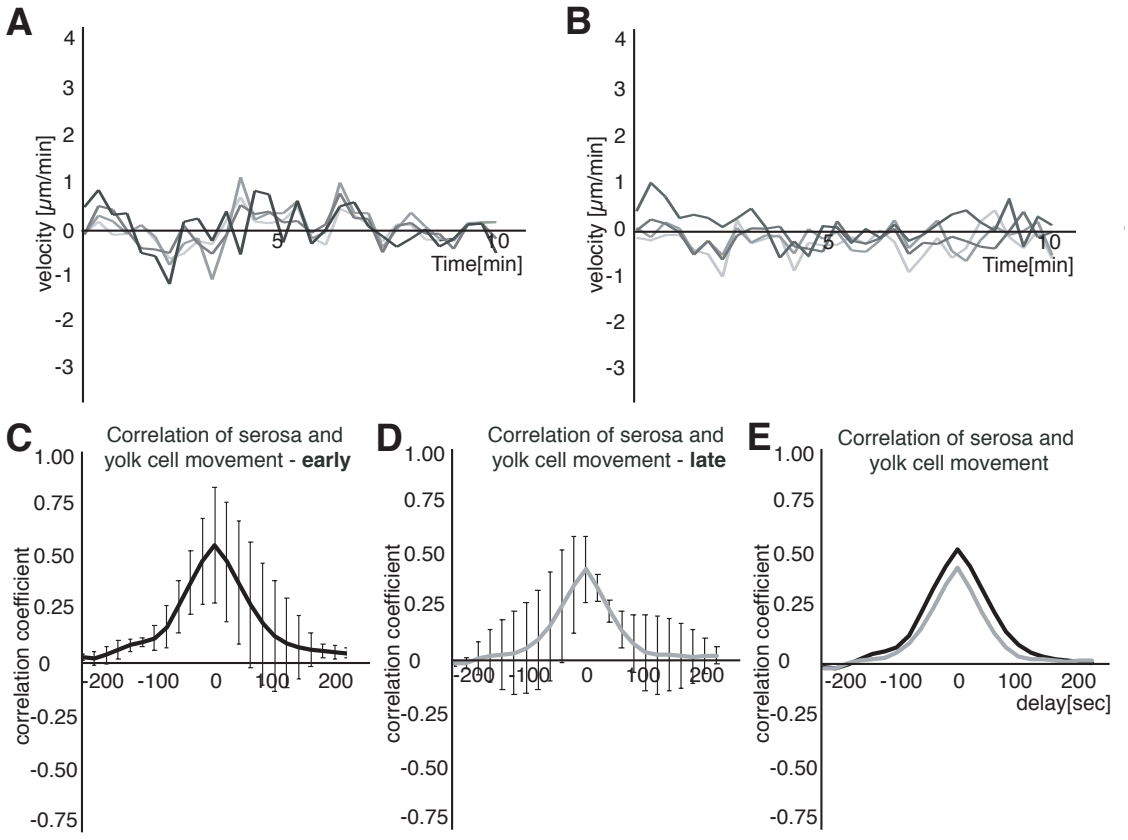

Figure 2.36: **Zen is required for early yolk sac oscillation and late tissue separation.**
A-B, Yolk flow analyzed on Mab-bsg-GFP stained embryos early – 90-120 min after onset of GBE (A) and late 140-200 min after onset of GBE (B), movements visualized by particle velocity toolkit (PIVLab-Matlab) and directionality of movements indicated by arrows (vector velocities). **C-E**, Average cross-correlation function of serosa cells and yolk cell indicate coupling early (black – 90-120 min after onset of GBE (C,E)) and remaining coupling late (grey 140-200 min after onset of GBE (D,E)) of serosa cells. Standard deviation of mean indicated as bars.

2.9.8 Serosa cell and yolk cell remain coupled when depleting *Mab-Mmp1*

Modulation of tissue-tissue connection, similar to that seen by separation serosa cells from underlaying yolk sac were in *Drosophila* previously associated with the M*atrix metalloprotease 1* (*Mmp1*) activity, which is involved in dissolving extracellular matrix (ECM) [Diaz-de-la-Loza et al., 2018, Glasheen et al., 2010].

To test whether this matrix metalloprotease was involved in altering the interaction of the both tissues the *Megaselia* orthologue of *Mmp1* (*Mab-Mmp1*) was cloned and found to be expressed in yolk sac nuclei [Caroti et al., 2018]. When *Mab-Mmp1* was knocked down serosa spreading was reduced at to a dorsal domain, suggesting serosa spreading was impaired [Caroti et al., 2018] (conducted by Francesca Caroti).

To understand how the knock down of *Mab-Mmp1* affects tissue-tissue coupling between serosa cells and yolk sac I quantified the movements by cross-correlation analysis of the tissues in (1) early stages (90-120 min) and in (2) late stages (140-200 min) corresponding to stages analyzed in wildtype (**Figure 2.37**). (1) The correlation of movements of serosa and yolk sac were, as observed in wildtype, high and comparable to wildtype and suggested a mechanical coupling of both tissues. (2) The observed correlation remained unchanged also in later stages and were significantly higher than in wildtype.

These results suggest that mechanical coupling stayed high which could explain the impaired serosa spreading.

In summary I could show that yolk cell and serosa cells were in tight contact after cellularization was completed and that the yolk cell might have a greater impact on development than described so far. In addition to that, I could investigate that a mechanical (pulsations) as well as a molecular mechanism (*Mab-Mmp1*) was involved in serosa cell decoupling from underlaying yolk sac ensuring the extraembryonic tissue to spread.

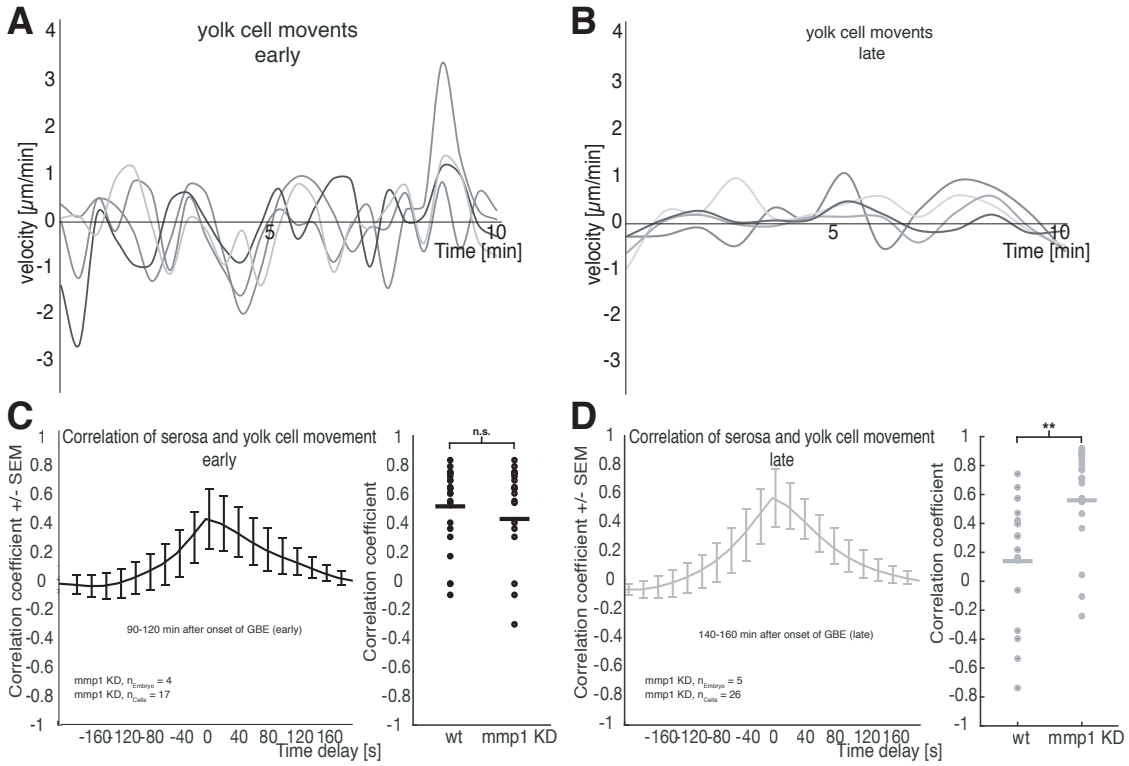

Figure 2.37: ***Mab-Mmp1* is required for free serosa spreading.**
A-B, Yolk flow analyzed on Mab-bsg-GFP stained embryos early – 90-120 min after onset of GBE (A) and late 140-200 min after onset of GBE (B), movements visualized by particle velocity toolkit (PIVLab-Matlab) and directionality of movements indicated by arrows (vector velocities). **C-D**, Average cross-correlation function of serosa cells and yolk cell indicate coupling early (black – 90-120 min after onset of GBE (C)) and remaining coupling late (grey 140-200 min after onset of GBE (D)) of serosa cells (Correlation coefficient of *Mab-Mmp1* KD means in contrast with wt data from Figure 2.36 (C,D right graphs). Standard deviation of mean indicated as bars (quantitative evaluation of confocal microscopy recordings in collaboration with Everado Gonzales) (adapted from Caroti et al., 2018).

3
Discussion

In my thesis I identified two biological innovations in early embryonic fly development. I characterized them by the precise description of differences on a cell or tissue level and identified changes/novelties in gene expression followed by a functional validation. This allowed me to link between cellular, molecular and phenotypic divergence.

In the first part I identified tall blastoderm cells as a feature of presumably higher fly species and small blastoderm cells as a feature of more basal flies. To characterize the function of tall cells and how they emerged I used a comparative approach to distinguish tall from small blastoderm cells and their formation using the fruit fly *Drosophila melanogaster* as a representative of tall cells and the midge *Chironomus riparius* as a representative of small cells. In my work I showed that a novel gene, called *slow as molasses* (*slam*), piggybacked onto an existing developmental process that fundamentally changed cell height in the blastoderm epithelium. I showed that this novel Rho/F-actin regulator controls epithelial cell lengthening by promoting a progressive extension of E-cadherin based adhesion along the basolateral membrane during evolution. My results also indicate that *slam* was the first of several novel zygotic genes that step by step altered the ancestral mode of blastoderm formation.

The second part describes analyses of embryonic and extraembryonic tissue separation in the scuttle fly *Megaselia abdita*. Here I took advantage of a previously described diversity in extraembryonic tissue development, where presumably higher flies develop a reduced extraembryonic tissue. Investigating the scuttle fly *Megaselia abdita* revealed decoupling of serosa cells from the subjacent yolk sac was necessary to ensure free spreading of the serosa to cover and protect the embryo. The decoupling was promoted by the *Matrix metalloprotease 1* (*Mab-Mmp1*) in combination with active pulsations. Interfering with this mechanism led to a prolonged connection to the yolk sac with a phenotype similar to a reduced extraembryonic tissue. The reduction of extraembryonic tissue here pretty much coincides with the transition from small cells to tall cells.

3.1 The transformation of small cells to tall cells

3.1.1 Tall columnar cell formation is driven by F-actin and E-cadherin in *Chironomus*

In the first part of this thesis, I identified the newly emerged gene *slam* as a key element that can instruct a blastoderm with short cells to become a blastoderm with tall columnar cells. When placing *slam* in a more basal system (*Chironomus*, which has no *slam*) consisting of small cells in its blastoderm, I found *slam* localized to the basolateral membranes, taking over its function which resulted in tall blastoderm cells (**Figure 2.15**). This elongation was likely driven by a progressive extension of E-cadherin based adhesion along basolateral membranes (**Figure 2.18**). I could show that this novel yet simple mechanisms integrated seamlessly into the existing machinery of *Chironomus* by reorganizing existing components (e.g., F-actin and E-cadherin). My hypothesis on the mechanism driving this cell elongation is based a proposed mechanism in planar cell-cell dynamics. There, epithelia reshape actively by the generation of small patches of stable cortical actin that might immobilize and induce clustering of E-cadherin which is key in cell-cell adhesion. These proposed F-actin/E-cadherin patches in the formation of tall blastoderm cells then extend along the apical to basal axis of adjacent lateral membranes. This might act as a mechanism that effectively zips cells together. The observed lateral accumulation of E-cadherin suggests an analogous mechanism to cell zippering in tissue culture [Vasiouhin et al., 2012]. There, patches of lateral adhesion form a self-organized zipper that progressively extends contacts. The finding that the lateral positioning of E-cadherin is involved in cell elongation is supported by the finding that cell height is reduced when the amount of E-cadherin is reduced (**Figure 2.19**). The local knockdown (KD) and its phenotype can be rescued by providing E-cadherin mRNA again (**Figure 2.20**). Surprisingly, the effects are locally restricted, suggesting a cell-autonomous mechanism.

One other mechanism that could promote cell lengthening is a mechanism that was proposed as a function of *slam* before. Here, guided vesicle fusion at the basal site is suggested to take part in the elongation of lateral membranes [Stein et al., 2002; Lecuit et al., 2002]. Vesicle fusion during *Drosophila* cellularization happens at two distinct places: a subapical domain close to the adherens junctions and a basal domain at the furrow canal [Figard et al., 2016]. These Golgi derived vesicles are important for cell elongation [Figard et al., 216]. When interfering with the secretory trafficking of the vesicles by Brefeldin-alpha, cells in the blastoderm stage appear 1/3 shorter in the *Drosophila* embryo [Figard et al., 2016; Sciaky et al., 1997]. I found that the columnarization in *Chironomus* was possible through a surplus of membrane, stored in apical villi, that got used up to elongate lateral membranes, however not reaching cell heights of *Drosophila* (*Drosophila* 31 µm vs 28 µm in *Chironomus* embryos overexpressing *slam* (slam$^{OE)}$). To test whether vesicle fusion was involved in *slam* promoted cell elongation in *Chironomus* it would be possible to interfere with vesicle trafficking similarly as for *Drosophila*.

Another previously proposed structure involved in cell lengthening are microtubules [Koonce et al., 1987; Guild et al., 2017]. It was shown that interfering with microtubules using drugs can affect with cell elongation in single cells [Gervais and Casanova, 2010]. However, it is unclear whether microtubules themselves generate the elongating force or whether they just stabilize incremental increases in length mediated by other processes. One proposed active microtubule-driven process of single cell columnarization is "microtubule sliding", which supposedly extends a microtubule-bundle like a "telescope". Examples for this mechanism are suggested to be in place in amoeba [Koonce et al., 1987] and cone cells of teleost retina [Troutt and Burnside, 1988]. However, insights gained by disrupting microtubules in *Chironomus* using specific drugs showed that cellularization still continues when interfering with microtubules after cellularization had started. Experiments on *Drosophila* show similar results and interfering with microtubules during cellularization has no effect on it [Foe and Edgar, 1993; Harris and Peifer, 2005]. This suggests that cell elongation is independent of microtubules. To further investigate the role of microtubules during cellularization it would be possible to follow microtubules dynamics together with membrane or actin dynamics and how these change after a specific

interference of microtubules.

Taking these facts into account, I propose that the formation of tall cells promoted by the novel gene *slam* is mainly driven by the lateral progression of E-cadherin ("zipper") but it remains to be tested whether other mechanisms that that were previously proposed to be involved in cell elongation (e.g., vesicle fusion or microtubule sliding) might assist the process.

3.1.2 Slam remodels the actin cytoskeleton in a cascade with RhoGEF2 establishing a second F-actin pool

Based on my results I speculate that the evolutionary origin of *slam* either extended or replaced the ancestral molecular mechanism of cuboidal blastoderm formation by opening of a second, basal F-actin polymerization site in addition with a lateral accumulation of E-cadherin. I used *Chironomus* as a representative of ancestral cuboidal blastoderm formation and investigated its wildtype development. I could show that *Chironomus* uses Diaphanous for subapical localization of F-actin, indicating a conserved role in cellularization already in the last common ancestor of *Chironomus* and *Drosophila* and likely in all flies.

This finding suggests that the addition of one scaffolding protein such as *slam* could facilitate the process leading to cell elongation by the reorganization of an existing machinery involving e.g., F-actin. F-actin is essential for building a scaffolding cytoskeleton supporting the cell and can also be involved in the motion of cells [Pollard and Cooper, 2013]. When the F-actin cytoskeleton gets reorganized it has the capacity to change cell morphology [Chalut et al., 2016; Chugh and Paluch, 2018; Chugh et al., 2017]. F-actin polymerization and F-actin dynamics are deeply conserved mechanisms that are tightly controlled in space and time by Rho GTPases which act together with GTPase-active proteins (GAPs) and guanin exchange factors (GEFs). GEF activity is necessary to activate signalling and GAP activity [Denk-Lobnig and Martin 2019]. F-actin dynamics and cell shape might be modulated by proteins that guide existing Rho activity to new

locations within the cell [van Unen et al., 2015; Müller et al., 2020].

My results show that *slam* is involved in re-localizing a Rho/F-actin machinery to a basolateral position where it opens a new actin polymerization point and hence can elongate membranes. Data from *Drosophila* support this finding where *slam*, a scaffolding protein, is also found at a basal position and acts together with RhoGEF2 and PatJ [Wenzl et al., 2010; Lecuit et al., 2002] and can interact with F-actin binding proteins such as Moesin, Par-3, Par-6 and Myosin II [Medina et al., 2002; Sen et al., 2012; Hutterer et al., 2004]. In addition, my results indicate a second pool of Diaphanous, which acts downstream of Rho at the basolateral position, supporting the idea of a re-localization of an existing machinery through *slam*. Data gained from *Drosophila* propose a cascade where *slam* and RhoGEF2 act together via Diaphanous to polymerize actin at the invagination front [Wenzl et al., 2010; Schmidt and Grosshans, 2018].

In *Drosophila* the establishment of this second basal actin polymerization site is actively involved in cell elongation by providing a huge contractile web with a force directed inward [Schejter and Wieschaus, 1993; Theurkauf, 1994]. This force is generated by actin depolymerization at the basal ring and active actomyosin contractility, which in turn reduces the total basal surface, which drives cell elongation [Xue et al., 2016]. In slam^{OE}embryos however, the establishment of a second actin pool was not contractile and likely was not actively involved in cell elongation. I hypothesize that the basal actin accumulation in slam^{OE}embryos is rather involved in establishing sites of E-cadherin patches which is on the one hand important for membrane extension (as discussed above) and on the other hand to hold the cytokinesis/cellularization ring open after it passed the nucleus to avoid ring closure at the basal site.

Data of *Drosophila* cellularization indicates a strong dependence on myosin II during the process, which is promoted by *slam* together with *dunk* [He et al., 2016; Acharya et al., 2014]. I showed that myosin was not involved in the blastoderm formation in *Chironomus* control embryos. Also, in slam^{OE}embryos myosin was not localized to the membranes indicating a myosin independent mechanism. I propose that a defined organization of myosin to the leading edge of the cellularization front could accelerate the process. This could be tested by overexpressing *dunk* in *Chironomus* and following the cellularization dynamics.

The results showing that *slam* is involved in the re-localization of cellular elements led me to hypothesize that *slam* could integrate seamless into a pre-existing cellular infrastructure influencing cell elongation.

3.2 The proposed ancestral mechanism

3.2.1 The ancestral mechanism of cellularization based on findings *Chironomus*

The postulated mechanism where *slam* acts as main organizer of tall cell formation by modulating the ancestral mechanism raises the question on the mechanism of small cell formation. My work is based on the artificial addition of genes into a present-day living organism, i.e. the *Chironomus* embryos. Based on my own work and results from literature, a possible mechanism for ancestral cuboidal blastoderm formation starts to emerge. In the following I will discuss my own as well as relevant findings in *Drosophila*.

The process of cellularization was studied and described intensively for *Drosophila* where it is compared to a mechanism that is similar to cytokinesis. In general terms cytokinesis is associated with a precise organization of the cleavage ring consisting of a contractile actomyosin structure. The establishment of this ring dependends on localization and activation of RhoGEF2 to the furrow canal and in turn activates myosin and the actin nucleator formin [Schwayer et al., 2016]. The arrangement of actin and myosin to the cleavage ring is suggested to be the driving force for ring closure by myosin sliding against actin leading to a reduction of ring perimeter and a cleavage. During closure, the ring has to be in close contact to the plasma membrane, which has been associated with anilin and septins. Anilin is a scaffolding protein and can interact with the core ring components actin and myosin. Septins are also scaffolding proteins that cross-link actin filaments into curved, tightly packed arrays and link the ring to the plasma membrane [Schwayer et al., 2016]. Anilin and septins have also been described to localize to the furrow canal in *Drosophila* cellularization [Piekny and Maddox 2010; Mavrakis et al. 2014]. One protein

of the septin family is Peanut (Pnut) [Adam et al., 2000], which is a maternally provided protein also found in *Chironomus*.

My hypothesis originates from the assumption that the ancestral mechanism of cellularization is based on a septin- and RhoGEF2-dependent mechanism very similar to cytokinesis. Accordingly, I envision that the main driver of cell elongation has been pnut, which was localized at the basal cell membrane, where it has been activated by RhoGEF2. This simple mechanism would follow a slow and linear dynamic, very similar to the one observed in *Chironomus*. In such a condition, any appearance of genes that scaffold and reorganize existing elements as F-actin and E-cadherin to a (baso-) lateral location will stabilize cell-cell adhesion. These patches of E-cadherin in turn accelerate membrane invagination resulting in taller cells. I showed that *slam* is one candidate that could facilitate the process to such an extent.

If cell elongation in *Chironomus* was driven by the establishment of a basal ring similar to cytokinesis rings this could explain that cells are closing up as soon as they passed the nucleus. Observations of cell tapering at the basal site in addition with data showing Dia/E-cadherin only in a subapical domain support this hypothesis. Possibly the lateral extension of F-actin/E-cadherin patches decreased the ring closure force to an extent that the cell elongated longer. However, this could not explain why *slam* became essential to tall blastoderm formation in *Drosophila* and related species (e.g., *Megaselia* **Figure 2.21**).

One possible lead comes from the cleavage furrow in planar epidermis division in *Drosophila*. Here the ingression is faster on the basal than on the apical side [Guillot and Lecuit, 2013]. This difference has been associated with E-cadherin coupling to the cytokinetic ring and reports from *Drosophila* show that cadherins can replace anilin in the cleavage furrow formation and cytokinesis during spermatocyte division [Goldbach et al., 2010]. It remains to be determined whether the presence of Anilin and E-cadherin together at the cellularization front has a similar effect. It is likely that a replacement or new organization of the components involved led to a novel mechanism that is not functional when *slam* is missing. Here it would be necessary to follow Anilin over *Chironomus* cellularization in comparison findings in *Drosophila*.

The cleavage ring of usual cytokinesis next to Anilin and actin is also composed of myosin, which is important for an active ring closure. In *Drosophila*, cellularization and

basal ring closure was described to be dependent on F-actin depolymerization together with a myosin dependent mechanism [Xue et al., 2016; Martin, 2016]. However, I showed that *Chironomus* cellularization is independent of myosin, suggesting ring closure rather is driven by actin depolymerization. Cofilin has been described to actively depolymerize actin and a knock down of cofilin in *Chironomus* would be possible to test whether actin depolymerization would result in a slower cellularization or a loss in basal ring closure.

To further investigate how the ancestral mechanism functions, the role of Pnut, RhoGEF2 and Anilin could be analyzed by following their dynamics in vivo in combination with knock-down experiments.

Based on my data gained from small blastoderm formation I propose that *Chironomus* as a fly living today is a good model to test hypotheses regarding the ancestral mechanism of blastoderm formation. Likely, the mechanism is very similar to an usual cytokinesis using similar proteins just without cleaving two cells but forming membranes around individual nuclei by cytokinesis ring formation.

3.3 The evolution of a novel developmental program

3.3.1 Stepwise addition of novel genes

Slam is known as the main organizer of cellularization in *Drosophila*, and it is arguably the core element of the developmental program responsible for blastoderm formation [Wenzl et al., 2010; Acharya et al., 2014]. At the same time, *Chironomus* and many other insects provide living proof that a developmental program exists that can form a blastoderm without *slam*. To reconcile these seemingly contradictory findings, I propose that the innovation of *slam* has transformed blastoderm development in such a fundamental manner that it entirely replaced the ancestral mechanism. Very likely, the process of a single gene eradicating an existing developmental program has been relatively fast. These insights come from my analyses in *Megaselia*, a phoridaen species that shared its last common ancestor with *Drosophila* about 150 million years ago. *Megaselia*, like *Drosophila*,

possesses a *slam* orthologue, and it is likely that similarities of blastoderm formation in both species represent their shared ancestral state. Notably, knockdown of *slam* in *Megaselia* leads to complete loss of blastoderm formation just like in *Drosophila*, suggesting that already 150 million years ago (MYA) and briefly after its origin, *slam* had been essential and ancient mechanisms of cellularization were lost.

A genome wide screen of all available dipteran genomes showed that after *slam* emerged about 190 MYA, it never got lost again, while other newly emerged zygotically expressed genes got lost again in some species. These genes support blastoderm formation in *Drosophila* e.g., *nullo*, *serendipity alpha*, *bottleneck* and *dunk* [Merrill et al., 1988; Schejter and Wieschaus, 1993; Theurkauf, 1994; Mazumdar and Mazumdar, 2002; He et al., 2016].

The finding that *slam* was the first new zygotic gene, and the others appear later could suggest that new genes became added stepwise facilitating cellularization. To investigate this postulated addition of genes I added two of them (*dunk* and *bottleneck*) to *Chironomus* to identify their capacity to alter cellularization alone and in addition with *slam*.

In *Drosophila-dunk* is described to recruit myosin to the leading edge of cellularization and the formation of a contractile actomyosin web [He et al., 2016]. This web then contracts as a whole, resulting in a force directed inward involved in membrane elongation. Preliminary data suggest that the overexpression of *dunk* in *Chironomus* can alter the process to taller cells as well (**Figure 2.25**) suggesting myosin was recruited to the cellularization front assisting cellularization. This however needs to be confirmed by an overexpression of *dunk* together with myosin staining.

I hypothesize that the overexpression of *dunk* in *Chironomus* led to localization of myosin to the basal site. Since myosin is a motor protein, contractility could be increased resulting in an acceleration of the process of cellularization which in turn elongated cells. I further hypothesize that the overexpression of *dunk* and *slam* together could facilitate the process to an extent where tall cells are formed by the lateral adhesion and by myosin contracting at an accelerated speed. The result would be a cellularization which is similar in cell height and speed to cellularization in *Drosophila*.

Bottleneck, which is a scaffolding protein mostly required during early stages (slow phase) of cellularization, is involved in forming a hexagonal meshwork from which the

fast phase starts [Schejter and Wieschaus, 1993, Theurkauf, 1994]. During slow phase elements needed for subsequent fast invagination (up to 1 µm/min) are brought to the invagination front and tension is built up [Schejter and Wieschaus, 1993; Lecuit et al., 2002; Schmidt and Grossshans 2018]. After the establishment of the cellularization front the tension rich phase transits to a less tensile phase [Xue et al., 2016; Martin, 2016]. I hypothesized that the addition of *bottleneck* to the *Chironomus* cellularization would form a tension rich phase which in turn would result in taller cells by building up a contractile web. However, preliminary data show that *bottleneck* in *Chironomus* altered cell shape but not cell height significantly. To investigate whether *bottleneck* influences cellularization dynamics, the process could be followed live. Likely, *bottleneck* alone was not capable to alter the process and needs additional factors like *slam*.

The investigation of *slam* function in addition to the preliminary data of *dunk* and *bottleneck* let me hypothesize that *slam's* program was extended with the emergence of new genes to an efficient, fast, and precise process. Future work will be necessary to understand when *slam* became essential to the process and how other new factors became integrated.

3.4 The function of tall cells

3.4.1 Tall cells have an increased barrier function

My conclusion that *slam* became essential very quickly and never got lost again supports the idea that tall cells had an evolutionary advantage for the embryo. My hypothesis here was driven by the idea that tall cells might be of advantage for subsequent gastrulation, where cells change shape and rearrange dramatically. This depends on the supply of sufficient membrane material and by providing taller cells, membrane would only need to be remodeled. To test this hypothesis, I followed gastrulation of slam^{OE}embryos, but found germband extension slowed down and extension of the germband reduced. These observations suggest rearrangement of tall cells is either dependent on other/additional regulators in *Drosophila* and/or the extended adhesion along the basolateral membrane is

hindering cell rearrangement.

Changes in cell shape are often associated with a contractile actomyosin network i.e. T1 transitions [Kolsch et al., 2007; Sawyer et al., 2010]. By additional expression of Fog in slam^{OE}embryos, I aimed to activate the GPCR signaling pathway and respectively the contractile actomyosin network to increase T1 transitions in the ectoderm and observed that the process picked up in pace. These results suggest that the source dependent process of making tall cells might be advantageous by providing additional membrane material but needs a precise organization afterwards not yet given in *Chironomus*.

While gastrulation appeared slower in the first hours after blastoderm formation in slam^{OE}embryos, development into larvae was not affected suggesting the novel mechanism driven by *slam* effects cellularization only. The mechanism by which *slam* gets recruited to the membrane is not understood yet [Wenzl et al., 2010; Acharya et al., 2014] and it might be possible that *slam* can only bind to the ingressing membrane but not affect membranes in other epithelial tissues and therefore does not affect later development.

My reasoning behind the following ideas, to test whether the tall blastoderm cells had an evolutionary advantage at blastoderm stage, was driven by general epithelial properties. Epithelia in many contexts are described to provide a protective environment by acting as a selective barrier [Rojanasakul et al., 1992; Steinmetz et al., 2019; Kurn and Daly, 2021]. This suggests that the tall cells in slam^{OE}embryos or *Drosophila* might be an advantageous barrier to the outside. The *Chironomus* "test-tube" system provides an ideal model to test for differences in epithelia properties that depend on cell height / cell volume increase, since essentially two similar tissues can be compared consisting of either small or tall cells but comparable in all other measures. Using the comparative approach with *Chironomus* and *Drosophila* to test for functions of tall cells would be problematic as number of cells, embryo size and egg-shell are too diverse. To test for the advantage of tall cells I aimed to test for desiccation in the *Chironomus* blastoderm once with tall cells and once with small cells. My results show that the osmotic barrier function is significantly increased in embryos with tall cells (slam^{OE}embryos) suggesting that a comparable transformation in ancient fly blastoderm lowered constraints of early embryo desiccation. The appearance of columnar blastoderm formation within the fly phylogeny slightly predates, but roughly coincides, with a reduction of desiccation-protective extraembryonic

tissue formation [Schmidt-Ott and Kwan, 2016], suggesting that changes in blastoderm architecture lowered evolutionary constraints on a protective but resource-expensive developmental program.

3.5 Loss of serosa decoupling from yolk sac promoted a novel (reduced) tissue structure

3.5.1 Serosa cells and yolk sac in *Megaselia abdita* are two adjacent structures that have to decouple for free spreading

In the second part of my thesis, I investigated the two extraembryonic structures yolk sac and overlaying serosa cells in the scuttle fly *Megaselia abdita*. My analysis in *Megaselia* allowed me to identify cellular, epithelial, and functional properties of yolk sac and serosa. These include the pulsatile cell behavior of both tissues and serosa tissue-autonomous spreading by coordinated thinning and apical area expansion. In addition, I showed decoupling of serosa from the adjacent yolk sac during gastrulation was essential to free tissue spreading from a dorsal domain to close at the ventral site and cover the entire embryo. When interfering with the mechanism of decoupling, serosa spreading was delayed and remained in a dorsal domain similar to the reduced extraembryonic tissue, as e.g., the amnioserosa in *Drosophila*.

3.5.2 Free serosa spreading in *Megaselia* requires decoupling from yolk sac.

Area tracking of *Megaselia* serosa development identified three distinct phases of tissue spreading [Caroti et al., 2018]. These phases corresponded to either the (I) early,

"tethered", (II) paused and pulsatile or (III) a late, "freed" state of the serosa. In the first phase of serosa spreading, the serosa was still continuous with the ectoderm and thus part of a coherent epithelium. In the second phase serosa spreading was paused and showed substantial and frequent pulsations. In the third phase, the serosa had separated from amnion and ectoderm and was spreading freely over the embryo proper. Serosa spreading was completed with closure along the ventral midline [Caroti et al., 2018].

The analysis of the transition from (I) tethered to (II) paused to (III) free serosa spreading provided evidence for a change in tissue-tissue interaction between serosa and the underlying yolk sac. (I) First strong correlation of movements in serosa and yolk sac membranes were observed 90-120 minutes after the onset of germband extension (**Figure 2.32)**, indicating tight coupling between the membranes during paused serosa spreading. (II) During paused spreading a pulsatile behavior of serosa cells with a frequency of 4.3 min (**Figure 2.33)** could be observed suggesting a mechanical influence on tissue-tissue interaction. (III) After onset of free serosa spreading, i.e., 140-200 minutes after onset of germband extension (**Figure 2.31 F**), this correlation was reduced (**Figure 2.32**), indicating that onset of free serosa spreading coincided with a de-coupling from the yolk sac. I found that tissue-tissue coupling persisted in *Mab-mmp1* RNAi embryos for at least 140-200 minutes after the onset of germband extension, where tissue-tissue interactions between yolk sac and serosa remained comparable to that of wildtype embryos with paused serosa spreading (**Figure 2.37**). Complementing these findings, serosa spreading was impaired in *Mab-mmp1* RNAi embryos [Caroti et al., 2018]. These results suggest that free serosa spreading in *Megaselia* requires its de-coupling from the yolk sac.

Similar interactions between yolk sac and extraembryonic tissue have been reported previously in *Drosophila*, but at later stages of development, where they contribute to germband retraction and dorsal closure [Schöck et al., 2003; Narasimha and Brown, 2004; Reed et al., 2004; Goodwin et al., 2016]. Interactions of yolk sac and overlying epithelia have been long suggested to contribute to insect development [Handel et al., 2000; Benton et al., 2003; Schmidt-Ott and Kwan, 2016]. Together, these findings suggest that yolk sac regulated tissue spreading in *Megaselia* may be an example of a more common phenomenon by which properties and behavior of epithelia are in part defined through contact with the underlying yolk sac.

2.5.3 *Mab-Mmp1* remodels tissue-tissue interaction between serosa and yolk sac membrane

MMPs are found in various contexts and are described to be involved in the breakdown of extracellular matrices by breaking down collagens [Diaz-de-la-Loza et al., 2018; Glasheen et al., 2010]. This suggest that serosa spreads free when *Mmp1* had dissolved collagen structures in between serosa cells and underlying yolk sac. These findings indicate the formation of an extracellular matrix (ECM) between the two adjacent membranes, but it remains to be determined whether collagens, integrins or other components of an ECM are present and whether their interference might influence early development.

In *Drosophila* beta-PS integrin is located on the basal site of the amnioserosa and the yolk sac and is necessary to hold both tissues together as their adhesion is required for contraction of amnioserosa [Narasimha and Brown, 2004]. It is possible that a similar adhesion between yolk sac and serosa cells is present in *Megaselia* wt before free spreading. The finding that the knock down of *Mab-Mmp1* delayed serosa expansion suggests a weakening of the attachment and a remodeling of the ECM in *Megaselia* wildtype embryos. When this remodeling is not taking place, the serosa possibly uses another mechanism to spread free. I propose that the generation of a mechanical force could assist serosa decoupling which might be accomplished by active pulsations as discussed in the next paragraph. In addition to an adhesion through molecules like integrins early studies already showed that at the end of cellularization, when blastoderm cells had formed together with the yolk sac membrane, stalks described as “cytoplasmic continuity” [Rickoll, 1976] remained connected to the yolk. Microtubules that are organized as inverted baskets above each nucleus elongate into the yolk as cellularization starts and remain connected via these stalks into the yolk. Possibly these stalks also have to be remodeled for a free serosa spreading but this remains to be tested.

Taken together these findings show that serosa cells are in tight contact with the underlying yolk sac that needs to be resolved by *Mab-Mmp1*, assisted by active pulsations to ensure a free serosa spreading.

2.5.4 Pulsations are a feature of serosa cells

While knockdown of *Mab-Mmp1* delayed splitting, it did not inhibit it [Caroti et al., 2018]. This may be caused by an incomplete knock out, but more likely because other factors play a role. My results suggest that in addition to enzymatic activity a mechanical contribution by short term pulsations found in serosa and yolk sac could contribute to a free spreading. These pulsations became particularly pronounced in the phase just prior to the detachment of the serosa from yolk sac. When interfering with yolk sac F-actin using Cofilin, frequency of pulsations changed and delayed serosa spreading in 20% of the embryos, suggesting decoupling from the underlying yolk sac is supported by mechanical forces (pulsations). This finding could possibly explain the observed delayed serosa spreading despite *Mab-Mmp1* knock down in *Megaselia* embryos. Further investigations showed that pulsations also depend on cell fate, when transforming serosa into amnion cells by *zen* KD, pulsations where abolished suggesting it takes several conditions to spread e.g., cell thinning, separation from underlying tissue by *Mab-Mmp1* and mechanical pulsations. Loss of one element may be strong enough to change development.

2.5.5 Evolutionary perspective

In an evolutionary context, in particular in the transitions from amnion and serosa to the amnioserosa, the loss of epithelial spreading may have been driven by loss of *Mmp1* expression in the yolk sac and subsequently manifested by coordinated changes in the expanding as well as the underlying membranes. Consistent with this hypothesis *Drosophila* lacks *Mmp1* expression at early stages of development in the yolk sac suggesting a change in tissue-tissue interaction may have been part of the origin of amnioserosa.

The current model on the origin of amnioserosa focuses on the serosa differentiation by zen activity. Here, the absence of zen led to the formation of a non-spreading dorsal extraembryonic tissue [Rafiqi et al., 2008; Rafiqi et al., 2012; Schmidt-Ott and Kwan 2016]. My results in part support the idea and I was able to show that cells do not pulsate and spread in absence of zen but in addition found that serosa development depends on

free tissue spreading promoted by *Mab-Mmp1*.

In summary, these results illustrate how the *Drosophila* amnioserosa may have originated from a rather ancient change in tissue-tissue interaction presumably in combination with a change in *zen* expression.

Conclusion

My thesis covers two instances of biological innovation in the early fly embryo. I was able to characterize these innovations on a cellular, molecular level and genomic level. Central to my studies was a comparative approach that used non-model fly species that represent more basal branches of the insect order as a starting point to uncover innovations that are characteristic for the fruit fly Drosophila melanogaster and its very close relatives.

1) The innovation of tall cells at the blastoderm stage in higher flies

In summary, I established the *Chironomus* embryo as a test-tube-like system with naive, cuboidal tissue architecture. In contrast to working in *Drosophila*, the *Chironomus* system lacks possible redundancies known to be present in more derived systems such as *Drosophila*. The *Chironomus* system thus provided me an unprecedented opportunity to address the mechanisms of blastoderm columnarization. The deliberate addition and removal of selected molecular components allowed me to reveal how a single new gene had the power to change the architecture of a tissue dramatically. Based on my findings in this thesis I propose that the established comparative approach using *Drosophila* and *Chironomus* blastoderm was powerful to study questions from EvoDevo but also to gain more general insights on the function of epithelial cells.

2) The innovation of prolonged tissue-tissue connection resulting in a reduced extraembryonic tissue spreading in higher flies

Studying the interactions of the two adjacent structures, yolk sac and serosa cells, allowed me to identify that the yolk sac impacts early dipteran development. Prolonging the interaction of yolk sac to overlaying serosa cells led to a reduced serosa spreading resulting in a novel tissue structure like the reduced extraembryonic tissue in *Drosophila*. This suggests tissue-tissue interaction as a mechanism that controls extraembryonic tissue spreading. The model *Megaselia abdita* to study cellular dynamics by staining the two adjacent tissues with subsequent flow analysis here was a powerful tool to identify and characterize these tissue-tissue interactions.

In summary, I have described two biological phenomena that exemplify biological innovation in organismal development. First, I showed that the connectivity of two tissues can be key variable in the evolution of tissue behavior and function. As tissues interact in animals at various stages of development, I propose that changes in the biomechanics of tissue-tissue connectivity have likely contributed to innovations also in other contexts. Second, I revealed that a single new gene can have the capacity to transform the architecture of epithelial cells, and that this change results in advantageous tissue properties. My results outline a plausible path of how newly emerged genes can take advantage of a highly plastic and adaptive cytoskeleton to found developmental programs from scratch. Given the deep conservation of cytoskeletal building blocks and core regulators, it appears very possible that similar mechanisms contributed to convergent innovations throughout the animal kingdom. And, as more and more genomes are sequenced and non-model species become available for functional studies, it may have never been more exciting to continue asking: how does biology innovate?

4

Materials & Methods

4.1 Material

Experiments were conducted in a standard molecular biology laboratory with general equipment. Molecular work has been conducted essentially as described in Sambrok and Green (2001); specific methods are described in the following. All solutions were prepared with standard reagents: use of autoclaved MilliQ water; use of normally autoclaved glassware; use of autoclaved pipette tips. Specific items are listed below.

4.1.1 Organisms

Organism	Strain
Drosophila melanogaster	W1118
Chironomus riparius	Meigen, Bergstrom strain
Megaselia abdita	Sander strain

4.1.2 Chemicals

Name	Company	Catalogue Number
Agar	Roth	5210.2
Agarose	Peq-Gold	35-1020
Ampicilin	Sigma	A9518
Bleach	DanKlorix	

Chloroform/Isoamylalcohol	Sigma	25666
Dinatriumhydrogenphosphat	Grüssinu	12133
DNA ladder ready mix	Thermo Scientific	SM1173
dNTP	Sigma	D7295
EDTA	Applichem	A3553
Ethanol	Sigma	52603
Ethidiumbromide	Roth	2218.2
Ethylenediaminetetraacetic Acid	Sigma	34549
Formaldehyde	Sigma-Aldrich	252549
Gel Loading Dye	NEB	10047936
Glacial acetic acid	Merck	607002006
Glycerol	Sigma	54997
Hablocarbonoil 27	Sigma-Aldrich	8773
Hablocarbonoil 700	Sigma-Aldrich	8898
Haptane	Roth	8654.3
Isopropanol	Sigma	69694
Methanol	Sigma-Aldrich	322415
Natriumactate	Grüssing	1131
Natriumchlorid	Sigma	31434
NTP	Thermo Scientific	R0481
Phenol/Chloroform/IAA	Roth	A156.1
Potasium Acetate	Grüssing	12001
Potasium Chloride	Applichem	A3582

Potassium dihydrogen phosphate	Applichem	3620
RNase Inhibitor	Roche	11801800
Sodium Dodecyl Sulfat	Roth	CN30.2
Tris base	Roth	4855.2
Tryptone	Sigma-Aldrich	T9410
Tween-20	Sigma	P1379
Blocking solution	Roche	11 921 637 001

4.1.3 Small compound inhibitors

Name	Company	Catalogue number	Concentration
Alpha amanitin	Sigma-Aldrich	A2263	50 µg/µl
Cycloheximide	Sigma-Aldrich	66-81-9	0.5 mM
Colchicine	Sigma-Aldrich	C9754	5 mM
H1152 ROK inhibitor	Enzo	ALX-270-423-M001	10 mM
SMIFH2	Sigma-Aldrich	344092	100 nM

4.1.4 Immunohistochemistry

Fluorescent dyes

Name	Company	Catalogue number	Concentration / Dilution
Phallacidin	Invitrogen	B607	1:50 (stock 200 units/ml)

DAPI	Molecular Probes Life Technologies	D1306	5 ug/ml

Antibodies

Name	Company	Catalogue number	Concentration / Dilution
Anti-GFP Chicken IgY unconjugated 2mg/ml	Life Technilogies	1A10262	1:250
Donkey Anti Chicken Alexa 594	Jackson	703 505 155	1:250
Anti-alpha-tubulin Conjugated with Alexa 488	Sigma-Aldrich	16-232	1:250

4.1.5 Injections RNA and recombinant proteins

Name	mRNA / dsRNA	Concentration
basigin-eGFP	mRNA	2.0 µg/µl
bottleneck	mRNA	1.1 µg/µl
cofilin	mRNA	3.3 µg/µl
Dme-E-cad-GFP	mRNA	2.0 µg/µl
dunk	mRNA	1.0 µg/µl
Ecad	dsRNA	0.8 µg/µl
eGFP-Gap43	mRNA	1.7 µg/µl

eGFP-slam	mRNA	2.2 µg/µl
fog	mRNA	1.13 µg/µl
mmp1	dsRNA	3.9 µg/µl
myosin-GFP	mRNA	1.2 µg/µl
slam	mRNA	1.0 µg/µl
zen	dsRNA	See PhD Thesis Caroti, 2017

Recombinant proteins	**Concentration**
Lifeact-GFP	1.8 µg/µl
Lifeact-mCherry	2.0 µg/µl
TexasRed-Histone H1	0.7 µg/µl

4.1.6 Media and Solutions

Media	**Composition**
LB	Tryptone 10g/l Yeast Extract 5g/l Sodium chloride 10g/l
LB-Amp Plates	Tryptone 10g/l Yeast Extract 5g/l Sodium chloride 10g/l Agar 15g/lAmpicillin 50µg/
Lysis Buffer	NaOH 8g/l SDS 10g/l ad 1l H_2O

Neutralisation Buffer	$C_2H_3KO_2$ 3M
PBS	NaCI 80 g KCl 2g $Na_2 HPO_4$ 14.4g KH_2PO_4 2.4g ad 1l H_2O
PBT	PBS (1x), Tween-20 0.1%
Resuspension Buffer	Tris base 6.06 g/l $Na_2EDTAx2 H_2O$ RNase A 100mg/l ad 1l H_2O
SOC	Tryptone 20 g Yeast extract 5 g NaCl 0.5 g ad 1l H2O
TAE	Tris base 242 g/l Glacial acetic acid 5.71% EDTA 50mM

4.1.7 Kits

Name	Company	Catalogue Number
Capping-Kit	Cellscript	C-SCCS1710
Gibson assembly	Invitrogen	A46626
PolyA-Kit	Cellscript	C-PAP5104H
QIAquick Gel Extraction	Qiagen	28706
TOPO TA cloning Kit	ThermoScientific	450641

4.1.8 Enzymes and Buffers

Name	Company	Catalogue Number
Antarctic Phosphatase	NEB	M0289S
Antarctic Phosphatase Reaction	NEB	B0289S
BglII	NEB	ER0082
BsaI	NEB	R0535
Cutsmart Buffer (10x)	NEB	B7204S
DNase Turbo	ThermoScientific	AM2238
Dpn1	NEB	R0176R
EcoRI	NEB	R3101S
Gibson Assembly mix	NEB	E2611
HF Buffer (5x)	NEB	B0518S
HindIII	NEB	R0104S
iProof Polymerase	Biorad	1725300
NcoI	NEB	ER0571
NotI	NEB	R3189S
PacI	NEB	R0547S
Proteinase K	Invitrogen	25530-015
Q5 DNA Polymerase	NEB	M0491S
RNA Polymerase SP6	Ambion	00830286
RNA SP6 polymerase	Roche	10810274001
RNaseA	Thermo Scientific	EN0531
SacI	NEB	R3156S

SalI	NEB	R3138S
T4 ligase	NEB	M0202S
T4 ligation buffer	NEB	B0202S
XbaI	NEB	R0145S

4.1.9 Plasmids

Plasmid	Stock number
Bnk in pSP expression vector	LP553
Cri-E-cad in pSP expression Vector	LP554
Dme-e-cad in pSP expression vector	LP572
Dme-slam in PCS2 expression vector	LP483
Dunk in pSP expression vector	LP524
eGFP-slam in pSP expression vector	LP668
GAP43-eGFP in pSP expression Vector	LP 595
Mab-basigin in pSP expression vector	LP647
Mab-cofilin in pSP expression vector	LP648
Mab-mmp1 in pSP expression vector	LP337
Zen in pSP expression vector	LP197

4.1.10 Disposables

Name	Company	Catalogue Number
Cover slip	Marienfeld	0101122_214
Dry yeast	RUF, Aldi	

Filter paper	Machery-Nagel	MN 615 1/4
Glass capillaries	Hilgenberg	
Microloader tips	Eppendorf	5242956003
Microscope slide	Roth	H878
Needles	Harvard apparatus	30-0019, GC100F-10
Parafilm	Sigma-Aldrich	P8299
Parsley	Tro-Kost	
Petri dish	Grainer Bio-one	632181
Reaction tube 0.5 ml	Eppendorf	30124332
Reaction tube 1.5 ml	Eppendorf	30125150

4.1.11 Instruments

Instrument	Company
Agarose gel documentation	Mitsubishi Biometra P93
Electroporator	MicroPulser BioRad
Heatblock	Mixing Block MB-102, Bioer
Incubator	Incubation Shaker Model G25, New Brunswick Scientific Co. Inc., Edison, USA
Injector	Eppendorf FemtoJet Express
Needle puller	Flaming, Brown Micropipette Puller Sutter Instrument CO., model P-97
Spectrophotometer	DS-11+, DeNovix
Tabel top centrifuge	Eppendorf Centrifuge 5417R
Thermocycler	S1000 Biorad, Hercules, CA, USA

Vortex	Vortex Mixer 7-2020, neoLab

4.1.12 Microscopes

Instrument	Company
Binocular	Zeiss Stemi 2000, Nikon SMZ18
Confocal	Leica SP8 with a HC PL APO 63x/1.30 Glyc CORR CS2 objective
Leica DIC	Leica DB5000 10x objective
Nikon DIC (Live)	Nikon Eclipse Ti with a 20x objective (Nikon Plan Apo 20x/0.75 OFN25 DIC N2)
Spinning Disk	Nikon eclipse VoxTi with a 100x objective
Stereoscope	Zeiss Axio Vert.A1

4.1.13 Software

Software	Company
Geneious 6.1.6	Biomatters Limited, New Zealand
Illustrator CS6	Adobe, USA
ImageJ	Schindelin et al., 2012 (http://fiji.sc/ImageJ)
Leica software	LasX
Matlab R2016a	The MathWorks, Inc., Natick, Massachusetts, United States
Matlab R2018b	The MathWorks, Inc., Natick, Massachusetts, United States
Nikon software	NIS Elements

4.2 Methods

4.2.1 Fly keeping

Culture keeping: A laboratory culture of *Chironomus riparius* (Meigen, Bergstrom strain) was maintained at 25 ˚C and a constant 17/7-h day/night cycle as previously described [Caroti et al., 2015]. Experiments in *Drosophila melanogaster* were carried out using strain w1118 (BDSC Stock # 5905, donated by Micheal Ashburner, University of Cambridge) acquired from the Ingrid Lohmann's Lab (COS, Heidelberg). *Megaselia abdita* culture was acquired from Urs Schmidt-Ott (The University of Chicago, Chicago, USA), which had previously received the cultures from Johannes Jäger (Centre for Genomic Regulation, Spain). The culture was maintained at 25 ˚C with a constant 16/8-h day/night cycle.

Egg collection: Eggs of *Chironomus* were collected in a water filled glass dish that sat in a basket full of adult flies (50 – 200 adults) over night. Usually, all stages of early development could be found in a collection of around 100 synchronized eggs in one egg package. The preferred stage was used for subsequent experiments or eggs stored at room temperature until further use. Eggs of *Drosophila* were collected on a 1% agar apple juice plate with a droplet of food (fresh yeast in H_2O) and plate put to the flies for 15-20 minutes to ensure a synchronized deposition. Egg of *Megaselia* were collected on a 1% agar plate with a droplet food (mix of fish flakes, tiny bit of dry or fresh yeast in H_2O) for 15-20 minutes to ensure a synchronized deposition. Collected embryos were stored on the agar plate at 25 ˚C until further use (e.g., fixation or injection).

4.2.2 Cloning, RNA synthesis and fluorescent protein generation

slam and GFP-slam: To generate a template for in vitro mRNA synthesis for the full-length coding sequence (CDS) of *slam* fused to GFP, a fragment encoding GFP-slam was

amplified by PCR from pMT-GFP-slam [Wenzl et al., 2010] (gift from J. Großhans) using primer pair 5'-GAATACAAGCTTGCTTGTTCTTTTTGCAGAAGCTCAGAATAAACGCTCAACTTTGGCAGATAAAATG/5'-AACAGGTCTCTTCGATCAGACCTCCACGGCCCTCCGGTCCATCAG, digested with HindIII and SalI, and ligated in the respective cloning sites in pSP35T as described [Urbansky et al., 2016]. The resulting pSP-GFP-slam was subjected to site-directed mutagenesis with primer pair 5'-CGTGACCACCCTGACCTACGGCGTG/5'-AGGGTGGGCCAGGGCACG to add a GFPF65L mutation that resulted in pSP-eGFP-slam. mRNA of full-length slam was generated using pCS2-Slam as template [Wenzl et al., 2010].

Megaselia-basigin: Mab-basigin was essentially cloned as described [Caroti et al., 2018]. Mab-bsg was identified from genome and transcriptome sequences. A fragment encompassing the full open reading frame was PCR amplified using Primer 5'-GGCTCCGCCGGCTCCGCCGCCGGCTCCGGCGAGGTGATGGTGAGCAAGGGCGAGGAGCTG / 5'-TTTATCTGCCAAAGTTGAGCGTTTATTCTGAGC and used in a Gibson Assembly to generate a 3' fusion with eGFP in a pSP expression vector (pSP-Mab-bsg-eGFP). RNA was in vitro transcribed using SP6 Polymerase (Roche), capping and polyA-tailing was performed using ScriptCap Cap 1 Capping System and Poly(A) Polymerase Tailing Kit (CellScript).

Gap43-eGFP: To visualize membranes, a GAP43-eGFP fusion construct was used. To obtain a template for mRNA synthesis, the Gap43-eGFP coding sequence was generated by in-frame Gibson cloning of the Gap43 encoding sequence, a short linker (GSAGSAAGSGEV), and a previously published pSP vector with 3'-terminal eGFP pSP-Mab-bsg-eGFP [Caroti et al., 2018].

Diaphanous: A fluorescent reporter for subcellular Diaphanous localization was generated using the GFP-Dia-N fragment that was described previously [Rousso et al., 2013]. To obtain the template for mRNA synthesis, GFP-Dia-N was PCR amplified from GFP-Dia-N-pUAST-attB (gift from B. Shilo) using primer pair 5'-AACAGGTCTCACATGGTGAGCAAGGGCGAGGAGC TGTTCACCGG/5'-AACAGGTCTCTTC-

GACTACGCCACACCATTAGCCTCCATCAA, digested with BsaI and SalI, and ligated by matching overhangs into NcoI/SalI digested pSP35T. The Kozac sequence was optimized using site-directed mutagenesis with primer pair 5'-TTGGCAGATAAAAT-GGTGAGCAAG/5'-AGTTGAGCGTTTATTCTG, resulting in pSP-GFP-Dia.

E-cadherin: The template for mRNA encoding a fluorescent reporter for subcellular localization of E-cadherin was generated by in-frame Gibson cloning of E-cadherin and a short linker (GSAGSAAGSGEV) into a pSP vector carrying a 3' terminal eGFP CDS. The fragment encoding full length E-cadherin and linker was amplified from pBabr-5sqh-E-Cad-stf-mRuby3-3sqh (unpublished, gift from YC Wang) using primer pair 5'-CGCTCAACTTTGGCAGATAAAATGTCCACCAGTGTCCAGCGAAT-GTC/5'-CCTCGCCCTTGCTCACCATCACCTCGCCGGAGCCGGC; the pSP backbone including eGFP was amplified using 5'-CCATGGTGAGCAAGGGC-G/5'-TTTATCTGCCAAAGTTGAGC. RNA was in vitro transcribed using SP6 Polymerase (Roche). Capping and polyA-tailing were performed using ScriptCAP 1 Capping System and Poly(A) Polymerase Tailing Kit (CellScript). A *Chironomus* orthologue of E-cadherin (Cri-E-cad, GenBank_XXXXXX) was identified from transcriptome sequences and cloned after PCR amplification from cDNA. The template to generate Cri-Ecad double-stranded RNA (dsRNA) comprised pos. 2677 to 3695 (pos. 1 refers to first nucleotide in ORF). The fragment was amplified by PCR with primer pair 5'-TAATAC-GACTCACTATAGGGAGACCACGCTGTTGACAAGAGCGGATCGA/
5'-TAATACGACTCACTATAGGGAGACCACCCTCGCATTGTTGGCG-CATATG with included T7 promotors. dsRNA synthesis was carried out as described [Urbansky et al., 2016]. Lifeact-mCherry was generated as a recombinant protein as described [Caroti et al., 2018].

Cofilin: The template for mRNA encoding Cofilin was generated by in-frame Gibson cloning of Cofilin into a pSP vector (LP595). The fragment encoding full length Cofilin amplified from *Megaselia* cDNA using primer pair 5'-AACGCTCAACTTTG-GCAGATAAAATGGCATCTGGAGTAACCGTTTCTG/5'-GTGGTA-ACCAGATCCTCTAGATTATTGACGATCGGTTGCGCGC. mRNA was in vitro

transcribed using SP6 Polymerase (Roche). Capping and polyA-tailing were performed using ScriptCAP 1 Capping System and Poly(A) Polymerase Tailing Kit (CellScript).

4.2.3 Immunohistochemistry.

Embryo fixation: Embryos were fixed for 40 minutes in a mixture of 8.2% formaldehyde in PBS (137 mM NaCl, 2.7 mM KCl, 10 mM Na2HPO4, 2 mM KH2PO4, pH 7.4) and n-heptane (700 µl PBS, 200 µl 37% formaldehyde, 200 µl n-heptane). For devitellinization of *Chironomus* and *Drosophila* embryos, all liquids were removed and 500 µL of n-heptane and then 500 µL of 95% ethanol were added. Embryos were shaken vigorously by hand for 40 seconds. Embryos were then washed in 90% ethanol and stored in 90% ethanol at 4 ºC (not longer than 2-3 weeks). *Megaselia* devitellinization was done manually (as described PhD Thesis Caroti, 2016). Vitellin membrane was removed using 2 sharp needles with embryos on an agar plate covered with 90% ethanol to ensure they would not dry out.

Phallacidin and DAPI staining: Staining of DNA and F-actin were carried out essentially as described with minor modifications [Urbansky et al., 2016; Caroti et al., 2018]: the Phallacidin stock (200 units/ml, Invitrogen B607) was diluted in PBS (1:50), and embryos were stained for 3 hours at room temperature. After an incubation time of 2 hours DNA was stained by using 4',6-diamindino2phenylidole (DAPI, Life Technology D1306) at a final concentration of 5 µg/ml and incubated for another hour, followed by several washes in PBS.

Anti-GFP antibody staining: To reveal the localization of eGFP-fusion proteins in fixed tissues, embryos were first injected with mRNA encoding the respective reporter at pole cell stage. Following fixation and methanol-free devitellinization, antibody staining against GFP was carried out essentially as described Urbansky et al., 2016. Briefly, embryos were rehydrated, washed, blocked with 5% blocking solution (Roche: 11 921 637 001) in PBT for at least two hours at room temperature, and then incubated with primary antibody (1:250, anti-GFP chicken IgY unconjug. 2mg/ml; Life Technologies, A10262)

in 5 % blocking solution overnight at 4 °C. Embryos were washed and incubated with secondary antibody (1:250, donkey anti-chicken Alexa 594, Jackson, 703-505-155) for 3.5 hours at room temperature. Embryos were then washed, transferred to glycerol/PBS and mounted for imaging.

Microtubule antibody staining: To detect microtubules same protocol as for the anti-GFP detection was used. Microtubules were detected using anti-alpha-tubulin conjugated with Alexa488 (1:250, Sigma-Aldrich, 16-232) with fixation and blocking as described above and incubation overnight at 4 °C.

***In situ* hybridization**: For *in situ* hybridization *Megaselia* embryos (control or injected) were heat fixed (28% (w/v) NaCl, 5% (v/v) Triton X100 in H_2O) 7 hours after egg lay. After some washing steps embryos were transferred to MeOH for storage at -20 °C. Embryos were manually devitellinized (as described in "Fly keeping"). *In situ* hybridization of *Megaselia* embryos was conducted as described previously [Caroti et al., 2018; PhD Thesis Caroti, 2016]. Embryos were cleared in Xylene first via ethanol and methanol washes transferred to PBT and treated with proteinase K (0.08 U/ml) in PBT. Then embryos were carefully transferred to HYB (50% Formamide, 5X SSC, Torula yeast 5mg/ml, Heparin 50 µg/ml, Tween-20 0.1% and filled up with H2O). The probe was prepared in HYB in a concentration of 1 - 2 ng/µl and hybridization performed over-night. Blocking was conducted using 5% goat serum and incubation with DIG-antibody carried out in a dilution of 1:2000 for 1 hour. Detection was done by NBT/BCIP (NBT 0,7mg/ml; BCIP 0,35mg/ml) staining for ddc for 3 hours, for bsg for 4 hours and for *Mmp1* 3.5 hours.

4.2.4 Injections of small compound inhibitors, mRNA, dsRNA, and recombinant protein.

General injection procedure: For injection embryos were collected at pole cell stage if not indicated otherwise. The jelly around the *Chironomus* eggs were removed by a 5 % bleach solution for for about 1 min and washed several times in H_2O afterwards. *Megas-*

elia and *Drosophila* embryos were bleached respectively in 50% or 100% bleach solution on a agar plate for 2 minutes and washed for 2 minutes under slowly running H_2O. Then embryos were aligned along a glass capillary, dried and covered with halocarbon oil (1+3 of 27-halocarbon oil and 700-halocarbon oil). For injection, the needles (Pulling protocol, *Mab*: P: 500; Heat: 500; Pull: 115; Vel:15; Time: 250; Pulling protocol *Cri* (2steps): Heat: 500, Pull: 100, Velocity: 10, Time: 250, the second phase with Heat: 550, Pull: 60, Velocity: 40, Time: 250) were backfilled with 0.2-0.5 µl (using micro loader tips) and opened by breaking the tip with a fine tweezer. Injections were carried out usually at an injection pressure of 600-800 and a constant pressure of 100 with 0.1 s injection time. After injection, the slides were placed in a moist chamber (a petri-dish with wet filter paper) for development until the desired stage.

Small compound inhibition in *Chironomus*: Small compound inhibitors were injected at the following concentrations: alpha-amanitin (50 µg/µl; (Edgar and Schubiger, 1986)), cycloheximide (0.5 mM; (Edgar and Schubiger 1986)), SMIFH2 (100 nM; (Rizvi et al., 2009) and Cytochalasin-D (2mg/ml), Colchicine (5 mM), H1152 (10 mM), Phallacidin (200 units/ml), Calyculin (Ishihara et al., 1989). alpha-amanitin and cycloheximide were injected at onset of blastoderm formation. Phallacidin, Cytochalasin D, colchicine and Rock inhibitor (H1152) were injected at syncytial blastoderm stage or at the onset of blastoderm formation as indicated in the text or figures; SMIFH2 and Calyculin-alpha was injected at the onset of blastoderm formation.

Overexpression experiments in *Chironomus*: Unless indicated otherwise, injection of capped mRNAs were performed at pole cell stage (about 2 -3 hours after egg lay) with the following concentrations: Dme-slam-eGFP (2.2 mg/ml) GAP43-GFP (1.66µg/µl) and Dme-E-cad-GFP (2 µg/µl), Dme-slam (2 mg/ml), fog 1.13 (mg/ml), Mab-myosin (light chain) (1.2 mg/ml), Dme-dunk (1 mg/ml), Dme-bottleneck (1 mg/ml), Mab-basigin-eGFP (3.3 mg/ml), Mab-cofilin (3.3 mg/ml).

Live nuclear labelling in *Chironomus*: Injection of Histone H1 was performed at pole cell stage (about 2h after egg lay) (0.7 µg/µl). Injection of recombinant Lifeact-mCherry (2

mg/ml) was performed before last nuclear division (about 6 hours after egg lay).

E-cadherin experiments in *Chironomus*: For global knockdown of E-cadherin in *Chironomus*, Cri-E-cad dsRNA was injected at nuclei migration stage, for local knockdown at late nuclei migration stage (after last nuclear division); concentration was 800 µg/µl. Restricted Cri-E-cad knockdown was established by a time series experiment in analogy to previously published work [Rafiqi et al., 2010]. Briefly, Cri-E-cad dsRNA was injected into the center of the embryo. If injection was carried out before onset of nuclear migration (corresponding to 3 hours after deposition and 4 hours prior to onset of blastoderm formation at 25 ˚C), cellularization did not start anywhere in the embryo and peripheral nuclear divisions were blocked. Restricted knockdown was then defined such that blastoderm formation continued and completed at the poles, but not the injection area in the center of the embryo. Ideal timing for E-cad dsRNA injection for global KD was thus determined to be at 5 hours after deposition (corresponding to 2 hours prior to onset of blastoderm formation at 25 ºC). Local rescue with E-cadherin-eGFP in Cri-E-cad RNAi embryos was carried out by injection after the penultimate syncytial nuclear division, about 1 hour before onset of blastoderm formation in a 3/1 mix with recombinant Lifeact-mCherry.

Actin staining in *Megaselia*: Injection of Lifeact-mCherry (2 mg/ml) into *Megaselia* for staining blastoderm/serosa cells were performed before last nuclear division (about 2.5 hours after egg lay at 25 ˚C). To stain yolk actin in *Megaselia* injections of Lifeact-GFP (1.1 µg/µl) were performed when cellularization was completed (about 3.5 hours after egg lay at 25 ˚C).

Overexpression experiments in *Megaselia*: To interfere with cortical actin in the yolk sac cofilin mRNA (3.3 mg/ml) injections were performed when cellularization was completed to restrict staining to yolk sac. To stain yolk sac membrane basigin-eGFP (3.3 mg/ml) was injected into *Megaselia* after cellularization was completed to ensure staining of the yolk membrane only, fast folding capacity of eGFP made detection possible about 90 minutes post injection (injections as described in Caroti et al., 2018).

Knock-down experiments in *Megaselia*: To knock down *Mmp1* dsRNA of *Mmp1* (3.9 mg/ml) was injected at early nuclear migration (about 2 hours after egg lay) in a 1:1 mix with Lifeact-mCherry (as described in Caroti et al., 2018). The injections to knock down zen (zen dsRNA (see PhD Thesis Caroti, 2016) was performed about 2 hours after egg lay. To knock down *slam*, dsRNA of *Mab-slam* was injected at about 2 hours after egg lay.

4.2.5 Microscopy

Imaging of cellularization (DIC and confocal): Dynamics of blastoderm formation in *Chironomus* were recorded using DIC and confocal microscopy. Embryos were imaged within their central third along their anterior-to-posterior axis without random orientation along the dorsoventral axis. Time lapse recordings with DIC were used to analyze progression of cellularization in embryos injected with alpha-amanitin, Cycloheximide, SMIFH2, Colchicine, or H1152 compared to water injected control embryos. Recordings were taken using a Nikon Eclipse Ti with a 20x objective (Nikon Plan Apo 20x/0.75 OFN25 DIC N2) for 2.5 hours in 2 minuntes intervals at the optical median plane of a sagittal section.

DIC imaging of extraembryonic tissue: Dynamics of yolk pulsations in *Megaselia abdita* were recorded using DIC microscopy. Embryos were aligned laterally or dorsally to obtain pulsations in the region of serosa anlage. Recordings were taken using a Nikon Eclipse Ti with a 20x objective (Nikon Plan Apo 20x/0.75 OFN25 DIC N2) for 4 hours in 20 seconds intervals at the optical median plane of a sagittal section.

Live confocal imaging: Time lapse recordings with confocal microscopy were performed to reveal F-actin dynamics via Lifeact-mCherry in otherwise wildtype embryos and embryos that were additionally injected with mRNA for *slam* and E-cad-eGFP. Time lapse recordings were taken by single-photon confocal imaging in a Leica system (SP8) using a 63x immersion objective (HC PL APO 63x/1.30 Glyc CORR CS2). Cellularization was recorded in 0.42 µm sections over a range of about 30 µm, with either single or simulta-

neous detection of mCherry and eGFP. Field of view was 1024x1024 pixels, with voxel size 0.24 x 0.24 x 0.42 µm and volumes were collected at 5 min intervals for 2.5 hours. Simultaneous confocal imaging *Chironomus*: Early embryonic development (2-7 h after egg lay) were recorded with simultaneous detection of TexasRed (Histone H1) and brightfield. Volumes were collected at 6 min intervals for 5 hours with a voxel size of 0.24 x 0.24 x 2 µm over a z range of about 50 µm. Immunohistochemically labeled embryos were imaged as confocal z-stacks (8bit) using 63x magnification and identical voxel sizes. Unless noted otherwise, images in figure panels are xz-reslices of z-stacks using an average intensity projection of 2.4 µm.

Simultaneous confocal imaging *Megaselia*: Embryos were injected in the syncytial blastoderm stage with either recombinant Lifeact-mCherry (wildtype analyses) or a 1:1 mix of Lifeact-mCherry and *Mab-Mmp1* dsRNA. Because a protein trap line equivalent to the *Drosophila basigin* reporter does not exist in *Megaselia* [Reed et al., 2004], we reasoned that injection of mRNA encoding Mab-bsg-eGFP into the yolk sac could mimic the desired properties of the *Drosophila* reporter as closely as possible and with minimal side effects in *Megaselia* . To express Mab-bsg-eGFP specifically in the yolk sac, capped mRNA of the reporter was injected after germband extension had started and yolk sac formation is thought to be completed [Rafiqi et al., 2010]. Time lapse recordings were taken along the dorsal midline anterior to the extending germband where serosa and yolk sac were in contact. For the analysis of early, pre-disjunction tissue interaction, recordings were taken 90 – 120 min after onset of germband extension; for the analysis of a post-disjunction tissue interaction, recordings were taken 140 – 190 min after onset of germband extension. Recordings were made by single-photon confocal imaging on a Leica system (SP8) using a 63x immersion objective (HC PL APO 63x/1.30 Glyc CORR CS2). Volumes were recorded in 15 to 20 confocal sections of 1 µm with simultaneous detection of mCherry and eGFP. Voxel size was 0.24 × 0.24×1 µm and volumes were collected at 20-s intervals for 10 min.

DIC imaging in situs: *In situ* stained embryos were imaged at a Leica DB5000 with a 10x Objective. Embryos were oriented by rolling them under the cover slip and images taken

in the DIC mode.

Spinning disk imaging: High resolution actin dynamics were taken from embryos injected in pole cell stage (2 hours AED) with *slam* and at nuclei migration (4 hours AED) with recombinant Lifeact-mCherry. Time lapse recordings were taken by Spinning Disk using a 100x immersion oil objective (100x N 1.4 Oil). Sections were recorded in 0.12 µm steps over a range of 20 µm with detection of mCherry. Voxel size was 0.067 x 0.067 x 0.12 and volumes were collected at 100 ms/frame over 5 minutes.

4.2.6 Embryo shrinking assay

Chironomus embryos were lined up, covered with oil, and injected with *slam* mRNA (slam^{OE}), H_2O (control), or left without injection (wt or unfertilized eggs). At the end of blastoderm formation, embryos were washed briefly with heptane to remove the halocarbon oil, immersed in 10x PBS, 5x PBS or 2.5x PBS, and embryo behavior was captured in time lapse recordings using a Nikon SMZ18. Differences in volume were approximated by differences in area in a single focal plane, with error bars indicating standard deviation.

4.2.7 Image analysis (Cellularization project)

General cell measurements: Unless otherwise noted, quantitative measures were carried out using FIJI [Schindelin et al., 2012]. Membrane length, cell height and maximal cell width were measured as line length; maximal cell width was measured at the apicobasal position that corresponded to the maximal area in the transverse cell section; columnarization of cells was calculated as the ratio of cell-height and maximal-cell-width.

Circularity measurements: Cell circularity was measured manually for fixed specimens stained with Phallacidin. Measurements were taken at the basal side (furrow canal) using the polygon tool (Fiji) in an en-face view. Membrane invagination depth was measured manually by the line tool in an xz-resclice and circularity plotted for the respectively ob-

tained depth. Circularity was calculated: C = 4 πA/P2 [A, area; P, perimeter].

Apical and basal tapering: The tapering index (TI) was calculated by subtracting the actual cell volume from the ideal volume of a cell column and then normalizing it to the ideal column volume. The tapering index was determined separately for the apical (from absolute cell apex to 5 µm height) and basal side of the cell (from 5 µm height to absolute basal).

Actin intensity measurement: The distribution of actin at individual membranes was measured manually along the emerging membrane using the "segmented line" tool in single plane cross-section. Intensities were subsequently plotted using the "plot profile" function. Kymograph heatmaps were generated from a mean of 10 membranes selected at each time point; plots were generated in Matlab (Surface Plot (Version 2016b)).

GFP intensity measurement: The distributions of GFP-slam and Dia-eGFP within a cell were analyzed by manually defining areas of cell outline (F-actin), nucleus (DNA), and cytoplasm (neither F-actin nor DNA) and then reporting the fluorescent signal indicating GFP-slam or Dia-eGFP relative to the total measured fluorescence in the same channel per cell. Figure panels were assembled and layouted in Adobe Illustrator.

Germband elongation tracking: Progression of the germband over time was measured using Matlab skript "Stackmarker" to follow the tip of the elongating germband. To extract the data points script "ExtractGBFromMask" was used and normalized with "GetNormalizedTimeForGB" and data potted using the scatter function.

4.2.8 Image analysis (Yolk project)

Cross Correlation: Quantification of cross correlation of yolk and membrane movement was done as using the Lucas-Kanade optical flow method which was implemented in the computer vision system toolbox in Matlab (Version 2016b). Scripts used for analysis were written by Everado Gonzales and provided on Github. Flow was analyzed for basigin

staining (yolk) and Lifeact staining (serosa) together with a manual segmentated mask of serosa cells. Each cell was analyzed separately using the script "MembraneXYolkFlow". Parameters were adjusted as followed: Smoothness: 0.03; Velocity difference: 0.05; Max. Iteration: 3

Auto Correlation: Quantification of autocorrelation of yolk movements was dine using the Horn and Schunk optical flow method which was implemented in the computer vision system toolbox in Matlab (version 2016b). Scripts used for analysis were written by Everado Gonzales and provided on Github or in the appendix. The oscillations of the yolk were analyzed in a window of 100x100 px as that movements form the extending germband have little or no effect on the analysis. The following parameters were used for DIC time lapse recordings: Smoothness: 0.02; Velocity difference: 0.03; Max. Iteration: 3. Auto correlation of time lapse recordings in which basigin-eGFP and Lifeact-mCherry were used as a marker by manually generated single cell segmentation as described above. The following parameters were used: Smoothness: 0.03; Velocity difference: 0.05; Max. Iteration: 3.

Flow velocity: Directionality of the flow was analyzed using Matlab tool PIVLAB. Movies used for the analysis were taken at a DIC with 20 x objective at a resolution of 20 sec. Parameters used for pre-processing: Wiener denoise set to 3. For analysis: Passes 32, 16,8. Strongest movements were observed in X and extracted via the export tool. Post processing: vecotors < -3 and > 3 were excluded since movements of this distance were not expected within the short frequency of the movies taken.

4.2.9 Statistics

Boxplots were generated by using Excel and statistical comparison were performed via Excel's implemented students t-test (two sided, unpaired). All samples fit normal distribution; P-values of student's t-test are indicated in the figure legend. The size of n (embryos and cells) is indicated on each figure.

Appendix

Following Matlab scripts (Matlab Version 2016b) were developed in collaboration with Everado Gonzales for the qunatitative evaluation of confocal microscopy recordings. Detailed description on the use of the scripts can be found in the Materials and Methods section.

Stack Marker

```
function Mask=StackMarker(Stack,MaskAlt)
%StackMarker(Stack)
%Displays all frames in Stack, and and uses user input to
% creates an output stack Mask.
%
%User input:
%-LeftMouseButton: marker
%-RightMouseButton: eraser
%-RightArrow: next frame
%-LeftArrow: previous frame
%-UpArrow: increase marker size
%-DownArrow: decrease marker size
%-e: zoom in!
%-q: zoom out!
%-a,w,s,d: navigate image
%-spacebar: toogle Play/Pause
%-r: rewind Stack
%-esc: close window, terminate function

Height=size(Stack,1);
Width=size(Stack,2);
Len=size(Stack,3);
HeightRange=Height;
WidthRange=Width;
   MaskAlt=false(size(Stack));
   end
%figure setup
ScreenSize = get(0,'ScreenSize');
H=figure('Position', ScreenSize);
set(H, 'KeyPressFcn', @KeyReader)
set(gcf,'ButtonDownFcn',@StartMarker)
set(gcf,'windowbuttonupfcn',@StopMarker)
set (gcf, 'WindowButtonMotionFcn', @MouseReader);
Pause=true;
try
   [y,Fs] = audioread('GunReload.wav'); %Can a man not have his fun?
   GunSound=true;
catch
   GunSound=false;
end %Try to read .wav file
WidthStart=1;
WidthEnd=WidthStart-1+WidthRange;

HeightStart=1;
HeightEnd=HeightStart-1+HeightRange;
X=0;
Y=0;
```

```
KernelRadius=3;
Kernel=strel('disk',KernelRadius);
ii=1;
while ishandle(H)
   Image=uint16(zeros(HeightEnd-HeightStart+1,WidthEnd-WidthStart+1,3));
   LocalMask=Mask(HeightStart:HeightEnd,WidthStart:WidthEnd,ii);
   Image(:,:,1)=Stack(HeightStart:HeightEnd,WidthStart:WidthEnd,ii)...
      +uint16(MaskAlt(HeightStart:HeightEnd,WidthStart:WidthEnd,ii)*10000);
   Image(:,:,2)=Stack(HeightStart:HeightEnd,WidthStart:WidthEnd,ii)...
      +uint16(LocalMask*10000);
   Image(:,:,3)=Stack(HeightStart:HeightEnd,WidthStart:WidthEnd,ii);
   imshow(Image,'InitialMagnification','fit')
   text(20,20,['Plane ',num2str(ii),' of ', num2str(Len)],'color',[0,1,0])
   text(20,30,['(X,Y) = (', num2str(X), ', ',num2str(Y), ')'],'color',[0,1,0])
   drawnow
   Mask(HeightStart:HeightEnd,WidthStart:WidthEnd,ii)=LocalMask;
   WidthRange=WidthEnd-WidthStart+1;
   HeightRange=HeightEnd-HeightStart+1;
   if ~Pause
      ii=ii+1;
   end
end
function KeyReader(src, event) %Keyboard event input function
   switch double(event.Character)
      case 120 % x
         error('stop')
      case 27 %Esc
         close
      case 32 %Spacebar
         Pause=~Pause;
      case 29 %RightArrow
        if ii<Len ii=ii+1; end
         LocalMask=Mask(HeightStart:HeightEnd,WidthStart:WidthEnd,ii);
      case 28 %LeftArrow
         if ii>1 ii=ii-1; end
         LocalMask=Mask(HeightStart:HeightEnd,WidthStart:WidthEnd,ii);
      case 31 %DownArrow
         if KernelRadius>1 KernelRadius=KernelRadius-1; end
         Kernel=strel('disk',KernelRadius);
      case 30 %UpArrow
         KernelRadius=KernelRadius+1;
         Kernel=strel('disk',KernelRadius);
      case 114 % r
         ii=1;
         LocalMask=Mask(HeightStart:HeightEnd,WidthStart:WidthEnd,ii);
         if GunSound        %Can he not?
            sound(y,Fs);
         end
      case 100 % d
         if WidthEnd+floor(WidthRange/10)<=Width
            WidthEnd=WidthEnd+floor(WidthRange/10);
            WidthStart=WidthStart+floor(WidthRange/10);
         end
         LocalMask=Mask(HeightStart:HeightEnd,WidthStart:WidthEnd,ii);
      case 97 % a
         if WidthStart-floor(WidthRange/10)>=1
            WidthEnd=WidthEnd-floor(WidthRange/10);
            WidthStart=WidthStart-floor(WidthRange/10);
         end
          LocalMask=Mask(HeightStart:HeightEnd,WidthStart:WidthEnd,ii);
      case 119 % w
          if HeightStart-floor(HeightRange/10)>=1
            HeightEnd=HeightEnd-floor(HeightRange/10);
            HeightStart=HeightStart-floor(HeightRange/10);
          end
          LocalMask=Mask(HeightStart:HeightEnd,WidthStart:WidthEnd,ii);
      case 115 % s
          if HeightEnd+floor(HeightRange/10)<=Height
            HeightEnd=HeightEnd+floor(HeightRange/10);
            HeightStart=HeightStart+floor(HeightRange/10);
          end
          LocalMask=Mask(HeightStart:HeightEnd,WidthStart:WidthEnd,ii);
      case 113 % q
                WidthRange=floor(WidthRange*4/3);
         if WidthStart+X-floor(WidthRange/2)>=1
```

```
            WidthStart= WidthStart+X-floor(WidthRange/2);
        else
            WidthStart=1;
        end
        if WidthStart+WidthRange-1<=Width
            WidthEnd=WidthStart+WidthRange-1;
        else
            WidthEnd=Width;
        end
        WidthRange=WidthEnd-WidthStart+1;

        HeightRange=floor(HeightRange*4/3);
        if HeightStart+Y-floor(HeightRange/2)>=1
            HeightStart=HeightStart+Y-floor(HeightRange/2);
        else
            HeightStart=1;
        end
        if HeightStart+HeightRange-1<=Height
            HeightEnd=HeightStart+HeightRange-1;
        else
            HeightEnd=Height;
        end
        HeightRange=HeightEnd-HeightStart+1;
                LocalMask=Mask(HeightStart:HeightEnd,WidthStart:WidthEnd,ii);
    case 101 % e
        WidthRange=floor(WidthRange*2/3);
        if X-floor(WidthRange/2)>=1
            WidthStart=WidthStart+X-floor(WidthRange/2);
        else
            WidthStart=1;
        end
        if WidthStart+WidthRange-1<=Width
            WidthEnd=WidthStart+WidthRange-1;
        else
            WidthEnd=Width;
        end
        WidthRange=WidthEnd-WidthStart+1;
        HeightRange=floor(HeightRange*2/3);
        if Y-floor(HeightRange/2)>=1
            HeightStart=HeightStart+Y-floor(HeightRange/2);
        else
            HeightStart=1;
        end
                if HeightStart+HeightRange-1<=Height
            HeightEnd=HeightStart+HeightRange-1;
        else
            HeightEnd=Height;
        end
        HeightRange=HeightEnd-HeightStart+1;

        LocalMask=Mask(HeightStart:HeightEnd,WidthStart:WidthEnd,ii);

    otherwise
        %chill
  end
end
function MouseReader(object, eventdata)
C=get(gca,'CurrentPoint');
X=floor(C(1,1));
Y=floor(C(1,2));
% if  ~(X>0&&X<Width&&Y>0&&Y<Height)
%     X=1;
%     Y=1;
% end
  end
function StartMarker(object, eventdata)
  Button=get(gcf, 'SelectionType');
     set(gcf,'windowbuttonmotionfcn',{@Marking,Button})
  set(gcf,'windowbuttonupfcn',@StopMarker)
  set(gcf, 'Pointer', 'crosshair' );

  Mask2=false(size(LocalMask));
  C=get(gca,'CurrentPoint');
  X=floor(C(1,1));%+WidthStart;
  Y=floor(C(1,2));%+HeightStart;
```

```
        switch Button
        case 'normal'
            if Y>0 && Y<size(Mask2,1) && X>0 && X<size(Mask2,2)
                Mask2(Y,X)=true;
                Mask2=imdilate(Mask2,Kernel);
                LocalMask=LocalMask+Mask2;
            end
        case 'alt'
            if Y>0 && Y<size(Mask2,1) && X>0 && X<size(Mask2,2)
                Mask2(Y,X)=1;
                Mask2=imdilate(Mask2,Kernel);
                LocalMask=LocalMask.*~Mask2;
            end
        case 'extend'
            LocalMask=false(size(LocalMask));
    end
end

function Marking(src,eventdata,Button)

    Mask2=false(size(LocalMask));
    C=get(gca,'CurrentPoint');
    X=floor(C(1,1));%+WidthStart;
    Y=floor(C(1,2));%+HeightStart;

    switch Button
        case 'normal'
            if Y>0 && Y<size(Mask2,1) && X>0 && X<size(Mask2,2)
                Mask2(Y,X)=true;
                Mask2=imdilate(Mask2,Kernel);
                LocalMask=LocalMask+Mask2;
            end
        case 'alt'
            if Y>0 && Y<size(Mask2,1) && X>0 && X<size(Mask2,2)
                Mask2(Y,X)=1;
                Mask2=imdilate(Mask2,Kernel);
                LocalMask=LocalMask.*~Mask2;
            end
        case 'extend'
            LocalMask=false(size(LocalMask));
    end

end
function StopMarker(src,evendata)
    set(gcf,'windowbuttonmotionfcn',@MouseReader)
    set(gcf,'windowbuttonupfcn','')
    set(gcf, 'Pointer', 'arrow');
end
end
```

Extract Germband from Mask

```
%extraction of coordinated from tracks (each point of the track is a "region" in the image, safed as a centroid)
%coordinates are safed in a table
function[GB] = ExtractGBFromMask( MaskStack )

Coordinates  = [];

for ii = 1:size(MaskStack,3)
    Image = MaskStack(:,:,ii);
    Centroid = regionprops(Image,'Centroid');
    if length(Centroid) > 0
        for jj = 1:length(Centroid)
            Coordinates = [Coordinates;Centroid(jj).Centroid];
        end

    end

end
```

```
%to calculate GBE from the total length of the embryo

GB = Coordinates(:,1)-Coordinates(1,1)/Coordinates(2,1)-Coordinates(1,1);
GB = GB/GB(2);
GB = (1-GB)*100;
GB = GB(2:end);


end
```

Get normalized time for germband

```
function [GBwithtime] = GetNormalizedTimeForGB(NormGB)
norm = NormGB > 9;
positivetime = transpose(1:length(norm(norm == 1)));
positivetime = positivetime-1;
negativetime = transpose(1:length(norm(norm == 0)));
negativetime = flipud(negativetime)*-1;
normalizedtime = [negativetime;positivetime];
GBwithtime = [normalizedtime NormGB];

end
```

Stack Reader

```
function Stack=StackReader(StackFile,Subsampling)
%Stack=StackReader(StackFile,Subsampling,Plotting,Speed)
%Read the .tif stack StackFile(string) and generate a double stack Stack.
%Boolean input Plotting plots every the image making a pause of
%1/Speed seconds. Also Subsampling...

display('Reading Image Stack')
tic

if nargin<2
   Subsampling=1;
end

InfoImage=imfinfo(StackFile);
mImage=InfoImage(1).Width;
nImage=InfoImage(1).Height;
NumberImages=length(InfoImage);
TStack=uint16(zeros(nImage,mImage,NumberImages));
TifLink = Tiff(StackFile, 'r');

for j=1:NumberImages
   TifLink.setDirectory(j);
   TStack(:,:,j)=uint16(TifLink.read());
end
TifLink.close();

if Subsampling>1

  TStack=TStack(1:Subsampling:end, 1:Subsampling:end,1:Subsampling:end);

end

Stack=uint16(zeros(size(TStack,3),...
            size(TStack,1),...
            size(TStack,2))); %Swap coordinates axes=>Z (not X) now main axis

for ii=1:size(TStack,3) %Transform to double stack
```

```
   Stack(ii,:,:)=TStack(:,:,ii); %Swap coordinates axes=>Z (not X) now main axis

end

toc

end
```

Flow analysis – Flow test

```
Scale=8;
opticFlow = opticalFlowHS('MaxIteration',5);

ScreenSize = get(0,'ScreenSize');
H=figure('Position', ScreenSize);

%while  ishandle(H)
   for ii=1:size(Stack,3)

      frameGray = Stack(:,:,ii);
      % Compute optical flow
      flow = estimateFlow(opticFlow, frameGray);
      % Display video frame with flow vectors
      Image=zeros(size(Stack,1),size(Stack,2),3);

      Image(:,:,1)=(flow.Orientation+ pi+0.000001)/(2*pi+0.00001);
      Image(:,:,2)=min(flow.Magnitude*Scale,1);
      Image(:,:,3)=max(frameGray,Image(:,:,2));

      Image=hsv2rgb(Image);
      Image=Image./max(Image(:));
      if ~ishandle(H)
         break
      end
      imshow(Image,'InitialMagnification','fit')
      %writeVideo(VideoObject,Image)

      drawnow

   end
%end
```

Separate cell masks (use before crosscorrelation)

```
MaskErode = MasterMask;
StrEl = strel('disk',3);

for ii = 1:size(MasterMask,3)

   MaskErode(:,:,ii) = imfill(MasterMask(:,:,ii),'holes');
   MaskErode(:,:,ii) = imerode(MaskErode(:,:,ii),StrEl);

end

SingleCellMask = bwlabeln(MaskErode,6);

clear StrEl ; clear ii
```

Crosscorrelation Yolk and Serosa

```
%% init
Start = 1;
End = size(MovieBasal,3);
CellIndex =1; %WT Early--> Mab4: 1,2/ Mab5: 6,9 /Mab8:8',9',11',12'/ Mab9: 3,5,6,7,9,11,13,14,15,16,18
        %Mab12: 2, 5, 6
    %WT Late--> Mab11: 1',2',3,5/ Mab14:3,5,6,7/
        %Mab15:1,2,3wtf?,4?,5?,6/ Mab17: 11,13

    %MMP1 Early--> MMP1_1: 1,2,3,4,5,6,~7'/ MMP1_3: 2,3,4,5/
        %MMP1_5: 2,3,4/ MMP1_6: 1wtf, 2,3

    %MMP1 Late-->  MMP1_19: 2,3,4/ MMP1_20: 1,2,4,6,7,8
        %MMP1_21: 1,2,4,5,6,7,9,10?/ %MMP1_22: 2,4,5,6,7
        %MMP1_23: 1,2',3?,4',5
StackBasal=double(MovieBasal(:,:,Start:End))/2^16;
StackApical=double(MovieApical(:,:,Start:End))/2^16;
Mask = SingleCellMask(:,:,Start:End)==CellIndex;

%% Generate Cell Outlines

CellOutline = false(size(Mask));
StrEl=strel('disk',3);

for ii = 1:size(Mask,3)
  Mask(:,:,ii) = imfill(Mask(:,:,ii),'holes');
  Mask(:,:,ii) = imclose(Mask(:,:,ii),StrEl);
  CellOutline(:,:,ii) = imdilate(Mask(:,:,ii),StrEl) - Mask(:,:,ii);
  CellOutline(:,:,ii) = imdilate(CellOutline(:,:,ii),StrEl);
end
%% Yolk & Membrane Flows

YolkFlowX = zeros(size(StackBasal));
YolkFlowY = zeros(size(StackBasal));
YolkDispX = zeros(1,size(StackBasal,3));
YolkDispY = zeros(1,size(StackBasal,3));

MembraneFlowX = zeros(size(StackApical));
MembraneFlowY = zeros(size(StackApical));
MembraneDispX = zeros(1,size(StackApical,3));
MembraneDispY = zeros(1,size(StackApical,3));

Scale=20;
Start=1;
Stop=size(StackApical,3);

opticFlowApical = opticalFlowLKDoG('ImageFilterSigma',0.2,'GradientFilterSigma',7,'NoiseThreshold',0.001);
opticFlowBasal = opticalFlowLKDoG('ImageFilterSigma',0.2,'GradientFilterSigma',7,'NoiseThreshold',0.001);

%opticFlowApical = opticalFlowHS('Smoothness',0.1,'VelocityDifference',0.05,'MaxIteration',3);
%opticFlowBasal = opticalFlowHS('Smoothness',0.1,'VelocityDifference',0.05,'MaxIteration',3);

H=figure('Position',get(0,'ScreenSize'));

for ii=Start:Stop% size(Stack,3)

  ApicalFrame = StackApical(:,:,ii);
  BasalFrame = StackBasal(:,:,ii);

  % Compute optical flow

  ApicalFlow = estimateFlow(opticFlowApical, ApicalFrame);
  MembraneFlowX(:,:,ii) =ApicalFlow.Vx.*double(CellOutline(:,:,ii));
  MembraneFlowY(:,:,ii) =ApicalFlow.Vy.*double(CellOutline(:,:,ii));
  Aux=MembraneFlowX~=0;
  MembraneDispX(ii) = mean(MembraneFlowX(Aux(:)));
  Aux=MembraneFlowY~=0;
  MembraneDispY(ii) = mean(MembraneFlowY(Aux(:)));

  BasalFlow = estimateFlow(opticFlowBasal, BasalFrame);
```

```
    YolkFlowX(:,:,ii) =BasalFlow.Vx.*double(Mask(:,:,ii));
    YolkFlowY(:,:,ii) =BasalFlow.Vy.*double(Mask(:,:,ii));
    Aux=YolkFlowX~=0;
    YolkDispX(ii) = mean(YolkFlowX(Aux(:)));
    Aux=YolkFlowY~=0;
    YolkDispY(ii) = mean(YolkFlowY(Aux(:)));

   % ----------------Plotting----------------%
    % Display video frame with flow vectors

    ApicalImage=zeros(size(StackApical,1),size(StackApical,2),3);

    ApicalImage(:,:,1)=(CellOutline(:,:,ii).*ApicalFlow.Orientation+pi+0.000001)/(2*pi+0.00001);
    ApicalImage(:,:,2)=min(CellOutline(:,:,ii).*ApicalFlow.Magnitude*Scale,1);
    ApicalImage(:,:,3)=max(ApicalFrame,CellOutline(:,:,ii).*ApicalImage(:,:,2));

    ApicalImage(:,:,1)=(ApicalFlow.Orientation+pi+0.000001)/(2*pi+0.00001);
    ApicalImage(:,:,2)=min(ApicalFlow.Magnitude*Scale,1);
    ApicalImage(:,:,3)=max(ApicalFrame,ApicalImage(:,:,2));

    ApicalImage=hsv2rgb(ApicalImage).*double(CellOutline(:,:,ii));


    BasalImage=zeros(size(StackBasal,1),size(StackBasal,2),3);

    BasalImage(:,:,1)=(Mask(:,:,ii).*BasalFlow.Orientation+pi+0.000001)/(2*pi+0.00001);
    BasalImage(:,:,2)=min(Mask(:,:,ii).*BasalFlow.Magnitude*Scale,1);
    BasalImage(:,:,3)=max(BasalFrame,Mask(:,:,ii).*BasalImage(:,:,2));

    BasalImage(:,:,1)=(BasalFlow.Orientation+pi+0.000001)/(2*pi+0.00001);
    BasalImage(:,:,2)=min(BasalFlow.Magnitude*Scale,1);
    BasalImage(:,:,3)=max(BasalFrame,BasalImage(:,:,2));

    BasalImage=hsv2rgb(BasalImage).*double(Mask(:,:,ii));

    subplot(1,2,1)
    imshow(BasalImage,'InitialMagnification','fit'); hold on
    subplot(1,2,2)
    imshow(ApicalImage,'InitialMagnification','fit'); hold on

    drawnow

end

clear opticFlowApical opticFlowBasal ApicalFlow BasalFlow

MembraneDispY = MembraneDispY(4:end);
YolkDispY = YolkDispY(4:end);


MembraneDispX = MembraneDispX(3:end);
YolkDispX = YolkDispX(3:end);


%% Movement XCorr

WindowSize = 11;

CrossCorrMem = zeros(WindowSize*2+1,length(MembraneDispY)-WindowSize);
CoeffsMem = zeros(1, length(MembraneDispY)-WindowSize);
LagsMem = zeros(1, length(MembraneDispY)-WindowSize);

CrossCorrY = zeros(WindowSize*2+1,length(YolkDispX)-WindowSize);
CoeffsYolk = zeros(1, length(YolkDispX)-WindowSize);
LagsYolk = zeros(1, length(YolkDispX)-WindowSize);

MembraneDispY = MembraneDispY - mean(MembraneDispY);

YolkDispY = YolkDispY - mean(YolkDispY);

[AutoCorrYolk,nAutoCorr]=xcorr(YolkDispY,'coeff');
[AutoCorrMem,~]=xcorr(MembraneDispY,'coeff');


WindowSize = 11;
```

```
CrossCorrMem = zeros(WindowSize*2+1,length(MembraneDispX)-WindowSize);
CoeffsMem = zeros(1, length(MembraneDispX)-WindowSize);
LagsMem = zeros(1, length(MembraneDispX)-WindowSize);

CrossCorrX = zeros(WindowSize*2+1,length(YolkDispX)-WindowSize);
CoeffsYolk = zeros(1, length(YolkDispX)-WindowSize);
LagsYolk = zeros(1, length(YolkDispX)-WindowSize);

MembraneDispX = MembraneDispX - mean(MembraneDispX);

YolkDispX = YolkDispX - mean(YolkDispX);

[AutoCorrYolkX,nAutoCorrX]=xcorr(YolkDispX,'coeff');
[AutoCorrMemX,~]=xcorr(MembraneDispX,'coeff');



for ii = 1:length(YolkDispY)-WindowSize

    [CrossCorrY(:,ii),n] = xcorr(MembraneDispY(ii:ii+WindowSize),YolkDispY(ii:ii+WindowSize),'coeff');
    %[CrossCorrY(:,ii),n] = xcorr(MeanDispYApical(ii:ii+WindowSize),MeanDispY(ii:ii+WindowSize),'biased');
    [~,idx] = max(CrossCorrY(:,ii));
    CoeffsYolk(ii) = CrossCorrY(idx,ii);
    %CoeffsY(ii) = CrossCorrY(n==0,ii);
    LagsYolk(ii) = n(idx);

    [CrossCorrX(:,ii),n] = xcorr(MembraneDispX(ii:ii+WindowSize),YolkDispX(ii:ii+WindowSize),'coeff');
    %[CrossCorrY(:,ii),n] = xcorr(MeanDispYApical(ii:ii+WindowSize),MeanDispY(ii:ii+WindowSize),'biased');
    [~,idx] = max(CrossCorrX(:,ii));
    CoeffsYolk(ii) = CrossCorrX(idx,ii);
    %CoeffsY(ii) = CrossCorrY(n==0,ii);
    LagsYolk(ii) = n(idx);

end

%% Plotting

figure
subplot(2,2,1)
plot(CoeffsYolk); hold on
axis([0 24 -1 1])
title('XCorr Coefficient Over Time')
xlabel('TimePoint')
ylabel('XCorr')
%legend('Y Disp','X Disp')
hold off

subplot(2,2,3)
plot(n,CrossCorrY,'--','LineWidth',0.5)
hold on
plot(n,mean(CrossCorrY,2),'LineWidth',3)
title('Y Displacement XCorr Accross Windows')
xlabel('Lags')
ylabel('XCorr')
hold off

subplot(2,2,2)
plot(YolkDispY*300,'-','Color',[0,0.6,0.6])
hold on
%plot(YolkDispX*100,'--','Color',[0,0.4470,0.7410])
plot(MembraneDispY*200, '-','Color',[1,0,0])
%plot(MembraneDispX*500, '--','Color',[0.8500,0.3250,0.0980])
hold off

title('Displacement Over Time')
xlabel('TimePoint')
ylabel('Adjusted Displacement')
legend('Yolk Y','Membrane Y')
%legend('Membrane Y','Yolk Y', 'Membrane X','Yolk X')
hold off

subplot(2,2,4)
plot(nAutoCorr,AutoCorrYolk)
hold on
```

```
plot(nAutoCorr,AutoCorrMem)
title('Displacement AutoCorrelation')
xlabel('Lags')
ylabel('XCorr')
legend('Yolk Diplacement','Membrane Diplacement')
hold off
```

Autocorrelation

```
%% init
Start = 1;
End = size(Movie,3);
CellIndex = 1; %WT Early--> Mab4: 1,2/ Mab5: 6,9 /Mab8:8',9',11',12'/ Mab9: 3,5,6,7,9,11,13,14,15,16,18
            %Mab12: 2, 5, 6
        %WT Late--> Mab11: 1',2',3,5/ Mab14:3,5,6,7/
            %Mab15:1,2,3wtf?,4?,5?,6/ Mab17: 11,13

        %MMP1 Early--> MMP1_1: 1,2,3,4,5,6,~7'/ MMP1_3: 2,3,4,5/
            %MMP1_5: 2,3,4/ MMP1_6: 1wtf, 2,3

        %MMP1 Late-->  MMP1_19: 2,3,4/ MMP1_20: 1,2,4,6,7,8
            %MMP1_21: 1,2,4,5,6,7,9,10?/ %MMP1_22: 2,4,5,6,7
            %MMP1_23: 1,2',3?,4',5

Stack=double(Movie(:,:,Start:End))/2^16;
Mask = SingleCellMask(:,:,Start:End)==CellIndex;
%% Generate Cell Outlines

CellOutline = false(size(Mask));
StrEl=strel('disk',3);

for ii = 1:size(Mask,3)
  Mask(:,:,ii) = imfill(Mask(:,:,ii),'holes');
  Mask(:,:,ii) = imclose(Mask(:,:,ii),StrEl);
  CellOutline(:,:,ii) = imdilate(Mask(:,:,ii),StrEl) - Mask(:,:,ii);
  CellOutline(:,:,ii) = imdilate(CellOutline(:,:,ii),StrEl);
end

%% Yolk & Membrane Flows
FlowX = zeros(size(Stack));
FlowY = zeros(size(Stack));
DispX = zeros(1,size(Stack,3));
DispY = zeros(1,size(Stack,3));

%% Flow Parameters
Scale=20;
Start=1;
Stop=size(Stack,3);

%opticFlow = opticalFlowLKDoG('ImageFilterSigma',0.05,'GradientFilterSigma',0.1,'NoiseThreshold',0.1);
opticFlow = opticalFlowHS('Smoothness',0.5, 'VelocityDifference',0.1,'MaxIteration',20);

H=figure('Position',get(0,'ScreenSize'));

%% Display Optical Flow
for ii=Start:Stop% size(Stack,3)

   Frame = Stack(:,:,ii);
   BasalFrame = StackBasal(:,:,ii);

   % Compute optical flow

   Flow = estimateFlow(opticFlow, Frame);
   FlowX(:,:,ii) =Flow.Vx.*double(Mask(:,:,ii));
   FlowY(:,:,ii) =Flow.Vy.*double(Mask(:,:,ii));
   Aux=FlowX~=0;
   DispX(ii) = mean(FlowX(Aux(:)));
   Aux=FlowY~=0;
```

```
    DispY(ii) = mean(FlowY(Aux(:)));

   % ----------------Plotting----------------%
    % Display video frame with flow vectors

    Image=zeros(size(Stack,1),size(Stack,2),3);

    Image(:,:,1)=(CellOutline(:,:,ii).*Flow.Orientation+pi+0.000001)/(2*pi+0.00001);
    Image(:,:,2)=min(CellOutline(:,:,ii).*Flow.Magnitude*Scale,1);
    Image(:,:,3)=max(Frame,CellOutline(:,:,ii).*Image(:,:,2));

    Image(:,:,1)=(Flow.Orientation+pi+0.000001)/(2*pi+0.00001);
    Image(:,:,2)=min(Flow.Magnitude*Scale,1);
    Image(:,:,3)=max(Frame,Image(:,:,2));

   % Image=hsv2rgb(Image).*double(Mask(:,:,ii));

    imshow(Image,'InitialMagnification','fit'); hold on

    drawnow

end

clear opticFlow Flow

%% Plotting
DispY = DispY(3:end);
DispX = DispX(3:end);

DispY = DispY - mean(DispY);
DispX = DispX - mean(DispX);

[AutoCorrY,nAutoCorrY]=xcorr(DispY,'coeff');
[AutoCorrX,nAutoCorrX]=xcorr(DispX,'coeff');


subplot(1,2,1)
plot(nAutoCorrY,AutoCorrY)
title('Displacement AutoCorrelation Y')
xlabel('Lags')
ylabel('XCorr')
hold off


subplot(1,2,2)
plot(nAutoCorrX,AutoCorrX)
title('Displacement AutoCorrelation X')
xlabel('Lags')
ylabel('XCorr')
hold off
```

Quiver Yolk Flow direction

```
function [QuiverSubsX,QuiverSubsY] = QuiverSampler(ImageX,ImageY,BlockSize)

if ~mod(BlockSize,2)
    BlockSize = BlockSize + 1;
end

BlockMiddle = round(BlockSize/2);
CentreMatrix = zeros(BlockSize);
CentreMatrix(BlockMiddle,BlockMiddle) = 1;

fun = @(block_struct) ...
      mean(block_struct.data(:)) * CentreMatrix;

QuiverSubsX = blockproc(ImageX,[BlockSize,BlockSize],fun,...
                        'TrimBorder',false,'BorderSize', [BlockSize,BlockSize]);
QuiverSubsY = blockproc(ImageY,[BlockSize,BlockSize],fun,...
```

```
                'TrimBorder',false,'BorderSize',[BlockSize,BlockSize]);

%QuiverSubsX = imresize(QuiverSubsX,size(ImageX));
%QuiverSubsY = imresize(QuiverSubsY,size(ImageY));
end
```

Publications

Caroti, F.*, Gonz lez Avalos, E.*, **Noeske, V.***, Gonz lez Avalos, P., Kromm, D., Wosch, M., Schütz, L., Hufnagel, L., & Lemke, S. (2018). Decoupling from yolk sac is required for extraembryonic tissue spreading in the scuttle fly Megaselia abdita. eLife, 7, e34616.

Noeske, V., Caglayan, E., Lemke, S. (2021). Single gene initiates evolution of epithelial architecture and function. Biorxiv https://doi.org/10.1101/2021.05.04.442636

*joint first authership

Figures from this thesis have been used in the preprint that can be found on biorxiv: https://doi.org/10.1101/2021.05.04.442636

Following figures from this thesis were adapted for the preprint:

Figure 2.3: Blastoderm cell architecture differes between *Chironomus* and *Drosophila*.
Figure 2.4: Early embryonic development in *Chironomus riparius* takes about 8 hours and 12 nuclear cycles until end of cellularization.
Figure 2.7: Cellularization in the *Chironomus* blastoderm follows a linear time course.
Figure 2.11: During blastoderm formation F-actin dynamics in *Chironomus* differ from actin dynamis in *Drosophila*.
Figure 2.12: Cellularization in *Chironomus* requires maternal transcripts.
Figure 2.14: Exhaustive comparative genomics in 172 fly species points to the emergence of slam about 190 MYA.
Figure 2.15: Overexpressing *slam* in *Chironomus* transforms short-cell- into rall-cell-blastoderm.
Figure 2.16: *sam* expression results in basolateral enrichment of Diaphanous.

Figure 2.18: E-cadherin based adhesion progresses along the basolateral membrane in slam^{OE}embryos.

Figure 2.19: E-cadherin is necessary for slam promoted cell elongation and blastoderm integrity.

Figure 2.20: A local source of E-cadherin is sufficient for the autonomous formation of columnar cells in slam^{OE}embryos.

Figure 2.23: Overexpressing of *slam* provides blastoderm with protection against water loss.

References

Acharya, S., Laupsien, P., Wenzl, C., Yan, S., & Großhans, J. (2014). Developmental Biology. Developmental Biology, 386(2), 371–384.

Adam, J. C., Pringle, J. R., & Peifer, M. (2000). Evidence for functional differentiation among Drosophila septins in cytokinesis and cellularization. Molecular biology of the cell, 11(9), 3123–3135.

Adam, J. C., Pringle, J. R., & Peifer, M. (2000). Evidence for functional differentiation among Drosophila septins in cytokinesis and cellularization. Molecular biology of the cell, 11(9), 3123–3135.

Afshar, K., Stuart, B., & Wasserman, S. A. (2000). Functional analysis of the Drosophila diaphanous FH protein in early embryonic development. Development (Cambridge, England), 127(9), 1887–1897.

Anderson, D. T. (1966). The comparative embryology of the Diptera. Annual Review of Entomology. Vol. 11, pp. 23-46.

Arnoult, L., Su, K. F., Manoel, D., Minervino, C., Magriña, J., Gompel, N., & Prud'homme, B. (2013). Emergence and diversification of fly pigmentation through evolution of a gene regulatory module. Science (New York, N.Y.), 339(6126), 1423–1426.

Barrett, K., Leptin, M., and Settleman, J. (1997). The rho gtpase and a putative rhogef mediate a signaling pathway for the cell shape changes in drosophila gastrulation. Cell, 91(7):905–15.

Benton, M. A., Akam, M., & Pavlopoulos, A. (2013). Cell and tissue dynamics during Tribolium embryogenesis revealed by versatile fluorescence labeling approaches. Development, 140(15), 3210–3220.

Bullock, S. L., Stauber, M., Prell, A., Hughes, J. R., Ish-Horowicz, D. and Schmidt-Ott, U.

(2004). Differential cytoplasmic mRNA localisation adjusts pair-rule transcription factor activity to cytoarchitecture in dipteran evolution. Development 131, 4251–4261.

Campos-Ortega JA, Hartenstein V. 1997. The Embryonic Development of Drosophila melanogaster. Berlin, Heidelberg, New York: Springer. ISBN 978-3-662-22489-2

Caroti, F., González Avalos, E., Noeske, V., González Avalos, P., Kromm, D., Wosch, M., Schütz, L., Hufnagel, L., & Lemke, S. (2018). Decoupling from yolk sac is required for extraembryonic tissue spreading in the scuttle fly Megaselia abdita. eLife, 7, e34616.

Caroti, F., Urbansky, S., Wosch, M., & Lemke, S. (2015). Germ line transformation and in vivo labeling of nuclei in Diptera: report on Megaselia abdita (Phoridae) and Chironomus riparius (Chironomidae). Development genes and evolution, 225(3), 179–186.

Caroti, Francesca (2016). PhD Thesis. Evolution of the extraembryonic tissue in flies: from Megaselia abdita to Drosophila melanogaster. Heidelberg, 2016

Cavey, M., Rauzi, M., Lenne, P.-F. & Lecuit, T. (2008). A two-tiered mechanism for stabilization and immobilization of E-cadherin. Nature 453, 751–756.

Chalut, K. J., & Paluch, E. K. (2016). The Actin Cortex: A Bridge between Cell Shape and Function. Developmental cell, 38(6), 571–573.

Chugh, P., & Paluch, E. K. (2018). The actin cortex at a glance. Journal of cell science, 131(14), jcs186254.

Chugh, P., Clark, A. G., Smith, M. B., Cassani, D., Dierkes, K., Ragab, A., Roux, P. P., Charras, G., Salbreux, G., & Paluch, E. K. (2017). Actin cortex architecture regulates cell surface tension. Nature cell biology, 19(6), 689–697.

Crawford, J. M., Harden, N., Leung, T., Lim, L. and Kiehart, D. P. (1998). Cellularization

in Drosophila melanogaster is disrupted by the inhibition of rho activity and 603 the activation of Cdc42 function. Dev Biol 204, 151–164.

Crawford, J. M., Harden, N., Leung, T., Lim, L., and Kiehart, D. P. (1998). Cellularization in drosophila melanogaster is disrupted by the inhibition of rho activity and the activation of cdc42 function. Dev Biol, 204(1):151–64.

Darwin C. 1839 The voyage of the Beagle, Natural History Library (1962 edn.). Norwell, MA: Anchor Press, pp. 379-380.

Davies JA (2013) Mechanisms of Morphogenesis ((2nd ed)) London/New York: Academic Press.

Denk-Lobnig, M. & Martin, A. C. (2019) Modular regulation of Rho family GTPases in development. Small GTPases 10, 122–129.

Diaz-de-la-Loza, M. D., Ray, R. P., Ganguly, P. S., Alt, S., Davis, J. R., Hoppe, A., Tapon, N., Salbreux, G., & Thompson, B. J. (2018). Apical and Basal Matrix Remodeling Control Epithelial Morphogenesis. Developmental cell, 46(1), 23–39.e5.

Farrell JA, O'Farrell PH. (2014). From egg to gastrula: how the cell cycle is remodeled during the Drosophila mid- blastula transition. Annual Review of Genetics 48:269–294.

Fernandez-Gonzalez, R., Simoes, S., Röper, J. C., Eaton, S., & Zallen, J. A. (2009). Myosin II dynamics are regulated by tension in intercalating cells. Developmental cell, 17(5), 736–743.

Figard, L., & Sokac, A. M. (2014). A membrane reservoir at the cell surface. BioArchitecture, 4(2), 39–46.

Figard, L., Wang, M., Zheng, L., Golding, I. & Sokac, A. M. (2016) Membrane Supply and Demand Regulates F-Actin in a Cell Surface Reservoir. Dev Cell 37, 267–278.

Figard, L., Xu, H., Garcia, H. G., Golding, I. & Sokac, A. M. (2013) The plasma mem-

brane flattens out to fuel cell-surface growth during Drosophila cellularization. Dev Cell 27, 677 648–655.

Foe VE, Odell GM, Edgar BA. (1993). Mitosis and morphogenesis in the Drosophila embryo:point and counterpoint. The Development of Droso- phila melanogaster. Vol. I. Cold Spring Harbor NY: Cold Spring Harbor Laboratory,; 149 – 300.

Foe, V. E., & Alberts, B. M. (1983). Studies of nuclear and cytoplasmic behaviour during the five mitotic cycles that precede gastrulation in Drosophila embryogenesis. Journal of cell science, 61, 31–70.

Fristrom D. (1988). The cellular basis of epithelial morphogenesis. A review. Tissue & cell, 20(5), 645–690.

Gervais, L., & Casanova, J. (2010). In vivo coupling of cell elongation and lumen formation in a single cell. Current biology : CB, 20(4), 359–366.

Giansanti, M. G., Bonaccorsi, S., Williams, B., Williams, E. V., Santolamazza, C., Goldberg, M. L., & Gatti, M. (1998). Cooperative interactions between the central spindle and the contractile ring during Drosophila cytokinesis. Genes & development, 12(3), 396–410.

Glasheen, B. M., Robbins, R. M., Piette, C., Beitel, G. J., & Page-McCaw, A. (2010). A matrix metalloproteinase mediates airway remodeling in Drosophila. Developmental biology, 344(2), 772–783.

Goldbach, P., Wong, R., Beise, N., Sarpal, R., Trimble, W. S., & Brill, J. A. (2010). Stabilization of the actomyosin ring enables spermatocyte cytokinesis in Drosophila. Molecular biology of the cell, 21(9), 1482–1493.

Goltsev, Y., Fuse, N., Frasch, M., Zinzen, R. P., Lanzaro, G., and Levine, M. (2007). Evolution of the dorsal-ventral patterning network in the mosquito, Anopheles gambiae. Development (Cambridge, England), 134(13):2415–2424.

Gompel, N., Prud'homme, B., Wittkopp, P. J., Kassner, V. A., & Carroll, S. B. (2005). Chance caught on the wing: cis-regulatory evolution and the origin of pigment patterns in Drosophila. Nature, 433(7025), 481–487.

Goodwin, K., Ellis, S. J., Lostchuck, E., Zulueta-Coarasa, T., Fernandez-Gonzalez, R., & Tanentzapf, G. (2016). Basal Cell-Extracellular Matrix Adhesion Regulates Force

Grosshans, J., Wenzl, C., Herz, H. M., Bartoszewski, S., Schnorrer, F., Vogt, N., Schwarz, H., and Muller, H. A. (2005). Rhogef2 and the formin dia control the formation of the furrow canal by directed actin assembly during drosophila cellularisation. Development, 132(5):1009–20.

Guild J, Ginzberg MB, Hueschen CL, Mitchison TJ, Dumont S. (2017) Increased lateral microtubule contact at the cell cortex is sufficient to drive mammalian spindle elongation. Mol Biol Cell. Jul 7;28(14):1975-1983.

Guillot, C., & Lecuit, T. (2013). Mechanics of Epithelial Tissue Homeostasis and Morphogenesis. Science, 340, 1185 - 1189.

Gunsalus, K. C., Bonaccorsi, S., Williams, E., Verni, F., Gatti, M., & Goldberg, M. L. (1995). Mutations in twinstar, a Drosophila gene encoding a cofilin/ADF homologue, result in defects in centrosome migration and cytokinesis. The Journal of cell biology, 131(5), 1243–1259.

Hacker, U. and Perrimon, N. (1998). Drhogef2 encodes a member of the dbl family of oncogenes and controls cell shape changes during gastrulation in drosophila. Genes Dev, 12(2):274–84.

Haies DM, Gil J, Weibel ER (1981) Morphometric study of rat lung cells. I. Numerical and dimensional characteristics of parenchymal cell population. Am Rev Respir Dis 123:533–541.

Handel, K., Grünfelder, C., Roth, S. et al. (2000) Tribolium embryogenesis: a SEM study of cell shapes and movements from blastoderm to serosal closure. Dev Gene Evol

210, 167–179 (2000).

Harris, T. J. C. and Peifer, M. (2005). The positioning and segregation of apical cues during epithelial polarity establishment in Drosophila. J Cell Biol 170, 813–823.

Havelka, J., Landa, V., & Landa, V. (2007). Embryogenesis of Aphidoletes aphidimyza (Diptera: Cecidomyiidae): Morphological markers for staging of living embryos. Eur. J. Entomol., 104(1), 81-87.

He, B., Martin, A., and Wieschaus, E. (2016). Flow-dependent myosin recruitment during drosophila cellularization requires zygotic dunk activity. Development, 143(13):2417–30.

Hehenberger E, Kradolfer D, Ko ¨ hler C. 2012. Endosperm cellularization defines an important developmental transition for embryo development. Development 139:2031–2039.

Hunter, C., & Wieschaus, E. (2000). Regulated expression of nullo is required for the formation of distinct apical and basal adherens junctions in the Drosophila blastoderm. The Journal of cell biology, 150(2), 391–401.

Hutterer, A., Betschinger, J., Petronczki, M. & Knoblich, J. A. (2004) Sequential roles of Cdc42, Par-6, aPKC, and Lgl in the establishment of epithelial polarity during Drosophila embryogenesis. Dev Cell 6, 845–854.

Ishihara, H., Martin, B.L., Brautigan, D.L., Karaki, H., Ozaki, H., Kato, Y., Fusetani, N., Watabe, S., Hashimoto, K., Uemura, D., Hartshorne, D.J., (1989). Calyculin A and okadaic acid: Inhibitors of protein phosphatase activity. Biochemical and Biophysical Research Communications 159, 871–877.

Jiménez-Guri E, Wotton KR, Gavilán B, Jaeger J (2014). A Staging Scheme for the Development of the Moth Midge Clogmia albipunctata. PLOS ONE 9(1): e84422.

Klomp, J., Athy, D., Kwan, C. W., Bloch, N. I., Sandmann, T., Lemke, S., & Schmidt-Ott,

U. (2015). Embryo development. A cysteine-clamp gene drives embryo polarity in the midge Chironomus. Science (New York, N.Y.), 348(6238), 1040–1042.

Kolsch, V., Seher, T., Fernandez-Ballester, G. J., Serrano, L., and Leptin, M. (2007). Control of drosophila gastrulation by apical localization of adherens junctions and rhogef2. Science, 315(5810):384–6.

Koonce, M., Tong, J., Euteneuer, U. et al. (1987) Active sliding between cytoplasmic microtubules. Nature 328, 737–739.

Kurn H, Daly DT. Histology, Epithelial Cell. [Updated 2021 May 10]. In: StatPearls [Internet]. Treasure Island (FL): StatPearls Publishing; 2021 Jan-. Available from: https://www.ncbi.nlm.nih.gov/books/NBK559063/

Kwan, C. W., Gavin-Smyth, J., Ferguson, E. L., & Schmidt-Ott, U. (2016). Functional evolution of a morphogenetic gradient. eLife, 5, e20894. https://doi.org/10.7554/eLife.20894

Lacy, M. E., & Hutson, M. S. (2016). Amnioserosa development and function in Drosophila embryogenesis: Critical mechanical roles for an extraembryonic tissue. Developmental dynamics : an official publication of the American Association of Anatomists, 245(5), 558–568.

Laprise, P., & Tepass, U. (2011). Novel insights into epithelial polarity proteins in Drosophila. Trends in cell biology, 21(7), 401–408.

Laurin, M., Gomez, N. C., Levorse, J., Sendoel, A., Sribour, M., & Fuchs, E. (2019). An RNAi screen unravels the complexities of Rho GTPase networks in skin morphogenesis. eLife, 8, e50226.

Lecuit T. (2004). Junctions and vesicular trafficking during Drosophila cellularization. Journal of cell science, 117(Pt 16), 3427–3433.

Lecuit, T., & Wieschaus, E. (2000). Polarized insertion of new membrane from a cyto-

plasmic reservoir during cleavage of the Drosophila embryo. The Journal of Cell Biology, 150(4), 849–860.

Lecuit, T., Samanta, R., & Wieschaus, E. (2002). slam encodes a developmental regulator of polarized membrane growth during cleavage of the Drosophila embryo. Developmental Cell, 2(4), 425–436.

Lemke, Steffen, Kale, Girish and Urbansky, Silvia. (2020). Comparing gastrulation in flies: Links between cell biology and the evolution of embryonic morphogenesis. Mechanisms of Development. 164.

Leptin, M. (1999). Gastrulation in Drosophila: the logic and the cellular mechanisms. The EMBO Journal, 18:3187–3192.

Leptin, M. and Grunewald, B. (1990). Cell shape changes during gastrulation in Drosophila. Development (Cambridge, England), 110(1):73–84.

Levayer, R., P.lissier-Monier, A. & Lecuit, T. (2011). Spatial regulation of Dia and Myosin-II by RhoGEF2 controls initiation of E-cadherin endocytosis during epithelial morphogenesis. Nat Cell Biol 13, 529–540 (2011).

M dina, E. et al. (2002) Crumbs interacts with moesin and beta(Heavy)-spectrin in the apical membrane skeleton of Drosophila. J Cell Biol 158, 941–951.

Martin AC, Kaschube M, Wieschaus EF (2009). Pulsed contractions of an actin-myosin network drive apical constriction. Nature.;457(7228):495-499.

Mavrakis, M., Azou-Gros, Y., Tsai, F. C., Alvarado, J., Bertin, A., Iv, F., Kress, A., Brasselet, S., Koenderink, G. H., & Lecuit, T. (2014). Septins promote F-actin ring formation by crosslinking actin filaments into curved bundles. Nature cell biology, 16(4), 322–334.

Mencarelli, C., Ciolfi, S., Caroti, D., Lupetti, P. and Dallai, R. (2011). Isomin: a novel cytoplasmic intermediate filament protein from an arthropod species. BMC Biol 9, 17.

Merrill, P. T., Sweeton, D., & Wieschaus, E. (1988). Requirements for autosomal gene activity during precellular stages of Drosophila melanogaster. Development, 104(3), 495–509.

Miller, K. G., & Kiehart, D. P. (1995). Fly division. The Journal of cell biology, 131(1), 1–5.

Miyamoto, D. M., & van der Meer, J. M. (1982). Early egg contractions and patterned parasynchronous cleavage in a living insect egg. Wilhelm Roux's archives of developmental biology, 191(2), 95–102.

Müller, P. M. et al. (2020) Systems analysis of RhoGEF and RhoGAP regulatory proteins reveals spatially organized RAC1 signalling from integrin adhesions. Nat Cell Biol 22, 498–511.

Munjal, A., Philippe, J.-M., Munro, E. and Lecuit, T. (2015). A self-organized biomechanical network drives shape changes during tissue morphogenesis. Nature 524, 645 351–355.

Narasimha, M. and Brown, N. H. (2004). Novel functions for integrins in epithelial morphogenesis. Current biology : CB, 14(5):381–385.

Piekny, A. J., & Maddox, A. S. (2010). The myriad roles of Anillin during cytokinesis. Seminars in cell & developmental biology, 21(9), 881–891.

Pignocchi C, Minns GE, Nesi N, Koumproglou R, Kitsios G, Benning C, Lloyd CW, Doonan JH, Hills MJ. (2009). ENDOSPERM DEFECTIVE1 is a novel Microtubule-Associated protein essential for seed development in Arabidopsis. The Plant Cell 21:90–105.

Planques, V., Warn, A. & Warn, R. M. (1991) The effects of microinjection of rhodamine phalloidin on mitosis and cytokinesis in early stage Drosophila embryos. Exp Cell Res 680 192, 557–566.

Pollard, Thomas & Cooper, John. (2009). Actin, a Central Player in Cell Shape and Move-

ment. Science (New York, N.Y.). 326. 1208-12. 10.1126/science.1175862.

Pope, K. L., & Harris, T. J. (2008). Control of cell flattening and junctional remodeling during squamous epithelial morphogenesis in Drosophila. Development (Cambridge, England), 135(13), 2227–2238.

Rafiqi, A. M., Lemke, S., Ferguson, S., Stauber, M., & Schmidt-Ott, U. (2008). Evolutionary origin of the amnioserosa in cyclorrhaphan flies correlates with spatial and temporal expression changes of zen. Proceedings of the National Academy of Sciences of the United States of America, 105(1), 234–239.

Rafiqi, A. M., Park, C. H., Kwan, C. W., Lemke, S., & Schmidt-Ott, U. (2012). BMP-dependent serosa and amnion specification in the scuttle fly Megaselia abdita. Development (Cambridge, England), 139(18), 3373–3382.

Reed, B. H., Wilk, R., Schöck, F., & Lipshitz, H. D. (2004). Integrin-dependent apposition of Drosophila extraembryonic membranes promotes morphogenesis and prevents anoikis. Current biology : CB, 14(5), 372–380.

Rickoll W. L. (1976). Cytoplasmic continuity between embryonic cells and the primitive yolk sac during early gastrulation in Drosophila melanogaster. Developmental biology, 49(1), 304–310.

Riggs, B., Fasulo, B., Royou, A., Mische, S., Cao, J., Hays, T. S., & Sullivan, W. (2007). The concentration of Nuf, a Rab11 effector, at the microtubule-organizing center is cell cycle regulated, dynein-dependent, and coincides with furrow formation. Molecular biology of the cell, 18(9), 3313–3322.

Riparbelli, M. G., Callaini, G., & Schejter, E. D. (2007). Microtubule-dependent organization of subcortical microfilaments in the early Drosophila embryo. Developmental Dynamics: an Official Publication of the American Association of Anatomists, 236(3), 662–670.

Ritter, R. (1890). Die Entwicklung der Geschlechtsorgane und des Darmes bei Chirono-

mus. 1:1–21.

Rizvi, S. A., Neidt, E. M., Cui, J., Feiger, Z., Skau, C. T., Gardel, M. L., Kozmin, S. A. and Kovar, D. R. (2009). Identification and characterization of a small molecule inhibitor of formin-mediated actin assembly. Chem Biol 16, 1158–1168.

Rothwell, Wendy & Sullivan, William. (2000). The centrosome in early Drosophila embryogenesis. Current Topics in Developmental Biology. 49. 409-447.

Rousso, T., Shewan, A. M., Mostov, K. E., Schejter, E. D. and Shilo, B. Z. (2013). Apical targeting of the formin Diaphanous in Drosophila tubular epithelia. Elife (Cambridge) 2, e00666.

Royou, A., Sullivan, W., & Karess, R. (2002). Cortical recruitment of nonmuscle myosin II in early syncytial Drosophila embryos: its role in nuclear axial expansion and its regulation by Cdc2 activity. The Journal of cell biology, 158(1), 127–137.

Sambrook, Joseph. (2001) Molecular Cloning : a Laboratory Manual. Cold Spring Harbor, N.Y. :Cold Spring Harbor Laboratory Press, 2001.

Sawyer, J.M., Harrell, J. R., Shemer, G., Sullivan-Brown, J., Roh-Johnson, M., and Goldstein, B. (2010). Apical constriction: A cell shape change that can drive morphogenesis. Developmental Biology, 341(1):5–19.

Schejter, E. D. and Wieschaus, E. (1993). bottleneck acts as a regulator of the microfilament network governing cellularization of the drosophila embryo. Cell, 75(2):373–85.

Schindelin, J., Arganda-Carreras, I., Frise, E., Kaynig, V., Longair, M., Pietzsch, T., Preibisch, S., Rueden, C., Saalfeld, S., Schmid, B., et al. (2012). Fiji: an open-source platformfor biologicalimage analysis. Nature methods, 9(7):676.

Schmidt-Ott, U., & Kwan, C. W. (2016). Morphogenetic functions of extraembryonic membranes in insects. Current opinion in insect science, 13, 86–92.

Schmidt, A. and Hall, A. (2002). Guanine nucleotide exchange factors for rho gtpases: turning on the switch. Genes Dev, 16(13):1587–609.

Schmidt, Anja and Grosshans, Jörg. (2018). Dynamics of cortical domains in early Drosophila development. Journal of Cell Science. 131. jcs212795. 10.1242/jcs.212795.

Schöck, Frieder & Perrimon, Norbert. (2003). Schock, F. & Perrimon, N. Retraction of the Drosophila germ band requires cell-matrix interaction. Genes Dev. 17, 597-602. Genes & development. 17. 597-602. 10.1101/gad.1068403.

Schwalm FE. (1988) Insect morphogenesis. In: Sauer HW, editor. Monographs in developmental biology.Vol. 20. Karger; Basel, Switzerland.

Schwayer, C., Sikora, M., Slováková, J., Kardos, R., & Heisenberg, C. P. (2016). Actin Rings of Power. Developmental cell, 37(6), 493–506.

Sciaky, N., Presley, J., Smith, C., Zaal, K.J., Cole, N., Moreira, J.E., Terasaki, M., Siggia, E., and Lippincott-Schwartz, J. (1997). Golgi tubule traffic and the effects of brefeldin A visualized in living cells. J. Cell. Biol. 139, 1137–1155.

Sen, A., Nagy-Zsv r-Vadas, Z. & Krahn, M. P. (2012) Drosophila PATJ supports adherens junction stability by modulating Myosin light chain activity. J Cell Biol 199, 685–698.

Shimmi, O., Umulis, D., Othmer, H., O'Connor, M.B., (2005). Facilitated transport of a Dpp/ Scw heterodimer by Sog/Tsg leads to robust patterning of the Drosophila blastoderm embryo. Cell 120, 873–886.

Sørensen MB, Mayer U, Lukowitz W, Robert H, Chambrier P, Jurgens G, Somerville C, Lepiniec L, Berger F. (2002). Cellularisation in the endosperm of Arabidopsis thaliana is coupled to mitosis and shares multiple components with cytokinesis. Development 129:5567–5576.

Stein, J. A., Broihier, H. T., Moore, L. A., and Lehmann, R. (2002). Slow as molasses is

required for polarized membrane growth and germ cell migration in drosophila. Development, 129(16):3925–34.

Steinmetz, P. R. H. (2019) A non-bilaterian perspective on the development and evolution of animal digestive systems. Cell Tissue Res 377, 321–339.

Stevenson, V., Hudson, A., Cooley, L., & Theurkauf, W. E. (2002). Arp2/3-dependent pseudocleavage [correction of psuedocleavage] furrow assembly in syncytial Drosophila embryos. Current biology : CB, 12(9), 705–711.

Suksuwan, W., Cai, X., Ngernsiri, L., & Baumgartner, S. (2017). Segmentation gene expression patterns in Bactrocera dorsalis and related insects: regulation and shape of blastoderm and larval cuticle. The International journal of developmental biology, 61(6-7), 439–450.

Sullivan, W., Fogarty, P., & Theurkauf, W. (1993). Mutations affecting the cytoskeletal organization of syncytial Drosophila embryos. Development (Cambridge, England), 118(4), 1245–1254.

Tautz, D., & Domazet-Lošo, T. (2011). The evolutionary origin of orphan genes. Nature reviews. Genetics, 12(10), 692–702.

Tcherkezian, J. and Lamarche-Vane, N. (2007). Current knowledge of the large rhogap family of proteins. Biol Cell, 99(2):67–86.

Theurkauf W. E. (1994). Actin cytoskeleton. Through the bottleneck. Current biology : CB, 4(1), 76–78.

Tram, Uyen & Riggs, Blake & Sullivan, William. (2002). Cleavage and Gastrulation in Drosophila Embryos. 10.1038/npg.els.0001071.

Treuting, P. M., Dintzis, S. M. and Montine, K. S. eds. (2017). Comparative Anatomy and Histology - A Mouse, Rat, and Human Atlas. Academic Press (London/New York).

Troutt, L & Burnside, Beth. (1988). The unusual microtubule polarity in teleost ret-

inal pigment epithelial cells. The Journal of cell biology. 107. 1461-4. 10.1083/jcb.107.4.1461.

Turner, F. R. and Mahowald, A. P. (1977). Scanning electron microscopy of Drosophila melanogaster embryogenesis. II. Gastrulation and segmentation. Developmental biology, 57(2):403–416.

Turner, F. R. and Mahowald, A. P. (1979). Scanning electron microscopy of Drosophila melanogaster embryogenesis. III. Formation of the head and caudal segments. Developmental biology, 68(1):96–109.

Uliana, J., Brancini, G., Hombría, J. C., Digiampietri, L. A., Andrioli, L. P., & Monesi, N. (2018). Characterizing the embryonic development of B. hygida (Diptera: Sciaridae) following enzymatic treatment to permeabilize the serosal cuticle. Mechanisms of development, 154, 270–276.

Umulis, D., Shimmi, O., O'Connor, M., Othmer, H., (2010). Organism-scale modeling of early Drosophila patterning via bone morphogenetic proteins. Dev. Cell 18, 260–274.

Urbansky, S., González Avalos, P., Wosch, M. and Lemke, S. (2016). Folded gastrulation and T48 drive the evolution of coordinated mesoderm internalization in flies. Elife (Cambridge) 5.

Urbansky, Silivia (2016). PhD Thesis. Turning the switch, fog and t48 control the mode of mesoderm internalization in flies. Heidelberg, 2016

van der Zee, M., Benton, M. A., Vazquez-Faci, T., Lamers, G. E. M., Jacobs, C. G. C., and Rabouille, C. (2015). Innexin7a forms junctions that stabilize the basal membrane during cellularization of the blastoderm in Tribolium castaneum. Development, 142(12), 2173–2183.

van Unen, J. et al. (2015) Plasma membrane restricted RhoGEF activity is sufficient for RhoA-mediated actin polymerization. Sci Rep 5, 14693.

Vasioukhin, V., Bauer, C., Yin, M. & Fuchs, E. (2000) Directed actin polymerization is the driving force for epithelial cell-cell adhesion. Cell 100, 209–219.

Wang, Y.-C., Ferguson, E.L., (2005). Spatial bistability of Dpp-receptor interactions during Drosophila dorsal-ventral patterning. Nature 434, 229–234.

Warn, R. M. and Magrath, R. (1983). F-actin distribution during the cellularization of the drosophila embryo visualized with fl-phalloidin. Exp Cell Res, 143(1):103–14.

Wenzl, C., Yan, S., Laupsien, P., & Großhans, J. (2010). Localization of RhoGEF2 during Drosophila cellularization is developmentally controlled by slam. Mechanisms of Development, 127(7-8), 371–384.

Wiegmann, B. M., Trautwein, M. D., Winkler, I. S., Barr, N. B., Kim, J.-W., Lambkin, C., Bertone, M. A., Cassel, B. K., Bayless, K. M., Heimberg, A. M., et al. (2011). Episodic radiations in the fly tree of life. 108, 5690–5695.

Wittkopp, P. J., Vaccaro, K., & Carroll, S. B. (2002). Evolution of yellow gene regulation and pigmentation in Drosophila. Current biology : CB, 12(18), 1547–1556.

Xue, Z. and Sokac, A. M. (2016). Back-to-back mechanisms drive actomyosin ring closure during Drosophila embryo cleavage. J Cell Biol 215, 335–344.

Yan, S., and Grosshans, J. (2018). Localization and translation control of slam in Drosophila cellularization. Fly, 12(3-4), 191–198.

Zheng, Liuliu & Sepúlveda, Leonardo & Lua, Rhonald & Lichtarge, Olivier & Golding, Ido & Sokac, Anna. (2013). The Maternal-to-Zygotic Transition Targets Actin to Promote Robustness during Morphogenesis. PLoS genetics. 9. e1003901. 10.1371/journal.pgen.1003901.

Acknowledgments

Als allererstes möchte ich mich bei dir, Steffen (Junior Prof. Dr. Steffen Lemke), bedanken, dass du mich die letzten Jahre so gut durch den PhD begleitet hast. Ich hätte mir keinen besseren Betreuer wünschen können. Deine Tür stand immer offen für mich und du hattest immer ein offenes Ohr. Vor allem bin ich gerne zu dir ins Office gekommen, wenn ich wieder neue, aufregende Daten hatte und diese direkt mit dir besprechen oder auch mal direkt die Aufregung mit dir vor dem Mikroskop teilen konnte. Aber auch danke dafür, dass du mir so viele Freiräume gelassen hast meine Ideen und Experimente so umzusetzen, wie ich es mir vorgestellt habe. Danke für diese tolle Zeit.

Zudem möchte ich dir, Jochen (Prof. Dr. Jochen Wittbrodt), danken. Du hast das Projekt von Anfang an mit begleitet und seit meinem Masterabschluss mitverfolgt. Danke, dass du in den TACs und darüber hinaus an dem Projekt mitgedacht und es immer gerne mitverfolgt hast. Ein großer Dank an dich Annika (Prof. Dr. Annika Guse), dass du mit so viel Enthusiasmus und Energie das Projekt währen der TACs und vor allem am Ende das Paper so vorangetrieben hast. Vielen Dank Michi (Dr. Michael Raissig), dass du dich mit uns auf Diskussionen außerhalb deines Feldes einlässt und mit in meinem Komitee dabei sein wirst.

Danke liebes Lemke Lab! So viele Stunden haben wir alle zusammen im Labor verbracht und viel zusammen gelacht. So viele die wir sind und waren und ich hier gerne kurz erwähnen und mich bedanken möchte. Als erstes Danke Silvi, du warst seit Tag 1 meiner ersten Lab Rotation bei Steffen und hast somit alle Hochs und Tiefs (zum Glück gab es davon sehr wenige) mitbekommen und hattest immer ein offenes Ohr. Ich werde es sehr vermissen zur Begrüßung ein lautes Viiooolaa zu hören. Ein ganz großer Dank geht an dich Maike, deine herzliche Art und dein Lachen sind einfach ansteckend. Wie häufig haben wir mit Silvi und Naima einfach nur gelacht. Und natürlich auch ein riesen Dank für deine Hilfe im Labor um beim Klonieren auch über deinen Laborwechsel hinaus. Danke Atalay, leider bist du jetzt schon kein Mitglied des Lemke Labors mehr, aber ich denke sehr gerne an die Zeit mit dir als Bay-Nachbar zurück „Tamam, tamam“. A big thank goes to Francesca. Thank you for your assistance in the lab and the fun times we had in the lab during, lunch time and the beer hours. Thanks to all other members of the Lemke lab who are still and have been in the lab. Thanks for all your support.

Liebe Paula, vielen, vielen Dank an dich. Ich habe so gerne mit dir zusammen an Matlab gearbeitet und ich habe so viel von dir gelernt (nicht nur über Matlab). Ich freue mich, dass wir bis heute so gut befreundet sind und werde das Schreiben der PhD-Thesis immer mit den zwei tollen Wochen bei euch verbinden.

Danke lieber Ever. Danke, dass du so geduldig mit mir zusammen an Matlab gear-

beitet hast und dir immer die Zeit genommen hast mir alles zu erklären. Und natürlich danke für Kletterausflüge und gemeinsame Abende. Ich hoffe wir machen bald mal eine Radtour zusammen.

Danke Linda für Einladungen zum Frühstück, für die tolle Radtour und Zeit im Office. Danke Ira, ich erinnere mich so gerne an unsere gemeinsame Fahrt ins Blaue und gemeinsame Kaffees.

Der wahrscheinlich größte Dank geht an dich Naima. Danke, danke, danke. Ohne dich hätte ich den PhD wahrscheinlich gar nicht erst angefangen. Ich weiß gar nicht, wie ich in diesen paar Zeilen sagen soll, wie unglaublich toll die Zeit mit dir im Labor und weit darüber hinaus war. Was haben wir nicht alles zusammen erlebt, waren auf der Welt unterwegs, waren in der Unteren und am nächsten Morgen wieder im Lab, haben von Frühstück bis Abendessen alle Mahlzeiten zusammen eingenommen. Die PhD-Zeit wäre nicht die gleiche gewesen ohne dich.

Ich möchte an dieser Stelle auch meinen engsten Freunden Danken. Danke liebe Freizeitspaß in HD-Gruppe, für all die tollen Tage und Abende, die wir zusammen verbracht haben. Danke Lisa, Alycia und Neza für die tolle WG-Zeit und weit darüber hinaus. Danke Lisa für dein Organisationstalent und deine Torten und einfach alles. Danke Moritz, dass du uns so gerne in deinem Garten und deinem Pool empfangen hast. Den Garten werde ich immer mit meiner PhD-Zeit verbinden. Danke Daniel und Moritz für die Genever-Abende. Danke Felix, Jacob, Anna, Freddy. Danke an Franz, Alycia, Tobias, Eva und Jan, dass ihr euch die Zeit genommen habt, die Arbeit Korrektur zu lesen. Danke Anne, dass du mich schon so viele Jahre und durch so viele Lebensphasen mit begleitet hast.

Mit der größte Dank geht an meine Familie. Danke, dass ihr mich immer unterstützt habt. Ohne euch, Mama und Papa, wäre ich heute nicht, wo ich bin. Danke, dass ich mich immer auf euch verlassen kann. Danke an meine Brüder Tobias, Jannik und Gabriel, wir sind alle so unterschiedlich und dadurch haben wir wirklich immer wieder interessante neue Themen zu diskutieren.

Danke, danke, danke Jan. Du hast mich so unglaublich unterstützt. Ohne dich hätte ich die letzten Monate nicht so gut durchgestanden. Danke für die tolle Zeit zusammen im Home-Office, die wir mit so vielen Stunden vor dem PC verbracht haben. Gut, dass wir beim gemeinsamen Radfahren und beim Pferd auch immer wieder zusammen abschalten konnten. Danke, dass du immer für mich da bist.

Declaration

Herewith I declare that I prepared the PhD Thesis " Single genes initiate novel epithelial structure in early fly development " on my own and with no other sources and aids than quoted.

Heidelberg, 2021